STUDIES ON THE MECHANISM AND INHIBITION OF TUBERCULOSIS CAVITATION

by

Michael Edward Urbanowski

A dissertation submitted to The Johns Hopkins University in conformity with the requirements for the degree of Doctor of Philosophy.

Baltimore, Maryland

May, 2018

Abstract

Tuberculosis is the leading cause of death due to a single infectious agent and is spread from person to person by coughed aerosols. Individuals with tuberculosis lung cavities spread disease more frequently than individuals without cavities. Unfortunately, few studies address the mechanistic drivers of tuberculosis. The first chapter of this manuscript describes the prevalence of cavitary tuberculosis among cases of active tuberculosis based on a retrospective study of 3000 autopsies. Our results show that the frequency of cavitation among cases of active tuberculosis is 15% and this statistic may inform computational models of disease transmission. One obstacle to studying the mechanism of tuberculosis cavitation is the difficulty in modeling tuberculosis cavities. Chapter 2 of this manuscript describes and characterizes a novel rabbit model of cavitary tuberculosis based on repetitive aerosol infection. We found that repetitive aerosol infection exacerbates disease and increases the frequency of cavitation from 25% for a single infection to 60-80% during repetitive infections even when the total exposure is the same between groups. These results suggest that repetitive exposure may drive worse disease and cavitation in high-incidence settings. Chapters 3 and 4 investigate the biochemical drivers of cavitation in tuberculosis. Previous studies suggest that extracellular matrix breakdown enables cavitation, but the identity of the host-expressed protein mediators of matrix breakdown remain unresolved. We applied the repetitive aerosol model described in Chapter 2 to study

small-molecule mediated inhibition of extracellular collagenases during cavity formation. Chapter 3 describes the inhibition of the collagenase MMPs by cipemastat. We found that cipemastat monotherapy was unable to reduce the frequency or extent of cavitary disease, suggesting that collagenase MMPs are not primary mediators of matrix breakdown. Chapter 4 describes preliminary studies on the inhibition of cathepsin K using odanacatib. These studies show strong support for cathepsin K as a mediator of cavitation and endorse odanacatib as an efficacious agent for pre-clinical investigations.

Acknowledgments

A lot of paths cross during the six years of doctoral studies. Many of these encounters influenced me tremendously. Often I wonder if my own path was nothing more than a random walk through time and space. But here, in this space, is where I get to thank the individuals who trusted that it was not.

Throughout the text I annotated the many authors who contributed to each set of studies. None of these studies could have been carried out by one person alone. In this section, I would like to focus on the more personal nature of these interactions and mention a few people who might not appear in the authorship lists.

First to my mentor, Bill Bishai, who has given me tremendous guidance, support, and encouragement during my studies. I feel truly honored that I was given the opportunity to work on the very important problem of tuberculosis cavitation. Then, to my thesis committee. Dr. Brendan Cormack, Dr. Marc Halushka, and Dr. Eric Nuermberger, all of whom patiently considered my many ideas and did their best to focus my attention when it was most important. Then to three additional Professors who I consider satellite mentors for their generous support and encouragement, but without any stakes in the game. Dr. Ralph Hruban inspired my passion for the history of tuberculosis. Dr. Paul Elkington was a brilliant and critical champion of my work. Finally, Dr. Sanjay Jain tirelessly supported my investigations.

I thank two talented researchers who taught me a thorough respect for the rabbit model. Dr. André Kübler and Dr. Brian Luna pioneered many of the techniques that I now take for granted, but which enabled the studies in this dissertation. Dr. Luna is one of the greatest teachers that I know and Dr. Kübler is equally so as an original and innovative investigator.

I thank all of the members of the Center for Tuberculosis Research at the Johns Hopkins School of Medicine. It is a wonderful place to work. There are a few people in particular that deserve a shout: Linda Brady, Dr. Dalin Rifat, Haidan Guo, Dr. Shichun Lun, Robyn Becker, Michael Pinn, Dr. Lee Klinkenberg, Dr. Gyanu Lamichhane, Dr. Jacques Grosset, Stef Krug, Julian Sanchez, Connie Williams, Gel-

trouda Demczuk, Dr. Bintou Ahmadou Ahidjo, Mariah Klunk, Kathryn Winglee, Kristina Bigelow, and Benjamin Merenbloom.

Thank you to Marjorie Kehoe and all the staff of the Johns Hopkins University Chesney Medical Archives for their patience, flexibility, and help during my research.

During my third year I was honored to serve as the Chief Graduate Student of the Pathobiology Graduate Program. I have never felt more alive or fulfilled in my life than during that year that I spent in service to my colleagues in the Pathobiology Program. I owe a debt of gratitude to all of the Pathobiology graduate students. Then also to Dr. Petros Karakousis and Dr. Kathy Gabrielson who invited me to be a TA for their classes. I received more from these experiences than I could ever hope to contribute.

I had two amazing program directors and role models in the Pathobiology program. Dr. Noel Rose and Dr. Lee Martin. I was lucky enough to interact with them bother personally. Dr. Rose's example encouraged me to be thoughtful, fair, industrious, and just a little bit snarky. Dr. Martin's example drove me to be knowledgeable, diligent, and steadfast in my ideas. Both are the epitome of scientists, researchers, and leaders. Dr. Rose and Dr. Martin worked in a team with Tracie McElroy, Stacey Morgan, and Nancy Nath. Tracie, Stacey and Nancy have helped me in more ways than I can possibly convey. Thank you.

I see tremendous value in being part of a graduate program. I learned the most from my friends and colleagues in Pathobiology. Here are a few names. To Samantha Semenkow and Anne Macgregor-Das who recruited me to the program and have been steadfast friends since. To my classmates Bo-Yi Sung, Sophie Lin, Jaeyeun Lee, and Devin Sabin.

I had the good fortune of owning a house while I was a graduate student, and so my mission was to fill it with the most creative and interesting people around. That is exactly what happened, though I had nothing to do with the recruitment and it was entirely by luck and their willingness to put up with me. So I kept learning in the hours after I left lab. To my housemates Drew Bell, Carolyn Tallon (practically), Clio Franklin, Eric Chow, Himavanth Reddy Gatla, Janelle Pickering, and David Yanagisawa.

I want to mention just a few more names in case you, the reader, should also cross paths with them. Then, you should take a few minutes to get to know them better, because they have enriched my life and inspired me to do better at every turn. First to Dr. Brad Poore. I have never met someone I respect more as a student, a scientist, a renaissance man, and a person. I am particularly thankful for the many nights of chess and his patience while we (mostly I) ranted about the evils of Amtrak (or whatever was important on that day). Then to Alvaro (*Doc*) Ordonez, whose intelligence is only matched by his compassion and respect for those around him, altogether making him super-human. We have gone on some marvelous adventures

during graduate school: El Cocuy Colombia, Alaska, Katahdin, The Presidentials, The AT of Shenandoah, but the greatest adventures are always our discussions. To Laurene Cheung who is the *most brilliant* experimentalist that I have ever met, but also the greatest citizen. I stand in perpetual awe of the precision she applies to her understanding of the world. To Beth Ihms who let me geek out with her. I am forever thankful that she allowed me to observe on the veterinary pathology service and I consider the times that I spent with her in the *tank* and at the zoo to be some of my greatest experiences in graduate school. Alright, then I must mention Patrick Border, *a man of extraordinary culture* (so said his fortune cookie once) and a true patriot in a time when our country needs it most. Lastly to Breann Yanagisawa, who is an exceptional scientist but who also shared with me her truly original ideas that could only be described as those of an artist.

I must thank Dr. Tobias Baskin, my first research mentor and long-time friend who inspired me with a love for experimental biology and encouraged me to apply to the Pathobiology Graduate Program at Johns Hopkins. Then there is Dr. Alex Cobb, the first post-Doc that I worked with. He is also great. Then finally to Dr. Robert Bertin who gave me my first microscope.

To Dr. Arthur M. Dannenberg who invited me into his house and let me talk with him for hours. It was an honor and very surreal. Often he spoke about his family who he loves and his computer, which never seemed to work. Sometimes we spoke about tuberculosis and I realized that very few of my thoughts on pathogenesis were original, he had had them all before. Should I be gifted with a long life, I hope that my fascination is captivated, as his is, forever.

I want to thank Michael Mahoney who past away last year. He was a gentle, wise, and accepting soul, also my great friend for over 20 years. I will never forgive the years of graduate school for taking away more time that I might have spent with him.

To Eva Shrestha, my best friend and companion on our many mutual adventures.

Finally, to my family. My father Ed, my mother Jean, and to my sister Kathryn. There are no words to express the love and respect that I have for them.

To all above, and those beyond this page.

Thank you.

Mike Urbanowski
2018.02.26

Dedication

To Eddie Urbanowski
1991-2003

My best friend and brother, who showed me how to fight disease from a hospital bed, and who inspires me to fight from a laboratory bench.

Contents

List of Figures

List of Tables

Introduction: the pathobiology of tuberculosis cavities

Michael E. Urbanowski · Alvaro A. Ordonez

"Out of the night that covers me,
Black as the pit from pole to pole,
I thank whatever gods may be
For my unconquerable soul.

In the fell clutch of circumstance
I have not winced nor cried aloud.
Under the bludgeonings of chance
My head is bloody, but unbowed.

Beyond this place of wrath and tears
Looms but the Horror of the shade,
And yet the menace of the years
Finds and shall find me unafraid.

It matters not how strait the gate,
How charged with punishments the scroll,
I am the master of my fate,
I am the captain of my soul."

Invictus by William Ernst Henley (1888).
Written from his bed as he battled with tuberculosis.

A lung cavity is the most dangerous consequence of pulmonary tuberculosis. Individuals that develop tuberculosis cavities are often sicker and more likely to aerosolize bacilli than those without cavities[1]. But, in the antibiotic era, cavities are contextualized as the extreme outcome of treatment failure and are one of the least-studied aspects of tuberculosis. In this introduction, we review cavities as dynamic physical and biochemical structures that interface the host-response with a unique mycobacterial niche to drive morbidity and transmission in tuberculosis. Our goal is to provide an insightful and thoughtful interdisciplinary review of the pathogenesis and consequences of tuberculosis cavitation.

To accomplish our goal, we examine insights from studies in epidemiology, pathology, pathophysiology, biochemistry and microbial ecology. Wherever possible, we draw parallels between these studies to build a more comprehensive conceptual model for the role of cavities in tuberculosis. Finally, we also highlight remaining enigmas surrounding tuberculosis cavities with the aim of helping researchers to design future studies.

The architecture of tuberculosis cavities

A lung cavity is a pathologic gas-filled space in the lung with a border, or wall, which has a density close to water[2]. A tuberculosis cavity is a cavitary focus caused by infection with a pathogen of the *Mycobacterium tuberculosis* (*M. tb*) complex. Among tuberculosis cavities there is considerable heterogeneity in size, morphology and wall-composition.

Examples of tuberculosis cavities at autopsy

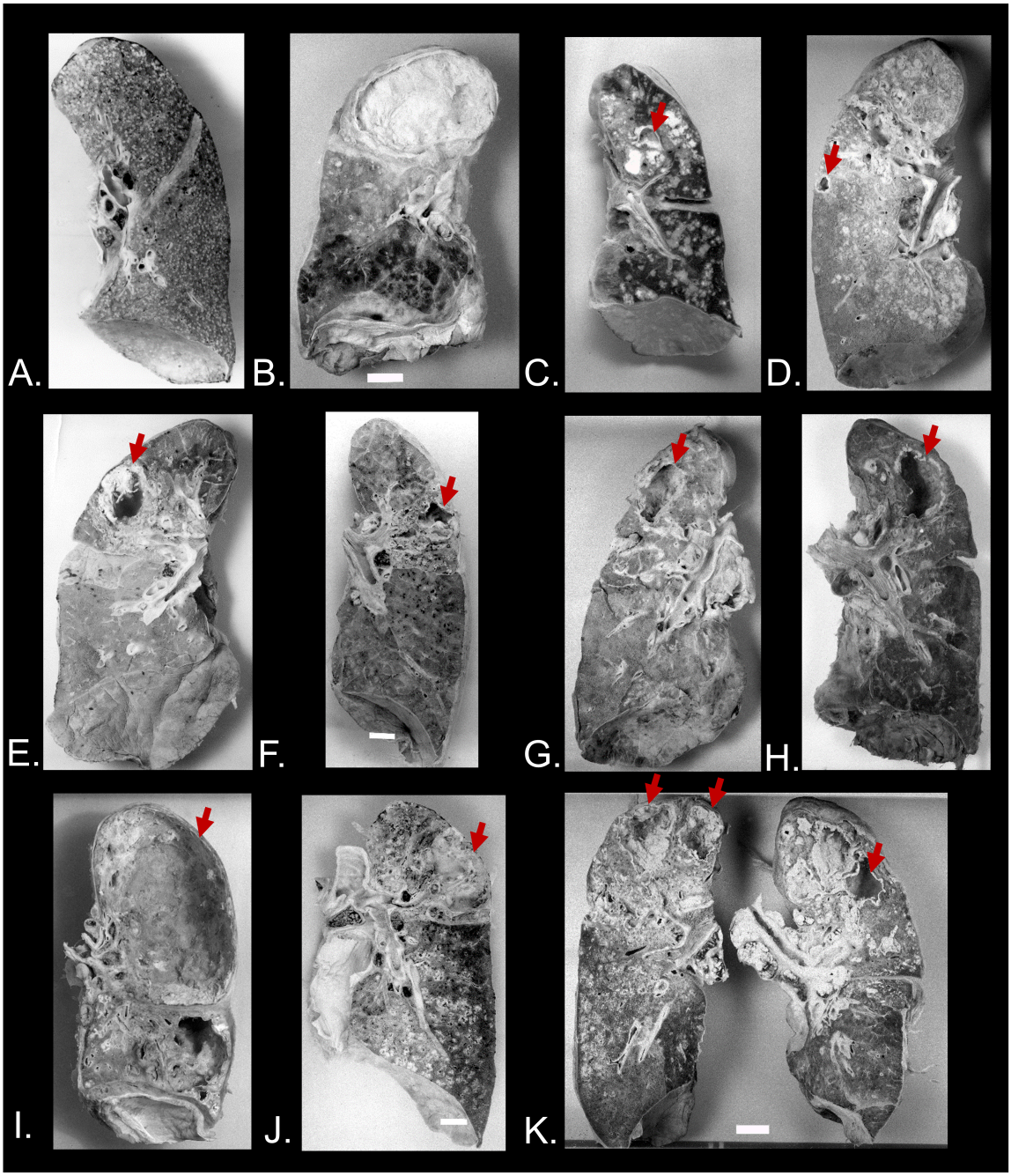

Figure I.1: Examples of tuberculosis lung pathology and cavities at autopsy. (A) The miliary pattern of tuberculosis in the lung. No cavities are present. (B) An example of a massive caseous tubercle in the lung. (C-K) Examples of tuberculosis cavities. Red arrows indicate cavities. (C-D) Two examples of cavities with nodular type morphology. The bright white regions in C are caseum. (E-H) Examples of intermediate size cavities, often within the apical lobe of the lung. (I-K) Examples of large apical cavities showing abscess-like morphology. In I the entire apical lobe has eroded. All images were obtained from the Johns Hopkins University Chesney Medical Archives and correspond to autopsy cases between 1920 and 1950. All images were collected from the Archives under IRB approval and used with permission.

Radiologic patterns of tuberculosis cavities

Radiologically, cavities are described by their size, shape, and wall thickness. Size is often correlated with the extent of disease[3]. Estimates for the average cavity size in adults with tuberculosis vary between 3 and 10 cm[4]. Small cavities can have diameters as small as 0.5 mm and demonstrate nodular morphology while large cavities fill entire lung lobes. The morphology of large cavities is often more complicated, consisting of multiple connected semi-cavernous air spaces embedded in a large area of consolidation and often in-association with smaller cavities eroded from the same dense abscess-like area[5]. It is likely that large cavities arise from the joining of multiple smaller cavitary foci within the same disease focus. Likewise, wall-thickness and shape may have diagnostic and prognostic value[6–8]. Thin-walled cavities often have well-defined inner and outer boundaries and small thin-walled cavities appear to arise from discrete nodules. Thick-walled cavities demonstrate a high potential for cavity growth and dynamic behavior, so eroding thick-walled cavities may be the precursors of larger thin-walled cavities as more caseum sloughs from the cavity wall.

Most large cavities occur in the lung apices while small nodular cavitites can occur throughout the lungs[2]. Importantly, the spatial pattern of pulmonary cavitation is similar to the spatial pattern of lung consolidation in tuberculosis. The mechanistic drivers of apically-oriented disease are still debated, but most studies agree that antigen-experienced immunocompetent individuals with active disease are at the greatest risk for extensive apical lung disease and cavitation[9]. At least two factors contribute to this pattern. First, an intact immune system likely drives extensive cavitation. Immunocompromised individuals, such as those with AIDS, are less likely to have lung cavities, but when cavitation does occur, the cavities are distributed throughout the lungs and more likely to have a small nodular appearance. Second, virulence factors associating with the mycobacterial pathogen also contribute

to cavitation. Individuals with pulmonary non-tuberculosis mycobacterial infections are also less likely to undergo extensive cavitation at the lung-apices and more likely to have distributed small nodular cavities[7].

The histologic architecture of tuberculosis cavities

The prototypical tuberculosis cavity wall contains three histologic regions.

1. **GP_A**: At the boundary between normal-appearing lung tissue and the cavity-wall begins a region of granulocytic pneumonia where the underlying alveoli and lung-tissue remains intact (GP_A), though filled with inflammatory cells. These inflammatory cells consist of activated macrophages, clusters of lymphocytes, and sporadic neutrophils among the resident pneumocytes, bronchial epithelial cells, and vascular endothelial cells already present in the lung.

2. **GP_E**: Moving towards the interior surface of the cavity-wall, is a region of granulocytic pneumonia where the alveolar structure is effaced (GP_E). This region also contains activated macrophages and occasional neutrophils. Lymphocytes are clustered sporadically, but fibroblasts are present and participate in pathologic collagen remodeling. This remodeling is visible with appropriate histologic stains as a fibrotic rim of varying density and thickness. Greater amounts of fibrosis are associated with older lesions. The GP_E contains sporadic multinucleated giant cells. The density of multinucleated giant cells is variable between lesions. Finally, the GP_E also contain regions of lipid-laden foamy macrophages. In some lesions, foamy macrophages concentrate along the inner boundary of the GP_E in a region of cell death. At this inner boundary, cells can be found with necrotic cell fragments. Intracellular acid-fast mycobac-

Example CT scan reconstructions of tuberculosis cavities

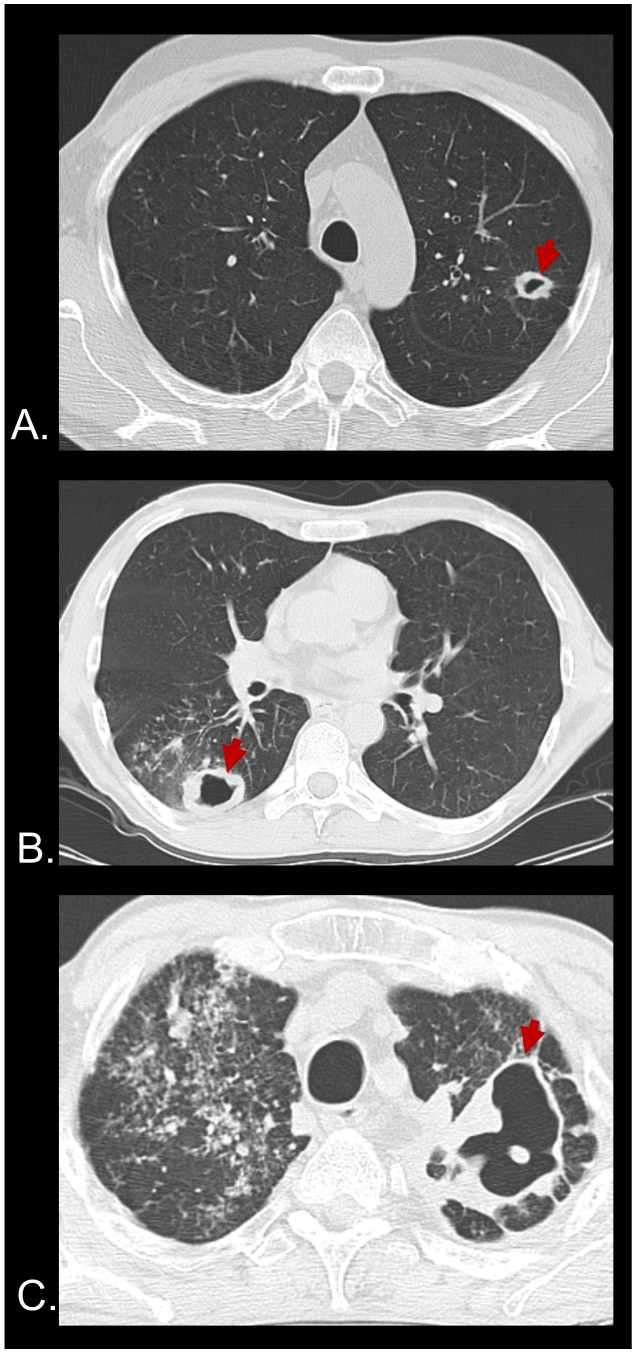

Figure I.2: Examples CT scan reconstructions of tuberculosis cavities. (A-C) All reconstructions are rendered in the transverse plane. Red-arrows indicate the cavity wall. (A) An example of a cavity showing nodular type morphology. (B) An example of an intermediate size cavity with thick walls. (C) An example a large abscess like apical cavity of the lung. All images were obtained from the NIAID TB Portals Program Website licensed as part of the Public Domain[10].

terial bacilli are found sporadically throughout the GP_E and their concentration is variable between intra-lesion regions and between different lesions.

3. **NL**: Along the interior surface of the cavity-wall is a layer of necrotic cellular debris (NL). The border between the GP_E and the NL is abrupt and marked by extensive cell necrosis. Extracellular fibrotic filaments are also rapidly depleted at the border between the GP_E and the NL leaving the NL devoid of extracellular matrix. The NL typically contains high concentrations of extracellular mycobacteria.

The clinical importance and epidemiology of tuberculosis cavities

Lung cavitation is a pathologic hallmark of post-primary tuberculosis, but it is hard to report the prevalence of cavitation among individuals with active tuberculosis since the actual prevalence depends heavily on the identity of the survey population. Some estimates show discordance between 10% and 50%[4,11]. Factors such as immune status[12], severity of disease, age, and screening modality all influence the risk of cavitation. In chapter 1 of this manuscript, we describe a study of 3000 tuberculosis autopsy records from the years between 1920 and 1950. Our study shows that the prevalence of cavitation among cases of active tuberculosis (where tuberculosis was clinically assessed as the cause of death) was 15%. Therefore, the fraction of individuals with cavities over all cases of active tuberculosis is relatively small.

Not all individuals with active tuberculosis show the same potential to transmit tuberculosis. In their historic experiment using guinea-pigs to "catch" transmission events from a specially ventilated tuberculosis ward, Riley *et al.*, noted that two of 62 patients involved in their study were responsible for the vast-majority of transmission

events[13]. These results suggest the existence of tuberculosis super-spreaders even among cases of active tuberculosis. Cavitation is a likely cause of the super-spreader phenotype, a hypothesis that is physically plausible since cavities allow the pulmonary airways to be continuous with high concentrations of bacteria along the inner edge of a cavity[14]. Moreover, tuberculosis cavities are associated with higher bacillary load in sputum[1] and the degree of sputum bacillary load is correlated with transmission[15]. Finally, Bailey *et al.* interviewed 292 cases of newly diagnosed tuberculosis and compared the interview results to the frequency of tuberculin-skin-test conversion among close contacts of the 292 cases[16]. The research team identified tuberculosis cavitation as the strongest factor associating with high rates of tuberculin-skin-test conversion among contacts. Therefore, it is likely that cavitation is the major driver of tuberculosis transmission.

In addition to driving transmission, several additional characteristics of cavities have clinical importance and make cavitary tuberculosis harder to treat.

1. **High concentrations of extracellular bacteria grow in the loose necrotic debris at the interior surface of the cavity[14,17].** In histologic studies, microscopic identification of acid-fast bacilli is insensitive due to the scarcity of bacilli in tubercles of granulomatous pneumonia. However, the necrotic debris along the inner walls of tuberculosis cavities often show a high concentration of bacilli. These bacilli are poised to slough off of the cavity wall and coughed out of the lungs.

2. **Genetic variability and drug resistance arise from the bacterial population bloom within the cavity.** Kaplan *et al.* investigated the genetic diversity of *M. tb* bacilli isolated from the lungs of patients with tuberculosis and found that the cavity surface was the site of the greatest bacterial proliferation and genetic diversification[18]. Describing Kaplan *et al.*'s work and others,

Yoder *et al.* reviewed the rates of drug-specific resistance patterns and compared these rates to the size of the bacterial population within cavitites[19]. The authors highlight that the tremendous increase in population size at the interior surface of the cavity meant that drug-specific resistance was likely to emerge within the cavity.

3. **Anti-mycobacterial drug penetration to the necrotic debris at the inner surface of the cavity is greatly reduced[20].** The wall of the cavity reduces penetration of chemotherapeutic drugs to the sites of high bacillary concentration within the necrotic debris. Factors such as reduced vascularity within the GP_E[21] and the non-specific binding properties of necrotic debris[22,23] contribute to suboptimal drug delivery. Finally, suboptimal drug concentrations within the cavity may provide a selective pressure that enriches for drug-resistant isolates.

4. **The interior layer of necrotic debris inside the cavity is protected from the immune system.** Host cells generally do not live within the necrotic layer of the cavity wall. Therefore, the regions of the cavity with the highest rates of bacterial replication coincides with an immune-sheltered zone.

5. **Healing processes are unable to regenerate the lung matrix destroyed during cavitation.** The extracellular matrix and basement membrane of the lung are destroyed during the pathogenesis of cavities. The healing response to lung matrix insult is pathologic fibrosis which does not support regrowth of the complex three dimensional architecture of the lung. Therefore, cavities often persist even after they are sterilized of mycobacteria or are replaced with scar tissue. Therefore, cavitation can lead loss of lung volume and chronic pulmonary deficits[24].

6. **Cavities that persist following curative therapy are at risk for sec-**

ondary colonization by opportunistic infections. If a cavity persists following curative therapy, the inner cavity wall remains an immune-sheltered site. Furthermore, fibrosis within the wall effaced the alveolar and bronchiolar architecture that normally supports innate immune defenses against inhaled opportunistic pathogens. The combination of high humidity, immune-sheltering, and lack of innate-defenses provide an opportunity for secondary colonization, often by species of *Aspergillus*[25].

Experimental models of tuberculosis cavitation

Modeling tuberculosis cavities for experimental studies and pre-clinical studies is difficult. Cavities are the consequence of chronic granulomatous inflammation and even among individuals with active tuberculosis, the frequency of cavitation is less than 50%. Dannenberg *et al.* summarized the animal models that develop cavities after experimental infection. As of 2006, these were limited to non-human primates and rabbits[26,27]. Importantly, the common mouse and guinea pig models do not, or rarely, develop cavities. The models of cavitary tuberculosis were reviewed by Helke *et al.* in 2006[28]. However, it has now been more than 10 years since this last comprehensive review and important advances in modeling cavities have been contributed by many investigators. In this section we describe a few of the characteristics and recent advances in modeling tuberculosis cavities.

Non-human primate models

Because of their genomic, physiological and immunological similarities with humans, non-human primates are a very valuable model for multiple infectious diseases, includ-

ing tuberculosis. Since the 1950s, non-human primates have been used to evaluate tuberculosis pathogenesis and have provided significant advances in the field[29–33]. Multiple *M. tb* strains (Erdman, H37Rv, 5159 and CDC1551) at different inoculum doses and infection routes (intratracheal instillation or aerosol delivery) have been evaluated in non-human primates[32,33]. Initial experiments performed between 1955 and 1975 included thousands of rhesus macaques and describe pathological findings, evaluate possible vaccines, and study the response to anti-tuberculosis therapies[34]. However, most research published during these decades did not describe cavitary lesions specifically, instead reporting them combined with other necrotic lesions[29,35–37]. More recently, cynomolgus macaques have been used as a model for tuberculosis, characterized by a lower progression to active disease compared to rhesus macaques[38,39]. After infection at low doses (approximately 25 CFU via bronchoscopic instillation), cynomolgus macaques develop active disease, latent infection or subclinical disease, thereby representing the spectrum of human *M. tb* infection[40–42]. In this model, cavitary lesions have been identified in approximately 15% of the infected animals[41,43]. The typical histopathological findings associated with cavitation include necrotic debris admixed with inflammatory cells ulcerating and expanding bronchial airways, eventually leading to cavities[42]. Capuano *et al.* reported the infection of 17 cynomolgus macaques with a low dose of *M. tb*, with two monkeys developing cavities by week 32-34 post-infection. At necropsy, large cavitary lesions were observed in the cranial (apical in humans) lobes with infiltration into airways[41].

Another non-human primate evaluated as a tuberculosis model of cavitation is the marmoset, which has significant advantages such as smaller size, propensity to bear dizygotic twins, ease of husbandry, availability of immunologic reagents and use as an accepted toxicology model[44,45]. Using common marmosets, Via *et al.* evaluated the lung pathology after infection with three strains of the *M. tb*-complex[46]. At necropsy, all of the animals showed evidence of pulmonary lesions consistent with

active tuberculosis. Half of the marmosets infected with *M. tb* CDC 1551 developed cavities after aerosol infection, but the animals infected with *M. tb* K04 (Beijing subfamily) or *M. africanum* strain N0091 had primarily invasive granulomatous pneumonia, more extra-pulmonary disease but no cavitation. Intratracheal infection with *M. tb* Erdman also resulted in extensive disease. Lung lesions in the animals infected with *M. tb* CDC 1551 had more defined margins, with peripheral fibrosis, less loose histiocytic infiltration, and lower bacterial loads in apparently normal lung, suggesting partial immunological containment[46]. A subsequent study showed that marmosets infected with *M. tb* CDC 1551 and treated with a standard four-drug combination (isoniazid, rifampin, pyrazinamide, and ethambutol) resolve disease faster compared to marmosets treated with isoniazid and streptomycin, measured by ^{18}F-FDG PET/CT[47]. While at the start of treatment (6 weeks post-infection), cavitary lesions were only evident in the CT of 1 out of 22 animals, 6 weeks after treatment, 11 (50%) marmosets had cavitary lesions. The bacterial burden of the cavities was significantly different between treatment groups. Based on these experiments, Cadena *et al.* evaluated a low bacterial burden model and bronchoscopically infected common marmosets with the more virulent *M. tb* Erdman strain or the less virulent CDC 1551 strain at low doses (1-7 CFU), following the disease progression with ^{18}F-FDG PET/CT[48]. The Erdman-infected animals had significant disease 4 weeks post-infection, while the marmosets infected with CDC 1551 had a slower progression with 1 of the 2 animals developing multiple cavitary lesions.

Rabbit models

Rabbits have been used as tools and models in the study of tuberculosis for over 100 years. Importantly, rabbits infected by aerosolized *M. tb* develop a spectrum of lesions similar to human disease, including cavities. Therefore, the rabbit model

is advantageous in investigations where the composition, structure, and spatial relationship between lesions are important for the hypothesis being tested. Rabbit lungs are also much larger than guinea-pig or mouse lungs, allowing investigators to collect and compare tissue from spatially distinct regions of infected lungs. Finally, rabbits are significantly cheaper and more efficient to house and maintain compared to non-human primates and the use of rabbits instead of non-human primates for mutually appropriate applications is consistent with the Three Rs of animal welfare in research.

The use of rabbits for tuberculosis research has two major disadvantages in contemporary studies. First, The paucity of rabbit-specific immunological reagents has limited the study of infection and immunity in rabbits. Second, rabbits are relatively outbred compared with murine models. Therefore, the rabbit response to *M. tb* infection is heterogenous and some rabbits develop a progressive syndrome while others successfully control the infection.

The most advanced experimental studies on the mechanism of cavitation have been conducted in rabbits. Here we briefly review the major advancements in rabbit models of tuberculosis cavitation during the past century.

1. **A robust immune response to mycobacterial antigen increases the likelihood of cavitation:** Lurie used rabbits extensively for his work on the pathogenesis and immune protection from *M. tb* infection[49]. The seminal mechanistic investigations on the cavity-inducing elements of the mycobacterial cell wall were conducted by Yamamura in rabbits during the 1950-80s[50–53]. Independently, Yamamura and Lurie both concluded that a robust immune response was necessary for cavity formation.

2. **Careful determination of the frequency of cavitation following aerosol infection:** In 1996, Converse *et al.* quantified cavitation in rabbits following

aerosol challenges of varying concentration and reported that approximately half of the rabbits had cavities following inhalation of 200-800 bacilli[54].

3. **The innovation of the bronchoscope-targeted instillation model:** Finally, Nedeltchev *et al.* provided an additional innovation of the rabbit model by generating cavities using bronchoscopic instillation of high-burden inoculum[55]. Nedeltchev's protocol used pre-sensitization of rabbits by intra-dermal injections of heat-killed *Mycobacterium bovis* to sensitize the immune system to mycobacterial antigen. The use of "sensitization" to drive cavitation was based on observations by Lurie and Yamamura, and the experiences of Dannenberg. The bronchoscope-target model was further refined and characterized by Kübler[56].

Based on the work by Dannenberg, Converse, Nedeltchev and Kübler, current rabbit models of cavitation fall into two groups. Each model has important but distinct characteristics for advancing research on tuberculosis cavitation.

1. **Cavitation by bronchoscope targeted instillation:** This model generates a single large necrotic focus reminiscent of abscess-like cavitation observed in cases of extensive lung disease. Cavitation often occurs after 1-month following inoculation, a much-shorter time-course than was reported by Wells and Lurie[57] following aerosol-delivered infection, but consistent with Yamamuras experiments which used trans-thoracic injection of cell-wall components to cause cavitation[50]. Therefore, this model is probably inappropriate for studies on the natural pathogenesis of cavities due to the artificial nature of the high-dose intra-bronchial inoculation. However, we highlight the strengths of this model for studies in lung-destruction and drug penetration into the caseum of cavity walls.

2. **Cavitation by aerosol exposure:** Cavitation by aerosol exposure is a better model for the natural pathogenesis of tuberculosis cavities. Rates of cavitation are historically variable between rabbits and between investigators. In our experience, 15-25% of rabbits receiving a day-1 implantation of approximately 2,500 CFU of *M. tb* (H37Rv) cavitate by week-10 following exposure. These rates are similar to the rates observed in humans with active tuberculosis. The typical cavity morphology is also different from cavities generated by bronchoscope targeted instillation and resembles tuberculosis cavities with nodular morphology.

In Chapter 2 of this manuscript we report a novel variation on the aerosol exposure model based on repeated aerosol exposure. In light of the work conducted by Dannenberg, Nedeltchev and Kübler on immune priming and cavitation, we wondered whether repetitive aerosol infection generated a different pattern of disease from a single aerosol infection, even when the total bacillary exposure was the same between groups. We found that repetitive aerosol exposure exacerbated both disease and cavitation. This insight may have important ramifications for epidemiological modeling of disease in high-incidence areas since cavitation is known to be a major driver of disease transmission. Moreover, we characterized the rabbit response to repetitive aerosol infection and showed that rabbits often developed multiple cavities per lung. Therefore, a repetitive aerosol exposure protocol may be most appropriate and efficient for pre-clinical studies investigating treatments to inhibit cavitation.

Mouse models

Mouse models of tuberculosis have been used for more than 50 years for understanding pathogenesis and the development and evaluation of new tuberculosis drugs and regimens[58]. The model is simple, inexpensive, tractable, and has the highest pre-

dictive value for clinical efficacy of combination regimens of any preclinical model[59]. Every drug regimen tested clinically for tuberculosis treatment in the 21st century has been tested first in the mouse model[60]. Until recently, mice had been overlooked as models of cavitary TB because commonly used mouse strains do not exhibit caseous pathology after infection with *M. tb*. However, recent development of the C3HeB/FeJ mouse model of cavitary tuberculosis provides a new model for studying cavities in an animal model.

The susceptibility of C3HeB/FeJ mice to *M. tb* infection is determined primarily at the *sst1* locus, which regulates the macrophage innate immune response to infection with intracellular pathogens[61,62]. Interestingly, C3HeB/FeJ mice are not deficient in the activation of T_h1 cytokine-producing T-cells or their migration to the lungs[63], macrophages in these mice have a reduced ability to control multiplication of *M. tb*, with these cells preferentially undergoing cell necrosis rather than apoptosis, associated with activation of the type-I interferon pathway and an exaggerated host inflammatory response[61,64]. After infection with *M. tb*, C3HeB/FeJ mice develop caseous lung lesions[61], which are also known to be hypoxic[65,66], and to undergo calcification similar to human TB[67]. Initial reports of occasional cavitation in C3HeB/FeJ mice[66–68] led to further investigation of their potential as a cavitary TB model. By using serial CT imaging, Ordonez *et al.* characterized pulmonary cavitation in C3HeB/FeJ mice after aerosol infection with two *M. tb* strains[69]. Cavities were observed in 47-61% of C3HeB/FeJ mice and the cavitation rate after *M. tb* HN878 (East Asian lineage) infection (40%) was similar to that observed with *M. tb* H37Rv (Euro-American lineage) (47%), although mice infected with HN878 were more likely to require euthanasia prior to the first imaging time point. The cavities observed shared features of human tuberculosis such as air-filled lesions with caseous debris in various stages of liquefaction and mixed inflammatory cells lining the cavity wall surrounded by encircling fibrosis. Unlike prior observations in rabbits, sensitiza-

tion with heat-killed bacilli prior to infection with *M. tb* HN878 (Beijing subfamily) was protective in C3HeB/FeJ mice, leading to increased survival, lower pulmonary bacterial burdens, and lower rates of cavitation during progressive disease and relapse compared to un-sensitized animals. After treating the same mouse model with non-curative combination chemotherapy, 11 of 18 (61%) mice developed cavities and were significantly healthier than those that developed cavities in the context of untreated infection, highlighting the potential for a chronic cavitary TB model[69].

Similar to tuberculosis, where multiple lesion types may occur simultaneously in lungs of patients with active disease[58,70,71], lesions in various stages of development with multiple different pathologies (pneumonia, necrosis and cavitation) have been observed in C3HeB/FeJ mice, thus modeling lesion-specific progression of pathology described in humans and NHPs[14,69,72]. These multiple lesion types provide an advantage in the evaluation of tuberculosis drugs which are known to partition differently into these lesions based on observations made in humans, mice and/or rabbits[20,73–76]. Multinucleated giant cells and cholesterol crystals, characteristic of human tuberculosis lesions[71], have also been observed in the C3HeB/FeJ model[69].

The pathogenesis of tuberculosis cavities

The pre-cavity tuberculosis lesions

There is no consensus histologic origin of tuberculosis cavities. Observational studies in tuberculosis patients are difficult since radiologic modalities are unable to reveal the biochemical composition of water-dense regions and because tissue samples are typically collected at a single time-point. However, defining the step wise pattern

of histologic events leading to cavitation is critical since these steps are translational targets for the prevention of extensive lung destruction and disease transmission.

As discussed above, radiologic observations support the conclusion that tuberculosis cavities arise from pre-existing dense lung areas. In addition to cavities, granulomas are well described in tuberculosis lung pathology and tuberculosis granulomas can be further attributed varying degrees of many different histologic characteristics including lymphocytic infiltration, lipoid character, fibrosis, central necrosis and liquefaction. Granulomas also appear in many different sizes from purely microscopic lesions to grossly visible lesions that are the characteristic tubercular nodules of a granulocytic pneumonia. In cases of more extensive lung disease, a large area of immune infiltrate, found often at the apices of the lungs, can consume an entire lobe and appear more similar to an abscess than a nodule. The pathogenic origins of these abscess-like regions in tuberculosis are still debated, so it is possible that these abscess-like areas are not simply large granulomas or the coalescence of multiple granulomas. For instance, Hunter proposes that morbidity in post-primary tuberculosis arises from an obstructive lobular pneumonia rather than the enlargement of microscopic granulomas[71].

Only a fraction of radiographic dense foci undergo cavitation so specific chemical and physical processes enable cavitation. One clue supporting the specificity of these processes comes from experiments by Luna *et al.*, who used serial CT scans in a rabbit model of tuberculosis cavitation and found that small increases in the central density of some tubercle lesions anticipated the development of cavities[77]. Complementing these studies, histologic observations in rabbit models show that the walls of cavities and necrotic granulomas are identical and that a cavitary focus is derived from a necrotic granuloma that underwent removal of its central necrotic debris. These studies also describe two specific histologic pre-cavity changes: extensive

central necrosis and extracellular matrix depletion. It is possible that these two histologic changes are responsible for the increase in density of pre-cavity lesions reported by Luna *et al.*

Evidence of necrosis can be observed sporadically through the GP_E region of the cavity wall but the interface between the GP_E region and the NL region is a boundary of complete cell death that renders the contents of the NL region devoid of live host cells. The mass of necrotic fragments in the NL region is described as caseous necrosis because of its cheese-like consistency. One common misconception is that liquefactive necrosis or liquefaction, a type of necrosis often observed in nervous tissue, is necessary for the formation of a cavity. Some necrotic granulomas may adopt the histologic identity of liquefactive necrosis, but observations in rabbits and mice, where caseous necrotic debris is observed in the airways of cavitating necrotic granulomas, show that liquefaction is not necessary for cavitation.

Depletion of the extracellular matrix in the lung also appears to be necessary for cavitation. The robust extracellular matrix of the lung is the basis for the mechanical compliance and elasticity that resists force induced trauma. In cavities and necrotic granulomas, pathologic matrix remodeling occurs throughout the GP_E region beginning with the effacement of the alveolar architecture and subsequent replacement with fibrotic matrix. At the boundary between the GP_E and the NL region, a second and more dramatic depletion of extracellular fibrils is tightly coupled with the boundary of extensive necrosis. The relative importance of matrix remodeling in the GP_E and its contributions to cavitation is unknown, but the importance of matrix depletion at the GP_E-NL boundary is paramount. Complete loss of extracellular matrix causes irreversible damage to the lung. In the absence of an extracellular scaffold, caseous necrotic debris can be evacuated with little mechanical resistance during the formation of a cavity.

The biochemical drivers of cavitation

The identity of the biochemical mediators of tissue destruction in tuberculosis remains one of the greatest unresolved drivers of cavitation. If the primary mediators of tuberculosis tissue destruction in necrotic granulomas are resolved then specific pharmacological intervention provides an opportunity to prevent cavitation without interfering with the beneficial aspects of the immune response[78].

The epicenter of tissue destruction, the boundary of complete necrosis and matrix-destruction between the GP_E and the NL, is pathologically striking and caught the attention of Dannenberg, Weiss, and colleagues in the 1960s. Dannenberg's laboratory performed experiments with *ex vivo* lung tissue from rabbits modeling tuberculosis lesions and showed that the necrotic debris within these lesions contained factors capable of hydrolyzing proteins, DNA and RNA[79–82]. Dannenberg also identified the lysosome-resident protein cathepsin D as a possible mediator of extensive tissue destruction[83,84].

In the 2000s, Friedland, Elkington and others showed renewed interest in the mediators of tissue destruction in tuberculosis[85,86]. Their hypothesis stated a specific role for extracellular matrix destruction in the pathogenesis of cavities and proposed host-expressed extracellular collagenases as the primary mediators of extracellular matrix degradation. This hypothesis was supported by transcriptomic data from tuberculosis patients showing increased expression of matrix metwalloproteinases (MMPs) in tuberculosis lungs[87–89]. These results were further corroborated by experiments in model systems. Volkman *et al.*, determined that the zebrafish homologue of human MMP-9 showed increased expression following infection with *Mycobacterium marinum*[90]. Kübler and colleagues performed an RNAseq analysis on tissue obtained from rabbits modeling tuberculosis pathology and found that tran-

scripts from members of the MMP and cysteine cathepsin families of extracellular proteases, specifically MMP-1, 12, 13 and cathepsin K, were enriched in the walls of cavities[56,91,92]. Finally, Ordonez *et al.* used optical imaging to localize mouse MMP-9 to sites of lung destruction in C3HeB/FeJ mice[69].

The MMP and cysteine cathepsin proteases are multi-membered conserved protein families with convergent roles in tissue remodeling. The MMPs are a group of 23 extracellular metallopeptidases that require zinc binding at their conserved catalytic sites for activity[93]. Likewise, the cysteine cathepsins contain 11 members which can be active in both lysosomal and extracellular environments[94]. Importantly, the MMPs and cysteine cathepsins share important properties that support a role in tuberculosis lung pathology. First, their expression is highly controlled by the initial translation of proenzyme forms requiring activation[93,95], by optimal activity in the extracellular environment, and by vulnerability to expressed inhibitory factors[94,96]. Second, members of the MMPs and cysteine cathepsin peptidase families have substrate specificity for elements of the lung extracellular matrix including collagen and elastin[97–100] . Finally, many of the transcriptional pathways that regulate MMP and cathepsin expression are downstream of immune-system receptors, suggesting that the expression of these proteases can be regulated in response to changes in the local inflammatory response[101–104].

Significant work is still necessary to clarify the role of extracellular proteases in tuberculosis pathology. First, the primary mediator or mediators of matrix destruction must be identified. Encouragingly, Rojas-Espinosa *et al.*, Kübler *et al.*, and Volkman *et al.*, all separately identified members of the MMP and cysteine cathepsin protease families as likely mediators of tissue destruction, defining important targets for future investigations[84,90,91]. Second, the consequences of matrix remodeling in the GP_E must be weighed against matrix depletion at the GP_E-NL boundary. It is

possible that irreversible tissue damage occurs well in-advance of matrix depletion but under the guise of pathologic fibrosis. Finally, a major challenge for researchers will be to discern whether the action of extracellular proteases can be uncoupled from the spatially co-incidental necrosis front. Matrix breakdown may be an accidental, though dangerous, consequence of the robust cell death that occurs at the GP_E-NL boundary, whereby dying cells release a milieu of normally sequestered proteolytic factors into the extracellular environment.

The biophysical drivers of cavitation

Although matrix destruction and caseous necrosis are necessary for cavitation, they are not sufficient. In radiology studies, numerous dense inflammatory foci appear but do not cavitate. Furthermore, in tissue sections from human and modeled tuberculosis lungs, large caseous, but not cavitary lesions are also common. Therefore, it is likely that factors other than biochemical mediators also help determine the likelihood that a caseous lesion becomes a cavity. Here, we review the biophysical factors that likely play a role in cavitation.

One possible determinate is proximity to an airway. In this explanation, caseous tubercles that do not breach an airway fail to cavitate because they cannot evacuate their caseous contents into the bronchial tree. This hypothesis predicts that larger lesions are at a greater risk of cavitation since they are more likely to connect to an airway but does not explain why large caseous foci often exist but do not cavitate. To explore this heterogeneity, Nagasawa *et al.*, undertook a series of autopsy studies in which the investigators created plastic casts of cavities and their draining bronchi[105]. Their work found a relationship between cavity-size and total bronchial drainage. An absolute minimum diameter of 0.3 cm was necessary for the

drainage of small cavitites, but larger cavities were drained by multiple, often larger, bronchi. Based on these observations, it is likely that some caseous foci enlarge but do not cavitate because they do not encounter bronchi that match the relative size necessary for cavitation.

Pressure may be another driver of cavitation. Working in separate models, Ihms and Urbanowski (unpublished) in rabbits and Ordinez *et al.*, in C3H3B/FeJ mice, noticed that small newly formed cavities often had a smooth surface at the interface between the necrotic debris and the cavity space, reminiscent of a gas bubble[69]. These findings were corroborated by studies on cavity morphology in tuberculosis patients[106]. We propose that these observations are best explained by a check-valve mechanism where small amounts of caseum initially block the draining bronchus. Inspiration creates negative pressure within a micro-cavity that allows small amounts of air to pass the check-valve. Relaxation of the respiratory muscles traps air in a positive-pressure bubble within the micro-cavity. During subsequent inspirations it is energetically favorable to reduce the negative pressure within the micro-cavity by evacuating more caseum to enlarge the cavity. This hypothesis also explains the dynamic wall thickness of thick-walled cavities which varies as caseum drains through the bronchus.

A positive-pressure model may explain the earliest cavitation events, but several observations argue against it as the penultimate model for cavity growth. First, many tuberculosis cavities, in humans and models, do not have a gas-bubble like appearance. Moreover, many large cavities have open connections between the cavity-space and the draining bronchus. Therefore, the mechanism of large-cavity growth is also unknown and requires further investigation. Ihms and Urbanowski *et al.*, undertook a study of cavity dynamics in a rabbit aerosol model of cavitation (unpublished) and concluded that the pull of lung tissue at the periphery of the cavity wall likely

aides during cavity formation and growth. Finally, it is also possible that a continuous cycle of matrix breakdown, necrosis, and caseum expulsion within the cavity wall leads to cavity enlargement.

We are unaware of any recent studies that attempt to describe cavities in a physical model, but we propose this as an important area of research. A biophysical model of tuberculosis cavities would allow researchers to integrate tissue-level biochemical changes as physical constants that contribute to cavity formation and enlargement. This approach will also require a collaborative team of biophysicists and experimental biologists.

Microbial drivers of cavitation

A cavity is not pathognomonic for *M. tb* infection and numerous bacterial and fungal pathogens are associated with cavitation. However, *M. tb* does cause the highest rate of cavitation among infectious pathogens. One possible explanation for this is that *M. tb*'s success in aerosol transmission is directly tied to its ability to become aerosolized via the bronchial-cavity space. In this perspective, *M. tb* evolved to cause a pathologic inversion of anatomical topology where the internal space of the granuloma becomes continuous with the air in the environment.

If *M. tb* evolved to cause cavities, then specific virulence factors of the *M. tb* bacillus must drive cavitation. Yamamura and colleagues investigated the cavity-inducing properties of purified components of the mycobacterial cell wall. In their experiments, the investigators noted that cavities could be caused by trans-thoracic injection of milligram quantities *M. tb* cell wall lysates directly into the lungs of rabbits[50]. To identify the cavity-causing elements of *M. tb*, they purified the protein fraction from the lipid fraction of the *M. tb* cell wall. Next, the investigators injected

these fractions into the lungs of rabbits. Yamamura *et al.*, found that if injected alone, both the protein and lipid fractions caused granulomas, but when injected together were they able to reconstitute the cavity-causing effect of *M. tb* lysates.

Yamamura *et al.*, also injected lysates from BCG, an attenuated laboratory strain derived from *Mycobacterium bovis*, and *Nocardia rubra* (a bacterial species in the same order as mycobacteria) and found that these injections were able to cause granulomas[51]. When injections with these lysates were complemented with the *M. tb* protein fraction, then cavity formation occurred. These observations suggest that some protein factor, not present in BCG or *Nocardia rubra*, is an inducer of cavitation in *M. tb* infection. Therefore, immunogenic proteins including ESAT6 and CFP10, encoded by genes of the RD-1 locus of virulent *M. tb*, but lost from the BGC genome, are obvious candidates[107].

Finally, Yamamura and colleagues also studied the cavity-inducing properties of the lipid fraction of the *M. tb* bacillus[52]. Trehalose dimycolate is the most prevalent glycolipid found in the *M. tb* cell wall and Yamamura *et al.*, found that trans-thoracic lung co-injection of trehalose dimycolate and the *M. tb* protein-fraction in a mixture was able to cause cavities. Elegantly, Yamamura resolved the minimally effective structure for cavity induction by substituting trehalose dimycolate with synthetic fatty-acids. Only synthetic species with long branched-chain fatty acids were able to substitute for trehalose dimycolate to cause cavities.

Taken together, Yamamura and colleagues showed that the molecular composition of the *M. tb* cell wall contains lipid and protein factors that confer cavity-causing specificity to virulent *M. tb* strains. However, Yamamura's work did not identify the pathways modulated by these virulence factors. To date, no investigators have reported intrinsic molecules of *M. tb* that are capable of directly mediating tissue destruction. Therefore, in careful consideration of Yamamura's seminal work, we hy-

pothesize that *M. tb* infection leads to a high rate of cavity formation by two complementary pathways. First, the protein fraction leads to the acquisition of cell-mediated immunity and the recruitment of lymphocytes to drive granuloma enlargement. Second, the lipid fraction provides a digestion-resistant substrate that accumulates in the endocytic compartment of phagocytes and acts as a stress-inducing factor for innate immune cells[108]. Necrosis, matrix breakdown, and cavity formation is driven by the summative effects of pro-inflammatory cytokines from recruited lymphocytes acting on lipid-stressed cells. There is also likely overlap between these pathways since ESX1 secreted proteins are known to cause macrophage activation and death while trehalose dimycolate similarly stimulates cytokine secretion and may act to prime T-cell immunity[109]. This model requires further interrogation and validation.

Immunological drivers of cavitation

Strong evidence implicates the adaptive immune response as a major driver of cavitation. HIV patients with low $CD4^+$ counts cavitate less often than patients with intact immune systems[110]. Furthermore, antigens that elicit a T-cell response appear to be highly conserved in virulent strains of *M. tb*[111]. Finally, the $CD4^+$ T_h1 response effectors are strongly tied to tuberculosis control in humans and TB models.

The generation of a T-cell response in tuberculosis is mediated by the activation of antigen-presenting cells that migrate to draining lymph-nodes. Subsequent expansion and homing of reactive T_h1-polarized T-cells to existing granulomas forms the lymphocytic cuff commonly observed around necrotic granulomas and cavities. T-cells at granulomas produce the soluble pro-inflammatory cytokines IL-2, IFN-γ, and TNF-α.

We propose a model in which the adaptive immune response to *M. tb* infection

acts as a pro-inflammatory switch with three effects that drive cavitation.

1. T-cell derived pro-inflammatory cytokines IFN-γ, and TNF-α activate macrophages and neutrophils in an attempt to kill *M. tb* bacilli. Cells near the center of the granuloma experience the highest concentrations of pyogenic cytokines and these signals cause a state of stress on innate immune cells that promotes necrosis at the center of the lesion.

2. T-cells provide signals to recruit and activate circulating monocytes to granulomas. Since vascular elements are intact within the GP_A but not the GP_E regions, inflammatory cells must traverse the GP_E region, homing along pyogenic cytokine gradients, toward the border of the NL. Migrating monocytes secrete matrix-degrading enzymes to allow movement through tissue matrix so the influx of immune cells may be the major driver of tissue matrix weakening and depletion within the GP_E region.

3. The cumulative effects of immune-cell activation and T-cell recruitment increases the oxygen demand of the granuloma and causes a hypoxic environment at the center of the granuloma and this hypoxia, in-turn, drives central necrosis.

Mycobacterial ecology inside the cavity

One of the most intriguing perspectives on cavitation considers the internal surface of the cavity as a unique mycobacterial ecosystem. In 2003, Jacques Grosset reviewed the pathogenesis of tuberculosis and clarified the most dangerous pathologic development: extracellular bacteria at the cavity surface[17]. Corroborating this assertion, Ors *et al.* found that the thickness of the cavity wall in tuberculosis patients correlated

with the degree of smear positivity[3]. Indeed, in both human studies and tuberculosis models, the caseum lining the cavity wall supports mycobacterial blooms with as many as 10^9 bacilli per cavity[14,112]. The caseum of the cavity contrasts with non-cavity lesions where *M. tb* bacilli concentration is heterogeneous and often undetectable[14].

The internal surface of the cavity is the anatomical site with the highest concentration of mycobacteria. Several factors support extensive bacterial replication within the cavity.

1. **The formation of a cavity dissipates anoxia, so oxygen may be the limiting resource for bacterial proliferation within the lung[113].** During *in vitro* studies, the change from an anoxic to oxygen-rich environment increases the doubling time and the concentration of bacteria achieved during the stationary-phase. Similar changes in growth kinetics probably occur within the caseum after a cavity forms.

2. **The caseum inside the cavity is immune-sheltered substrate, so bacterial replication is unchecked by phagocytes and neutrophils.**

3. **The wall of the cavity reduces the penetration of many anti-mycobacterial agents so that suboptimal concentrations chemotherapeutic drugs reach the replicating bacteria in the caseum.**

The superposition of high bacterial concentration with the potential for aerosolization has important clinical implications. In the pre-antibiotic era, surgical lung collapse therapy showed efficacy as a therapy for extensive pulmonary tuberculosis. More recently, Corbetta *et al.* used endobronchal one-way valves to cause regional hypoventilation and saw improvement in cavitary disease[114]. These observations implicate oxygen tension within a tuberculous cavity as a major factor governing the progression of cavity disease.

The cavity also provides an environment for genetic diversification and the acquisition of drug resistance among mycobacteria proliferating in the necrotic debris[115]. Kaplan *et al.* compared the genomes of *M. tb* isolates from lung resections and found that the explosive replication at the cavity wall led to heterogeneity at drug-resistance determining loci[18]. In a clinical setting, the delivery of suboptimal anti-mycobacterial drug doses to the caseum may enrich for drug-resistant mutants.

Many aspects of microbial ecology within the cavity remain unstudied, probably because of the difficulty in modeling tuberculosis cavities and obtaining specimens. However, with the recent advances in modeling cavities, it may now be possible to conduct detailed studies on bacterial physiology and growth state within cavities. For instance, transcriptional and proteomic studies on bacteria in caseum may help resolve conserved metabolic pathways necessary for proliferation in necrotic debris. Bacterial community architecture may also be organized in three dimensions, with a reservoir of progenitor bacteria near the GP_E-NL boundary where they are protected from the constant sloughing of caseum.

Healing of tuberculosis cavities

Destruction of the tissue extracellular matrix, fibrosis, and cavitation all cause irreversible damage to the lung. In autopsy cases from the pre-antibiotic era, the most common incidental finding consistent with healed tuberculosis was apical scarring, suggesting that the destroyed alveolar architecture of the lung is never replaced. Cavities may also persist for years after tuberculosis is cured and can become sites for opportunistic infections. Unfortunately, few treatment options exist for tuberculosis cavities. In this section, we review the small body of literature describing healing reactions and tuberculosis cavities.

Amberson followed 476 patients with cavitary tuberculosis in the pre-antibiotic era and found that only about 5% of cavities larger than 2 cm became radiologically invisible during prolonged observation[116]. In the remaining fraction of patients, about 30% of cavities shrank, and 65% remained the same size or enlarged. These percentages are likely changed following successful cure with antibiotics, since Ross and Kay later found that the majority of persistent tuberculosis cavities continued to have mycobacteria within the wall[117]. Following a series of pathology studies on chronic cavitary disease, Hermel and Gershon-Cohen proposed two mechanisms of cavity healing. In closed healing cavities resolve to scar tissue while in open healing, the wall of a cavity becomes extensively fibrosed and remains as an open structure within the lungs[106]

Significant efforts must still focus on the treatment of cavities. Open-healing of cavities is not ideal because cavities can later host opportunistic infections[118]. One therapeutic goal is to prevent the enlargement of existing cavities. Several treatment strategies are under investigation. First, Corbetta *et al.* explored the use of endobronchial one-way valves to reduce the concentration of oxygen within the cavity. The reduced oxygen concentration likely hinders bacterial growth and prevents further necrosis and matrix breakdown[114]. Another potential strategy is to treat with aerosolized antibiotics to dramatically reduce bacterial burden within the cavity[74]. These treatment paradigms require further investigation.

The ultimate goal of tuberculosis cavity treatment should be to replace the cavity with functional pulmonary tissue. This goal poses significant technical challenges to regenerative medicine since the lung is composed of a complex tree of alveoli, bronchi and blood vessels created in the context of the developing fetus[119].

A Foreword to the Dissertation

A tuberculosis cavity is the epicenter of advanced tuberculosis. Unfortunately, cavities are also one of the least-studied aspects of tuberculosis. In this review we describe the known processes that drive cavitation. The core elements of cavity pathobiology are a perfect storm of host and microbial factors that drive tuberculosis transmission and damage the lungs. We also reviewed recent advances in modeling cavities. Our goal is to provide researchers with a better understanding of the tools available for studying cavities and that these tools will be applied during research efforts to reduce morbidity and mortality in tuberculosis.

In the manuscript that follows, we present studies that advance our understanding of the mechanism and inhibition of cavitation in tuberculosis. Chapter 1 details a retrospective study conducted at the Chesney Medical Archives of the Johns Hopkins University. The study reviews 3,000 autopsies where evidence of tuberculosis was appreciated by pathologists working in the pre-HIV/AIDS era. The goal of this investigation is to describe the pathologic phenotype of extensive lung destruction in tuberculosis. Chapter 2 describes the challenges of modeling extensive lung destruction in tuberculosis and introduces a novel rabbit model for investigating lung destruction and cavitation in tuberculosis. Chapters 3 and 4 focus on identifying the biochemical drivers of cavitation (reviewed above). In chapter 3 we applied the repetitive aerosol rabbit model, characterized in chapter 2, to test the effects of pharmacological inhibition of the collagenase MMPs during cavity formation. In chapter 4 we show evidence for the role of cathepsin K in matrix destruction during tuberculosis.

Chapter 1

The prevalence of cavitation among cases of active tuberculosis

Michael E. Urbanowski · Marjorie Kehoe

"The tragedy is not that things are broken.
The tragedy is that things are not mended"

by Alan Paton.
Cry, The Beloved Country (1948)

1.1 Introduction

Cavitation is a well-described consequence of tuberculosis, but accurate estimates for the prevalence of cavitation among cases of active tuberculosis are rare. The textbook *Tuberculosis* (2004) provides the estimate of between 19 and 50%[4]. In their 2003 study, Gomes *et al.* reported that 36% of 153 patients in a retrospective radiographic study had lung cavities[11]. Differences in the modality used for cavity identification,

the characteristics of the survey population, and the most prevalent strain of *M. tb* in the study population likely contribute to discordance among estimates[120]. For instance, it is well established that low $CD4^+$ cell counts are associated with lower rates of cavitation in cases of HIV/*M. tb* co-infection[110]. Therefore, a study describing a population with high rates of AIDS may find a lower prevalence of cavitary disease than a study describing a population with low rates of AIDS. Alternatively, survey populations taken from inpatients at hospitals may be enriched for cases of severe tuberculosis and therefore more likely to develop cavities.

Despite the difficulty in determining the prevalence of cavitation in tuberculosis, the estimate may be critical for computational models of disease transmission[121]. In their seminal study, Riley *et al.* noticed that only two individuals were responsible for the vast-majority of transmission events on a tuberculosis ward[13]. Riley *et al.*'s study and those of others confirm the epidemiological importance of tuberculosis super-spreaders[122]. Super-spreaders are individuals who are more likely to spread tuberculosis among the larger population with tuberculosis[123]. For tuberculosis, it is estimated that about 20% of cases of active tuberculosis contribute to 80% of transmission events[124].

The pathologic phenotype that enables super-spreaders is likely the presence of a cavity. This is a physically plausible hypothesis since cavitation in tuberculosis causes high concentrations of mycobacteria to be continuous with the external environment via the bronchial tree. Further supporting this hypothesis, Bailey *et al.* developed a predictive model for skin-test conversion among close contacts of newly diagnosed cases of tuberculosis[16]. The investigators found that the probability of skin-test conversion for contacts of individuals with cavitary disease was 0.670, the highest probability of any factor involved in the study. This study is supported by case-studies of tuberculosis super-spreaders with confirmed cavitary disease[125,126].

Therefore, the prevalence of cavitary disease could be used to directly inform computational models about the prevalence of super-spreaders.

This chapter focuses on resolving the prevalence of cavitation among cases of active tuberculosis. To accomplish this goal, we received institutional review board permission from the Johns Hopkins University Chesney Medical Archives to create a database of tuberculosis autopsy cases. This database contains the major pathologic findings associated with 3000 autopsy cases where evidence of tuberculosis was reported between 1920 and 1950. To our knowledge, this is the largest retrospective cohort of tuberculosis autopsy cases where the entire set of non-biased pathologic findings is reported. These years were selected because they correspond to a time period when established terminology was used to describe autopsy findings consistent with tuberculosis but was before the use of antibiotics or the HIV epidemic, both of which are known to change the frequency of cavitation. Therefore, we report on the prevalence of cavitation among individuals with active tuberculosis at autopsy during the pre-antibiotic era.

Our findings reveal the prevalence of lung cavities among cases of active tuberculosis to be 15%. As part of our studies, we also generated a de-identified database of autopsy cases. Each autopsy case in the database is reconstructed with the full set of associated pathologic findings. Finally, we restructured the database using standardized terminology and an imposed inheritance hierarchy schema that enables comparisons between all phenotypes within the database. Our goal is to release this database as a tool to the tuberculosis research community.

1.2 Results

1.2.1 Construction of a database for tuberculosis autopsies.

Autopsies at the Johns Hopkins Hospital between from the years 1920 through 1950 were previously indexed by pathologists. These indexes defined a set of 159 pathologic findings associated with tuberculosis. Each index entry for a pathologic finding listed the autopsy case numbers that demonstrated the finding. The entire index for autopsies between 1920 – 1950 corresponded to approximately 3000 autopsies.

The 159 pathologic findings identified in the indexes were a set of non-standard terminology. This non-standard terminology was discordant for several reasons.

1. Variations on the terms used for pathologic findings were used by different pathologists to describe similar findings. From this dataset, an example of this inconsistency is the use of the term "lung tubercle" and "lung nodule".

2. Some pathologic findings represent compound findings while others represent single findings. From this dataset, an example of this inconsistency is use of the term "lung cavity with tubercles" and "lung tubercles" and "lung cavity."

3. Pathologists used different terms for pathologic findings during different periods of time. From this dataset, an example of this inconsistency is the use of the term "pediatric tuberculosis" which was indexed as a separate category of tuberculosis starting in the years 1927 — 1936 and may reflect the terminology preferences of a single pathologist.

The discordance in terms used for tuberculosis-associated pathologic findings reduced the ability to make comparisons among autopsy cases in the database. There-

fore, we created a modified version of the database with three major changes to the data architecture (Fig 1.1).

1. To rectify the variability in terminology we developed a set standardized pathologic terms and aggregated groups of autopsy cases indexed under synonymous terms into the same category (Fig 1.1C).

2. To rectify the use of compound terminology we generated a hierarchy that allowed compound terms to be inherited by non-compound terms. This hierarchy reflected both the architecture of the indexes and our knowledge of associated findings in tuberculosis pathology. For instance, autopsies where extrapulmonary disease was found were further indexed by the organs where pathologic changes were identified. In our hierarchy we created a master category of "extrapulmonary disease" and sub-categories for each organ. The autopsy cases listed in each organ sub-category inherited back to the master category "extrapulmonary disease" so that comparisons could be made between both the prevalence of organ-specific dissemination and between the prevalence of extrapulmonary disease and other findings (Fig 1.1C, Fig. 1.2)

3. To rectify the use of different pathologic terms during different periods of time we generated histograms of term-usage by year. We restricted out comparisons to years when terms were in use.

The complete list of findings and associated autopsies were deconvoluted using an Excel algorithm that re-associated each case with a binary matrix of findings. The result of iterating the deconvolution algorithm over the entire set of autopsies was a 2-dimensional matrix of autopsies and associated pathologic findings (Fig 1.1A and B).

Dataset restructuring to promote comparisons between pathologic phenotypes

A.

cavity	tubercle	caseation	pneumonia
1	2	2	1
2	5	3	3
3	6	6	10
4	8	9	11

autopsy	cavity	tubercle	caseation	pneumonia
1	1	0	0	1
2	1	1	1	0
3	1	0	1	1
4	1	0	0	0
5	0	1	0	0
6	0	1	1	0
7	0	0	0	0
8	0	1	0	0
9	0	0	1	0
10	0	0	0	0
11	0	0	0	11

B.

```
=IF(ISNA(VLOOKUP(ValuetoFind, RangetoFindValue, 1, FALSE)), 0, 1)
```

C.

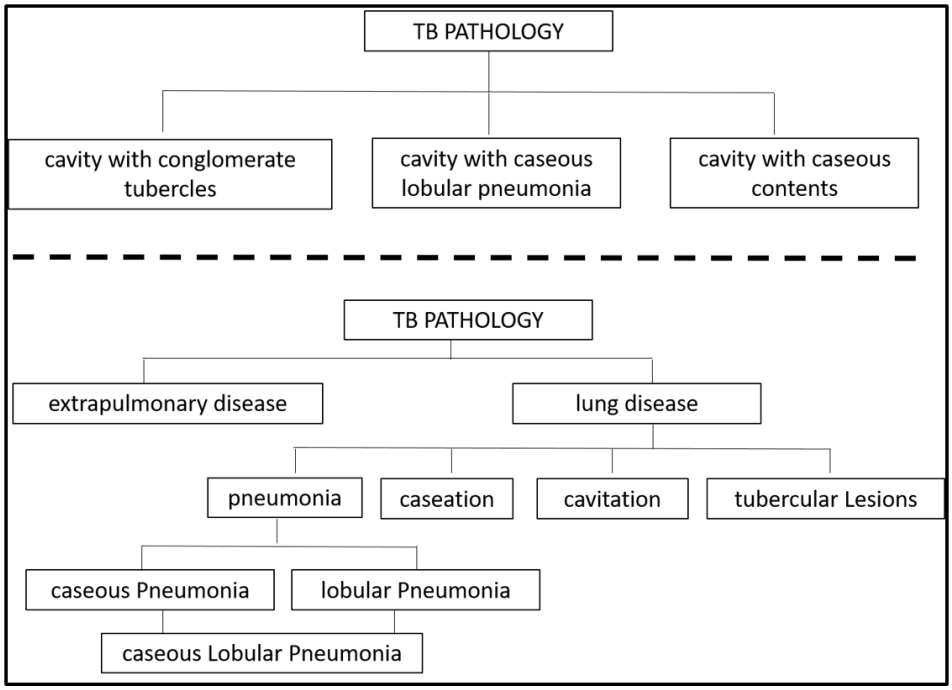

Figure 1.1: Methods of restructuring the tuberculosis autopsy dataset to promote comparisons between pathologic phenotypes. (A) Pattern of deconvolution. Data was received from the autopsy-record index as a set of pathologic findings and associated autopsy numbers. The Excel algorithm in B was applied to each column in the deconvoluted matrix to generate a 2-dimensional matrix of autopsy cases and their associated pathologic findings. (B) The Excel algorithm used in A. (C) An example of the creation of a dataset architecture with standardized terminology for pathologic findings. Top row shows an example architecture as copied directly from the autopsy index. Bottom row shows a hierarchial architecture created from the top-row dataset. Autopsy cases can appear in multiple categories. All higher categories inherit cases from connected lower categories.

1.2.2 The prevalence of tuberculosis cavities among cases of active tuberculosis was 15%

We filtered autopsy records from our 2-dimensional matrix for cases of active tuberculosis. Next we further selected autopsies for which we had looked at the original autopsy record and collected demographic data (age, gender, year-of-death) and had confirmed that the case was indexed correctly (Fig 1.3). Evidence of tuberculosis was found in 18% of all autopsies performed. These filters resulted in 844 autopsy records. Next we further filtered our 844 autopsy set for cases of active tuberculosis. We defined "active tuberculosis" as clinician-assessed tuberculosis described in the clinical notes before the time of death and where pathologists confirmed pathologic changes consistent with tuberculosis at autopsy. Therefore, it is possible that tuberculosis was not the primary cause of death for some of these autopsy cases, but was rather a co-morbidity. We found 337 autopsy cases of active tuberculosis corresponding to 40% of the autopsies where evidence of tuberculosis was found (Fig 1.3A).

The frequency of cavitation among the 337 autopsy records of active tuberculosis was 15% among active TB cases and 6.6% among all autopsies where evidence of tuberculosis was found (Fig 1.3B). We also report the frequency of several other common pathologic findings in our dataset as a percentage of all TB cases in the database and as a percentage of active TB cases (Fig 1.3B).

1.2.3 Cavities were most common in the age-range 45 — 55 years.

The most common age of cavitary tuberculosis may also inform computation models of transmission. For instance, it is unlikely that an infant with cavitary tuberculosis will have the same number of contacts as an individual who is 20 years old. Since we

know the age-of-death for autopsy cases in our database, we generated a prevalence histogram of cavities by age (Fig 1.4C). However, we noticed that the same histogram applied to all autopsy cases with active tuberculosis had a peak in the age range 0 — 5 years, indicating that more autopsies were performed on infants (Fig 1.4B). There are two likely reasons for this peak:

1. The prevalence of tuberculosis among children in the age-range of 0 — 5 years-of-life is higher than for other age groups.

2. The selection of cases for autopsy was biased toward infants.

To assess the frequency of cavities in each age group, we divided the prevalence of autopsies with cavities in each age group by the prevalence of autopsies with active tuberculosis in each age group. The resulting histogram showed that children between the ages 0 — 5 years do not have an increased prevalence of cavitation (Fig 1.4D). Rather, there was a peak in the prevalence of cavitation in the age-range 45 — 55 years of age.

1.2.4 "Case complexity diagrams" display the relative heterogeneity and complexity of autopsy cases with cavitary disease.

The 2-dimensional matrix of autopsy records contains higher-order phenotype patterns. To begin analyzing these pattern, we first asked about the relative prevalence in non-cavitary tuberculosis findings among cases of cavitary disease and non-cavitary disease (Fig 1.5). Our analysis showed that the prevalence of select pathologic findings was similar between cavitary and non-cavitary tuberculosis groups. The one exception was the presence of "tubercles" which had a higher prevalence in cavitary

tuberculosis than non-cavitary tuberculosis. To further understand these patterns we create a "case complexity diagram" (Fig 1.6). This diagram begins with an initial phenotype, in our example, cavitary tuberculosis. Cases are then clustered based on the binary presence or absence of cavitary disease. Along the x-axis are a set of arbitrary steps of case-complexity. After the initial grouping of cavitary disease from non-cavitary disease, we next searched for the next most prevalent pathologic finding in each subgroup. The algorithm was iterated for each subsequency sub-group over 7 levels of complexity.

The case complexity diagram shows that the findings of extrapulmonary disease in combination with lymphadenopathy and primary tuberculosis was the most common phenotype associated with both cavitary and non-cavitary disease. Tubercles were the only trait consistently enriched among cavitary tuberculosis. Finally, lung fibrosis was only found in cases of non-cavitary tuberculosis, though we are less confident about this conclusion since the number of individuals with fibrosis in the non-cavitary tuberculosis group was low.

1.3 Discussion

In this chapter we describe the creation of a dataset containing the complete pathologic phenotypes of 3000 cases with autopsy findings consistent with tuberculosis. We structured the dataset with standardized terminology for each discrete pathologic finding at autopsy and created an inheritance hierarchy for compound terminology. Finally, we used this dataset to provide a robust estimate for the prevalence of cavitation among all cases of active tuberculosis at autopsy. We report this prevalence as 15%. We also investigated the age distribution of cavitary disease and show that the rate of cavitation is roughly the same until the age range 45 — 55 years. These

findings may inform computational models of tuberculosis transmission by identifying super-spreaders. Importantly, the prevalence estimate of 15% and the associated age-specific prevalence estimates may overestimate the prevalence of cavitary disease since they are taken from hospital autopsy cases. The estimate of 6.6% prevalence of cavitation among all autopsies where tuberculosis pathology was found may be a better estimate for the prevalence of individuals with cavitary tuberculosis in the community.

The dataset contains higher-order patterns. As an example of a higher-order description of this dataset, we created a "phenotype complexity diagram" which shows the relative prevalence of each phenotypic trait associated with cavitary and non-cavitary tuberculosis. As part of this analysis, we noted that a greater prevalence of tubercles was specifically associated with cases of cavitary tuberculosis. We hypothesize that the extent of tubercules due to granulomatous pneumonia may correlate with risk for cavitation since more tubercles increase the chances of bronchial association. This hypothesis requires further investigation. It is possible that repetitive exposure leads to a phenotype where tubercles are prevalent throughout the lung and this prevalence increases the risk of cavitation. Chapter 2 of this manuscript addresses the influence of repetitive exposure on disease progression and cavitation.

We believe that this dataset could be useful to other investigators. Our intention is to release this dataset as an open resource as part of a peer-reviewed publication.

Architecture of the restructured dataset for all pathologic findings

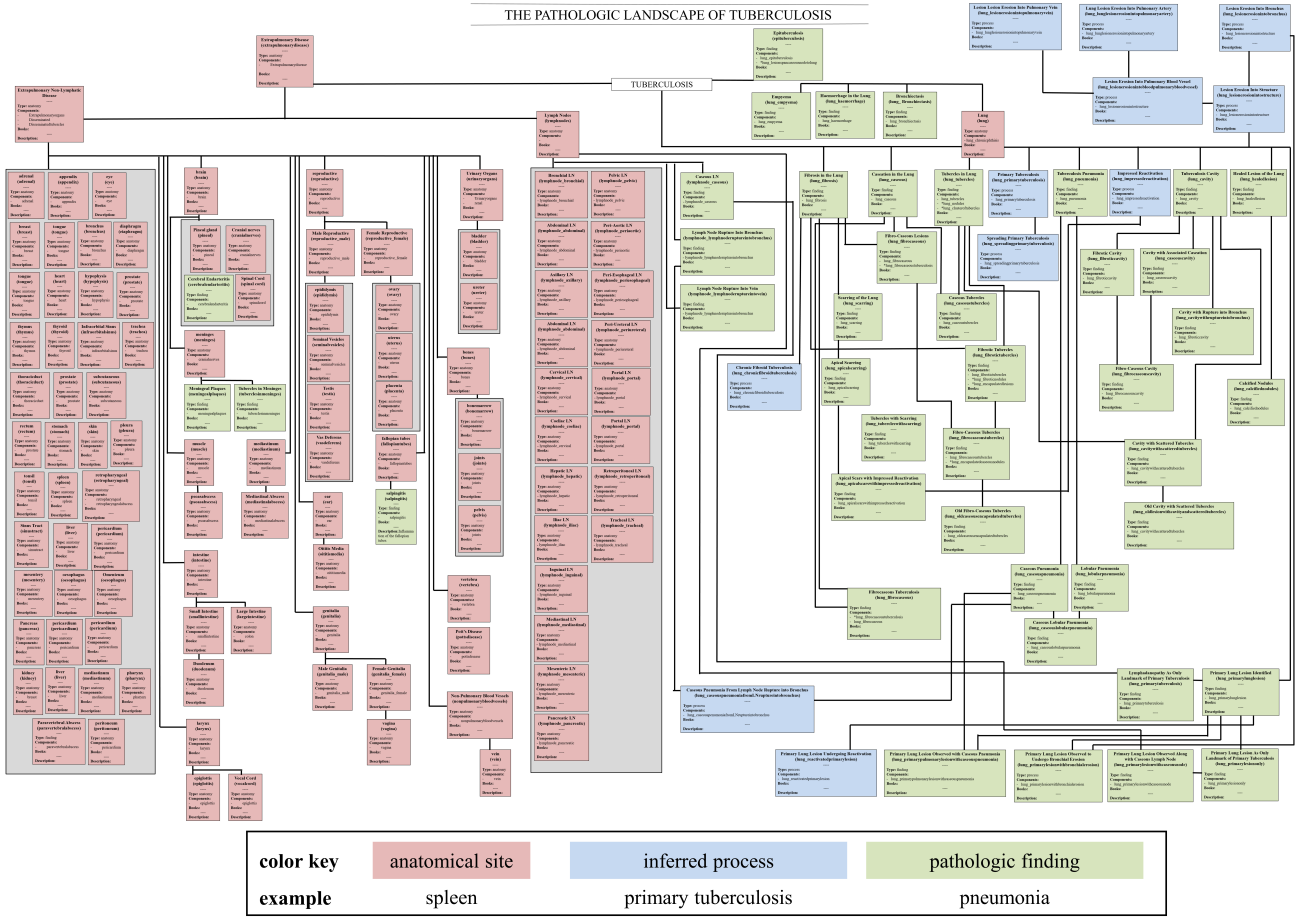

Figure 1.2: Architecture of the restructured dataset for all pathologic findings

The prevalence of pathologic findings among cases of tuberculosis.

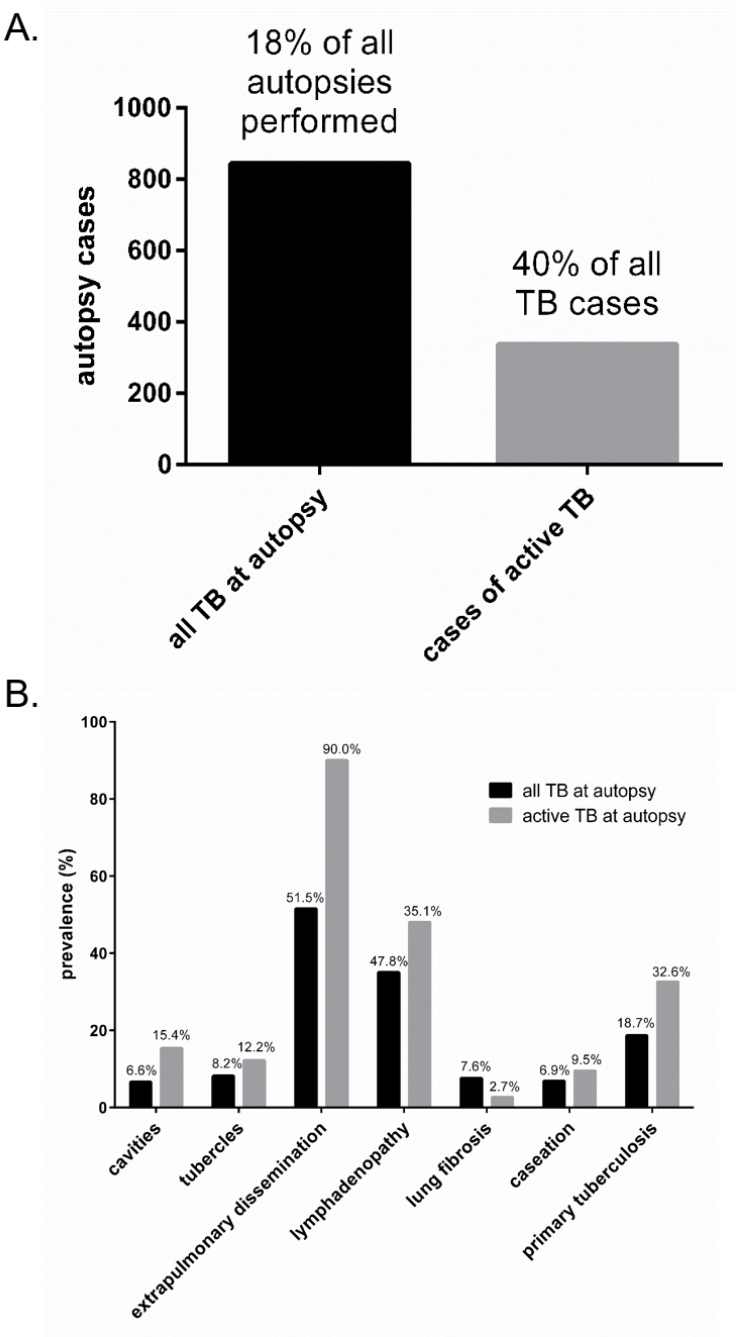

Figure 1.3: The prevalence of pathologic findings among cases of tuberculosis determined at autopsy. (A) Chart showing relative number of autopsy cases where findings consistent with tuberculosis were determined at autopsy compared to the prevalence of active tuberculosis cases in the same dataset. (B) Prevalence of various pathologic findings compared between the two groups in A.

The age distributions of tuberculosis autopsy cases.

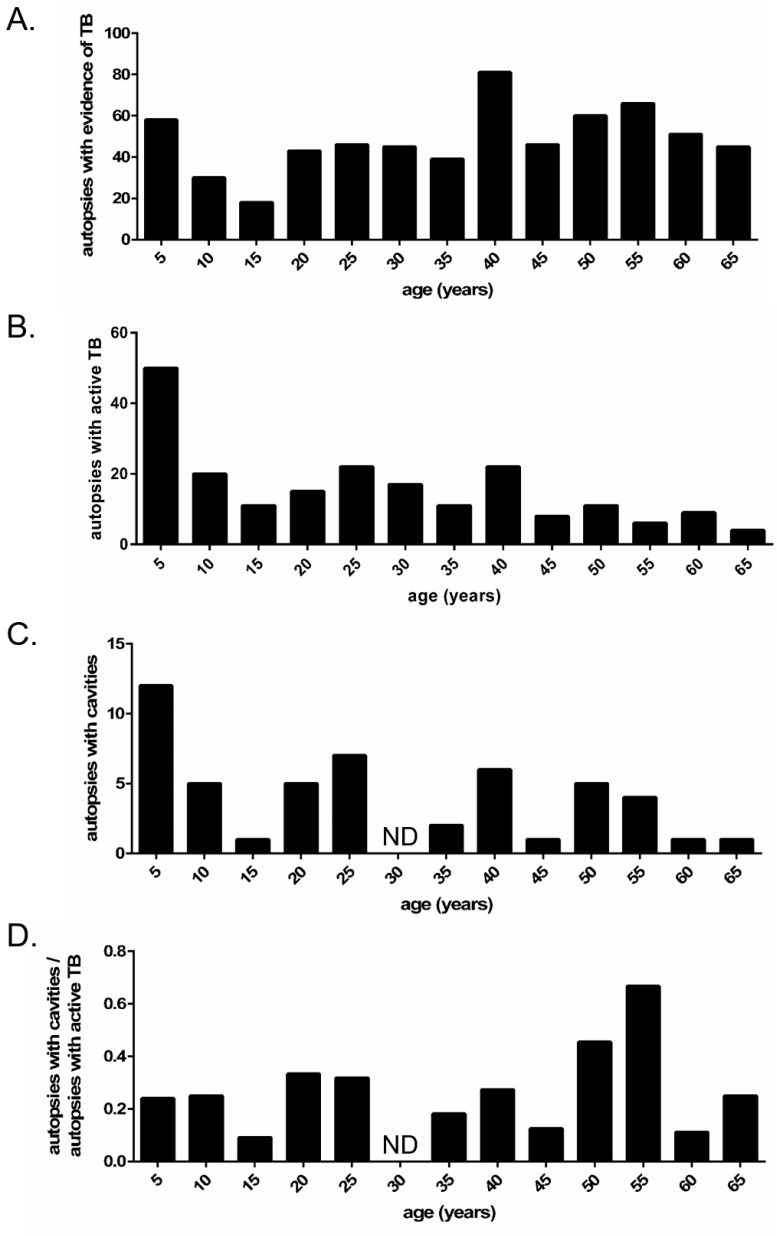

Figure 1.4: The age distributions of tuberculosis autopsy cases. Binning was in 5-year increments (A) Prevalence by age of all autopsies with evidence of tuberculosis. This histogram is composed of 844 unique autopsy records. (B) Prevalence by age of all cases of active tuberculosis. This histogram is composed of 337 unique autopsy recoreds. (C) Prevalence by age of cavities among cases of tuberculosis. This histogram is composed of 96 unique cases of cavitary tuberculosis. (D) Prevalence by age of cavities among cases of tuberculosis standardized to the prevalence of active tuberculosis in each age group. For all histograms "ND" indicates "No Data."

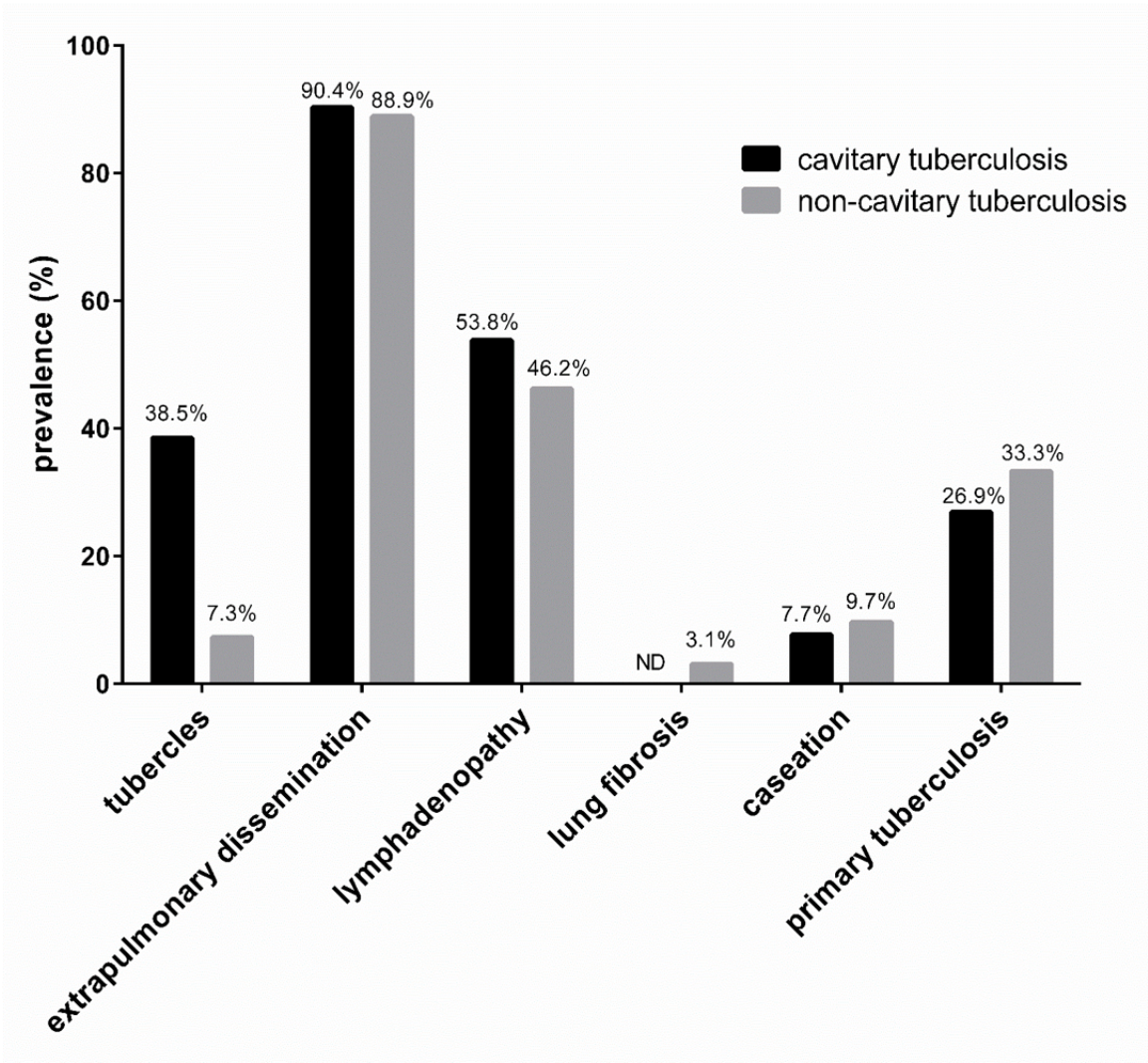

Figure 1.5: Prevalence of pathologic findings among autopsy cases with and without lung cavities. "ND" indicates no data.

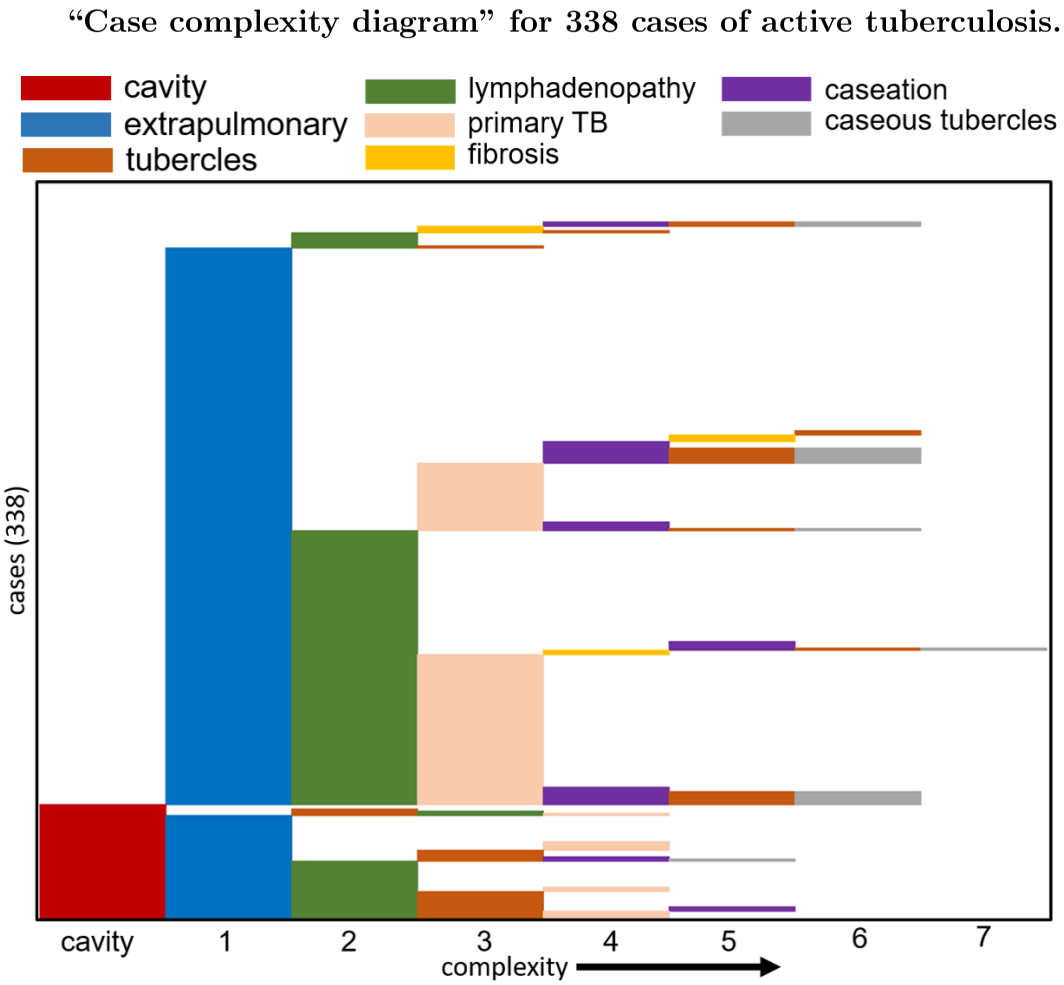

Figure 1.6: "Case complexity diagram" for 338 cases of active tuberculosis. Pathologic findings key: red = cavity, blue = extrapulmonary dissemination, orange = tubercles, green = lymphadenopathy, pink = primary tuberculosis, yellow = fibrosis, purple = caseation, grey = caseous tubercles.

Chapter 2

Repetitive aerosol exposure to model tuberculosis cavities

Michael E. Urbanowski · Elizabeth A. Ihms · William R. Bishai

"But at this point his life took the following turn. He had had to work hard and steadily for his examination, and had come home looking rather paler than a man of his blond, rosy type should do. Dr. Heidekind scolded, and insisted on a change of air; a complete change... it was that Hans Castorp should go for a few weeks to the high mountains before he took up his work in the yards."

by Thomas Mann.
The Magic Mountain (1924)

2.1 Introduction

Tuberculosis is a major cause of morbidity and mortality with 10.4 million new cases of tuberculosis and 1.4 million deaths in 2015[127]. Individuals with extensive lung disease develop a spectrum of gross lesions including diffuse inflammation, tubercles, caseous tubercles, and cavities. The most consequential of these lesions is the lung cavity.

Cavities are not specific to tuberculosis, but they are the greatest risk factor for transmission of bacilli[2,16,17,19]. Cavitary tuberculosis is also more difficult to treat than non-cavitary tuberculosis and is associated with the emergence of drug-resistance[18]. For patients with cavitary tuberculosis who are cured, the cavities may remain, offering a niche for other opportunistic infections[25]. Cavitary lesions that do resolve are associated with fibrotic scarring and chronically diminished pulmonary function[24,128] .

A perfect storm of pathologic features coincide within cavities to drive transmission and a reduced likelihood of treatment success. The interior surface of the cavity wall represents an immune sanctuary that permits high levels of extracellular bacterial proliferation[14,18]. Moreover, cavities often communicate with the conducting airways of the lung, providing a physical conduit for aerosolization and transmission of *M. tb* bacilli[27]. Finally, diminished vascularity and widespread necrosis within the cavity wall reduces the penetration of chemotherapeutic drugs[20–22,129].

Despite the importance of cavities to the natural history of tuberculosis, the mechanism of cavity formation in tuberculosis remains unclear. Histologically, cavities are thought to arise from necrotic granulomas, whose centers are both devoid of extracellular matrix. Pulmonary extracellular matrix is composed primarily of col-

lagen and elastin, which provide mechanical support to the lung while maintaining compliance and elasticity. The expression of collagenases leads to caseation, suggesting that matrix depletion may be an early mechanistic driver of cavitation[84,86,130]. Indeed, increased expression of collagenases is also associated with cavity formation in both animal models and tuberculosis patients[87,131] .

A limitation to studying tuberculosis cavitation is the lack of reproducible animal models[26,132,133]. Mice and guinea pigs rarely develop cavities while they do occur in non-human primate and rabbit models. Previous studies employed pre-sensitization with heat-killed tubercle bacilli together with a high-dose aerosol challenge, transthoracic challenge, or intrabronchial instillation[53–55]. While these methods result in cavitation in some animals, they also generate extensive pneumonitis making it difficult to monitor granuloma formation, necrosis and progression to cavity formation.

Here we describe a novel rabbit model for cavitary tuberculosis based on repetitive aerosol exposure. This model reliably generates multiple cavitary foci in 60 — 80% of study animals in a short period of time. Compared with single exposures of the same total bacterial burden, repetitive exposure generated more advanced disease and more cavitary foci, suggesting that repetitive exposure to aerosolized bacilli may be an important determinant for the severity of tuberculosis in high-incidence settings. Coincidentally, the number of exposures experienced by newly infected TB patients was recently reported as a risk factor for disease progression[134]. We also confirmed that this model develops human-like tuberculosis cavities where matrix depletion was a pathologic feature of cavity development.

2.2 Results

2.2.1 Repetitive aerosol exposure to *M. tb* causes a high frequency of cavitation in a rabbit model

Previous investigations suggested that sensitization with heat-killed mycobacteria prior to infection increased the frequency and severity of cavitation in rabbit models[55,56]. We reasoned that multiple aerosol challenges with virulent *M. tb* would provide a robust sustained immune-sensitizing effect while simultaneously antagonizing both the innate and adaptive defenses.

To test this hypothesis, we conducted a limited-power study by exposing rabbits to *M. tb* in two different patterns. For our studies we defined exposure as the product of the bacterial concentration in the aerosol inoculum and the total time spent in the aerosol chamber. One group of rabbits received five aerosol challenges with *M. tb* at a constant exposure of OD_{600} 0.05 spread evenly over a two week period. A second group of rabbits received a single aerosol challenge with *M. tb* where the aerosol exposure was OD_{600} 0.25, or five times that of a single exposure in the repetitive exposure group (Fig 2.1A). These challenges corresponded to an extrapolated day-1 bacterial implantation of 400 CFU per exposure in the OD 0.05 group and 2200 CFU per exposure in the OD 0.25 group (Fig 2.2). We confirmed that the cumulative exposure was the same for both groups by measuring the colony-forming units in the aerosol inoculum (Fig 2.1A).

To address the possibility that the infection chamber does not achieve aerosol concentrations of bacilli that are linearly correlated with the optical density of the aerosol inoculum, we performed a titration assay to compare the optical density of the aerosol inoculum with the day-1 implantation of bacteria in rabbit lungs, and

The pattern of repetitive aerosol exposure and disease outcomes

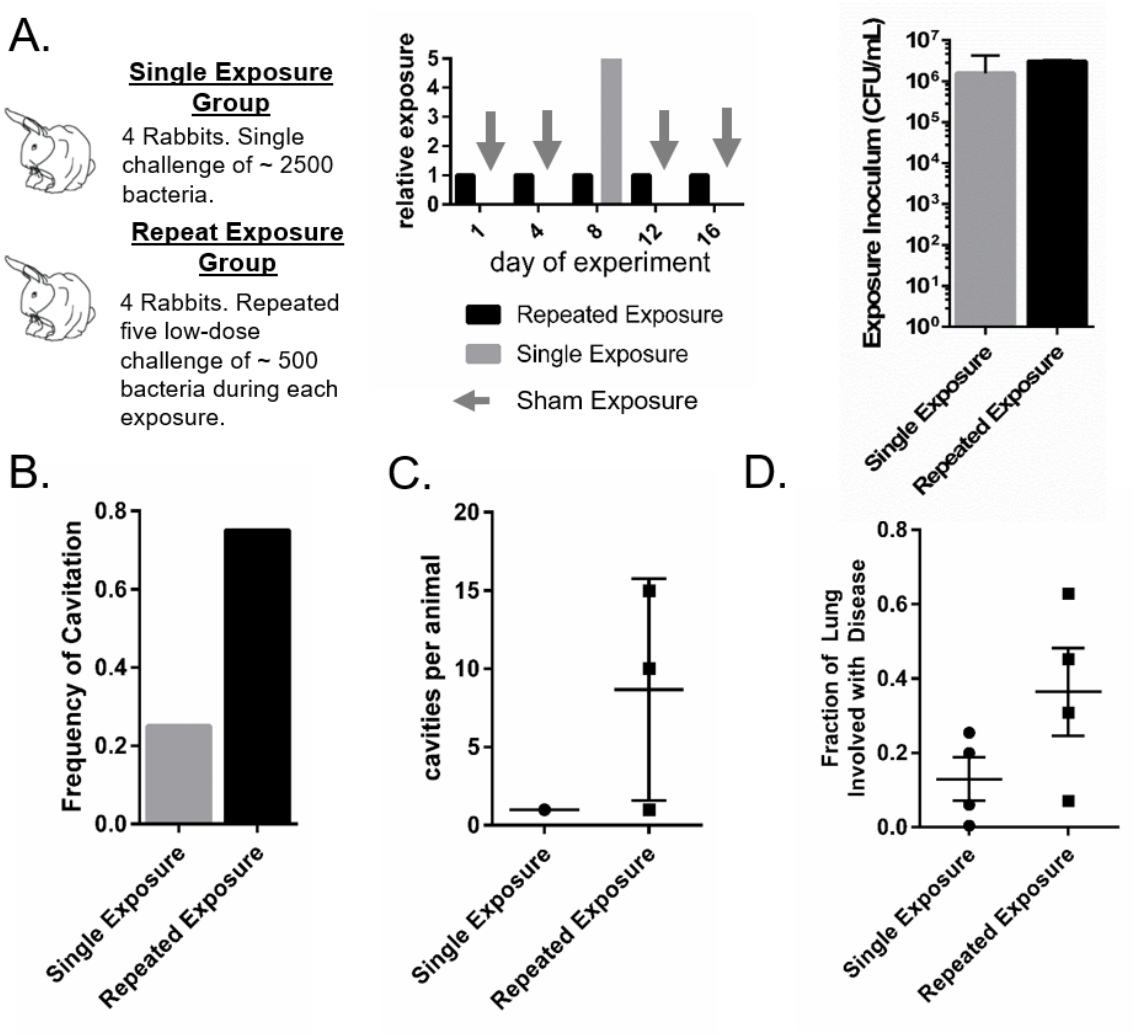

Figure 2.1: Infection parameters and disease patterns for rabbits challenged in the single and repetitive exposure groups. (A) Experimental exposure conditions and timing. Single exposure group rabbits received a single implantation with approximately 2500 bacteria on day 8 and sham exposures on days 1, 4, 12 and 16. Repetitive exposure group rabbits received five repetitive exposures resulting in implantation of approximately 500 bacteria on each of days 1, 4, 8, 12 and 16. Exposure was calculated based on the CFU in the aerosol inoculum. The repetitive exposure was calculated as the sum of the CFU/mL on each day of infection. (B) Frequency of cavitation among rabbits in the single and repetitive exposure groups. (C) The number of cavities per animal in the single and repetitive exposure groups. Cavity counts are only plotted for the animals that demonstrated cavitation. (D) Quantification of the fraction of lung identified as diseased by gross observation for rabbits in the single exposure and repetitive exposure groups.

showed a linear correlation in the optical density range used in these experiments (Fig 2.2). Based on this titration assay, Equation 2.1 relates the optical density of log-phase harvested inocolum to the recovered day-1 bacillary implantation in rabbit lungs. Equation 2.2 also relates the optical density of log-phase harvested inoculum to recovered day-1 implantation, but where data-points used to generate the standard curve are corrected for tissue-mediated CFU signal depression caused by plating onto agar with high concentrations of lung homogenate. The tissue-mediated CFU signal depression factor was calculated to be 9.63 ± 1.29. Equation 2.3 relates the bacterial count of log-phase harvested inoculum to the day-1 bacillary implantation in rabbit lungs. Our data indicate that it is likely that repetitive-exposure rabbits were infected on every occasion of exposure as bacteria were recovered from the lungs of all rabbits in the lowest optical-density exposure group of our chamber titration experiment (Fig 2.2).

$$y = 9418(x) - 27.24 \tag{2.1}$$

Slope 95% confidence: 8014-10823
Y-intercept 95% confidence: -842.3 - 787.8
R^2: 0.9999

$$y = 9352(x) - 34.06 \tag{2.2}$$

Slope 95% confidence: 9163 - 9541
Y-intercept 95% confidence: -75.81 - 143.9
R^2: 1.000

$$y = 0.0007037(x) - 250.0 \tag{2.3}$$

Slope 95% confidence: 0.0004879 - 0.0009195

Y-intercept 95% confidence: -2020 - 1520

R^2: 0.9139

We monitored rabbits using computer tomography (CT) scans. These data showed that 75% (3 of 4) of the animals in the repetitive exposure group experienced

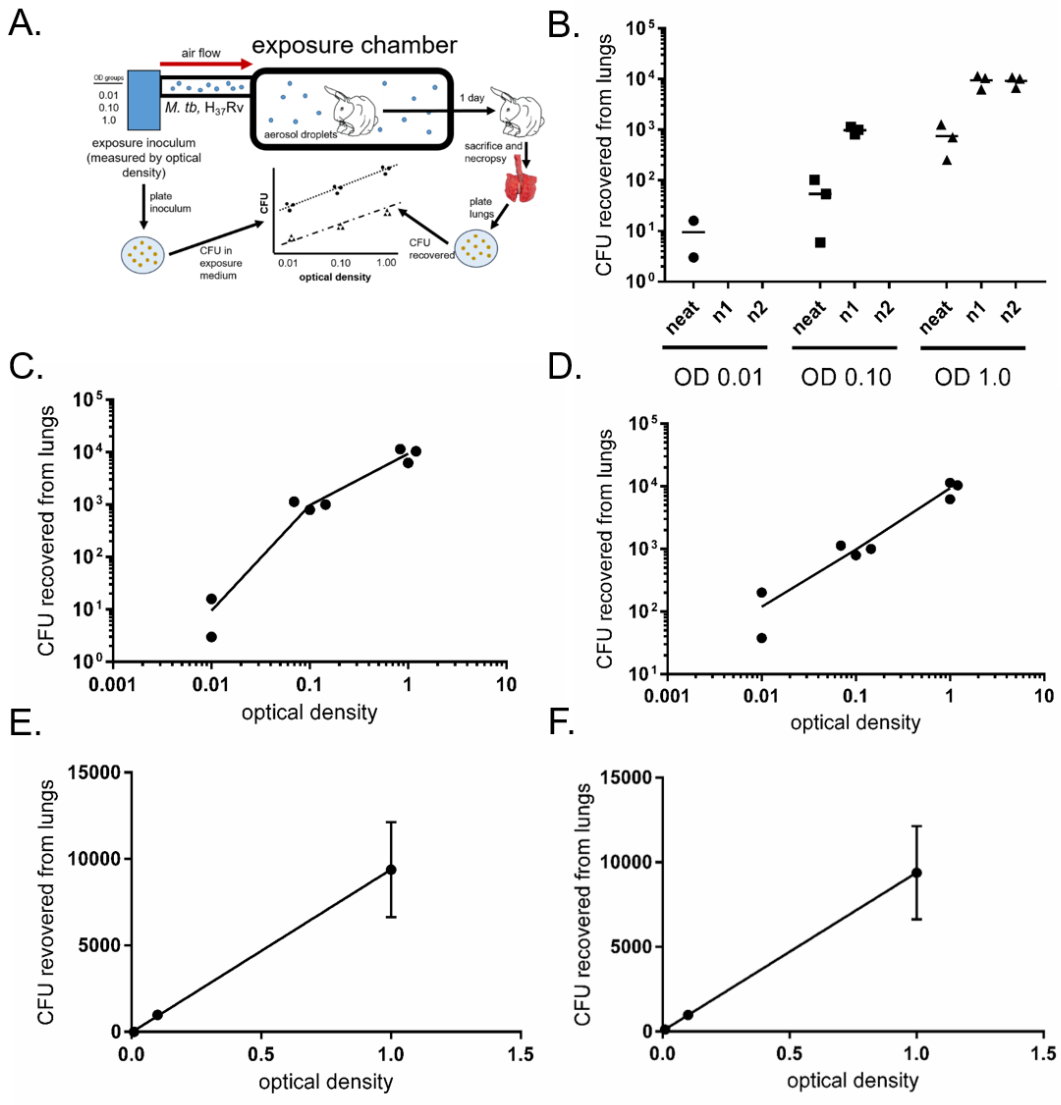

Figure 2.2: Titration of bacterial concentration in aerosol inoculum mapping optical density of aerosol inoculum to day-1 CFU recovered from rabbit lungs. (A) Experimental outline. (B) Bacteria recovered from rabbit lungs reported by optical density group and by dilution set. Three rabbits were used for each optical density group. (C) Optical density mapped to CFU counts using 10x dilution in the OD 0.1 and 1.0 range, and neat (undiluted) counts in the OD 0.01 range. (D) Optical density mapped to CFU counts using 10x dilution in the OD 0.1 and 1.0 range. Counts in the 0.01 group were adjusted for tissue-homogenates CFU signal depression by multiplying OD 0.01 data-points by the ratio of average signal depression between 10x and neat dilutions in the OD 1.0 group, shown in S1B. (E-F) Best-fit linear regression models based on the averages of data-points in each OD group in C and D. All equations are calculated for the best-fit line between data-points.

at-least one cavity versus 25% (1 of 4) of the animals in the repetitive exposure group (Fig 2.1B). Of those animals that developed cavities, those in the repetitive exposure group showed a trend toward more cavities per animal than those in the single exposure group (Fig 2.1C). On week-10 of the experiment, the rabbits were sacrificed and the lungs were fixed. Semi-quantitative gross pathologic analysis showed that rabbits in the repetitive aerosol group experienced worse lung disease than those in the single exposure group (Fig 2.1D and Fig 2.3). In light of the limited number of rabbits involved in this study, these data suggest that repetitive exposure caused an increase in the severity of disease as well as the frequency and severity of cavities.

2.2.2 Cavities from repetitive exposure formed quickly, showed dynamic behavior, and often persisted for many weeks

Focal matrix depletion precedes tuberculosis cavitation, so we sought to define the optimal treatment window for the prevention of cavitation as the weeks before the greatest frequency of cavitation. To study the dynamics of cavity formation generated by repetitive exposure to *M. tb*, we infected eight rabbits using the repetitive exposure protocol and observed their lungs using CT scans at weeks three, six, eight and 16. The overall frequency of cavitation in this study was 87% (7 of 8), further supporting our previous observations with the repetitive exposure method (Fig 2.4A). The greatest increase in the frequency of cavitation occurred between weeks 6 and 8, during which time the frequency of cavitation among rabbits increased from 11% (1 of 8) at week six to 50% (4 of 8) at week 8 (Fig 2.4A). Between week 8 and week 16, the frequency of cavitation increased modestly to 63% (5 of 8) but was marked by occasional resolution of existing cavities and the generation of new cavities.

Cavity morphology over time was observed by CT scan reconstructions. We

Comparison of fixed lungs from the single and repetitive exposure group rabbits

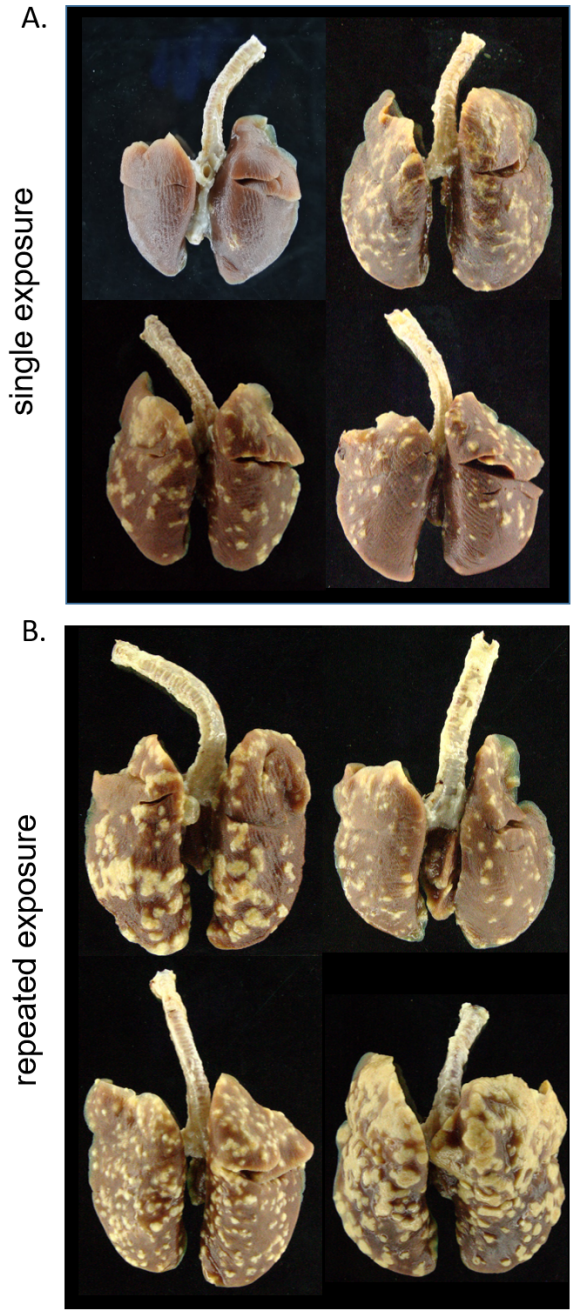

Figure 2.3: Gross images of formalin fixed lungs showing the dorsal aspect of the lungs. (A) Lungs from rabbits in the single exposure group. (B) Lungs from rabbits in the repetitive exposure group.

Patterns of cavity growth and shrink in rabbits infected by repetitive aerosol exposure

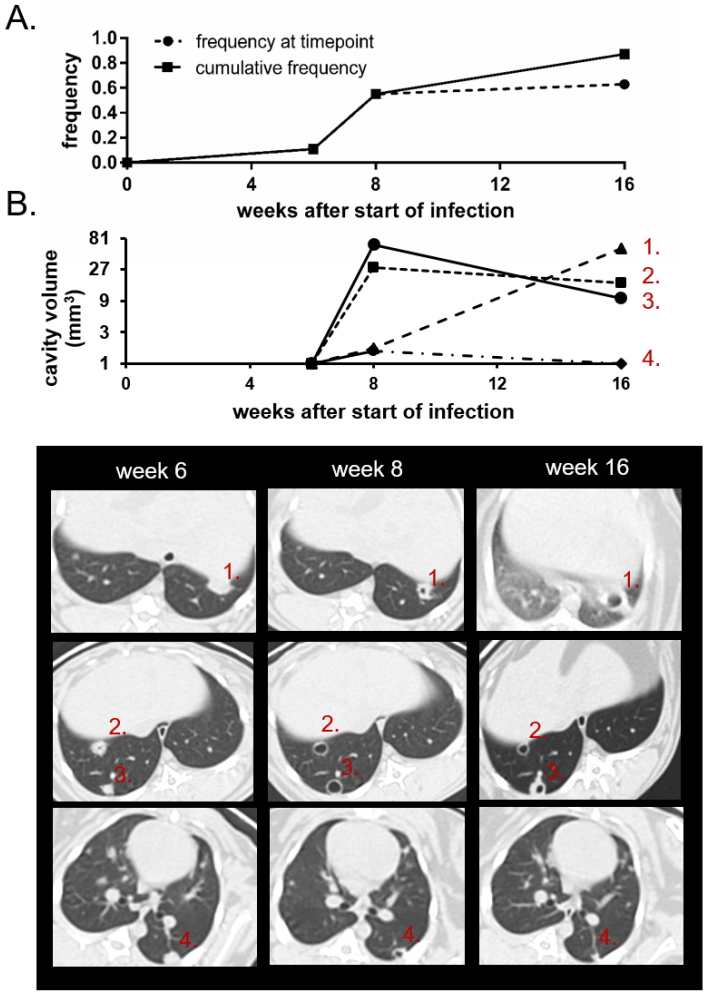

Figure 2.4: Timing of cavitation and cavity growth dynamics in the repetitive aerosol method. (A) The frequency of cavitation mapped to time after start of infection. The solid line indicates the cumulative frequency of cavitation among the cohort of 8 rabbits. The dashed line indicates the frequency of cavitation among the cohort at the specific time point and is distinguished from the solid line by the occurrence of cavity resolution. (B) Cavity volume mapped to time after the start of infection for four representative cavities demonstrating (1) continuous growth, (2, 3) growth and shrinking behavior, and (4) growth and resolution. Cavities were identified as lung volumes not connected to the normal bronchial structure with densities between -875 and -1024 Hounsfield units and points on the x-axis indicating a non-cavitary focus are plotted at the limit-of-resolution for the CT scanner. The y-axis is plotted using a logarithmic base 3 scale since measured volume varies closely as the cube of the radius of a spheroid object so that relationship among cavity volumes are more comparable to the two-dimensional reconstructions in C. (C) Transverse CT-scan reconstructions showing each of the foci identified in B.

used density segmentation analysis to identify cavities as air-filled spaces that were not connected to the bronchial tree. From this analysis, we identified three patterns of change in cavity morphology: (1) cavity growth (Fig 2.4B and C, example 1) (2) cavity shrinkage (Fig 2.4B and C, example 2 and 3), and (3) cavity resolution (Fig 2.4B and C, example 4). Together, these data demonstrate that cavities most-often formed between six and eight weeks after the initial aerosol exposure and were persistent though dynamic structures between weeks eight and 16 of the study.

2.2.3 The size of the pre-cavity consolidated focus does not impose a boundary on final cavity size

One potential hypothesis to explain the dynamic behavior of tuberculosis cavities proposes that the maximum size of a cavity is determined by the boundaries of the pre-cavity consolidated focus. If this hypothesis is true, then a conceptual model for tuberculosis cavitation should be straightforward and is comprised of the following steps:

1. Granuloma formation
2. Central matrix depletion and necrosis
3. Erosion of necrotic debris through a bronchus

We conducted a thorough study of the dynamics of cavity formation, growth and resolution using CT-scans generated from serial time-points (Fig 2.5). In this study, we considered the total lesion volume (V_{lesion}) as the volume of the cavity (V_{cavity}) plus the volume of consolidation around the cavity ($V_{consolidation}$). We then identified the full set of cavities generated during our repetitive aerosol exposure pilot

studies and plotted V_{lesion} for each of the serial CT time-points at weeks three, six, eight, and 16 following the start of the experiment (Fig 2.5A).

Approximately 50% of the cavities observed in this study were the largest at the initial time of observation and shrank by some degree in serial CT scans. About 25% of the cavities grew steadily over serial CT scans. About 20% of the cavities displayed dynamic growing the shrinking behavior. Finally, a minority of the cavities (4%) underwent complete resolution and were not radiologically apparent at the final CT-scan (Fig 2.5B and C). These findings suggest that cavity volume changes over time and can grow and shrink. Importantly, many of the cavities that demonstrated growing behavior showed V_{lesion} changes that grew by more than 2-times their initial volume, suggesting that the volume of a pre-existing consolidated focus, or pre-existing cavity, does not impose a boundary on the final cavity size.

Next, we asked whether the size of the initial consolidated focus limits the absolute size of the cavitary lesion (V_{lesion}). We used serial CT scans taken at week 6 and later. We identified all instances of consolidated foci and new cavities in each of these scans. Next, we identified the preexisting consolidated focus in the CT-scan taken from the imaging time-point immediately preceding the scan where the lesion was identified. Common anatomical landmarks were used to identify the most-probably precursor consolidated focus. Finally, we reported the ratio of V_{lesion} to the size of the preexisting consolidated focus ($V_{lesion,\ t\text{-}1}$) (Fig 2.5D and E).

These data demonstrate that cavitation is often accompanied by a rapid (two-weeks or less) expansion event. Most ratios for solid lesions, foci that did not cavitate, remain close to 1.0. However, cavitation was accompanied by an average 1.87 times expansion in the size of the lesion (range: 0.67 9.30) (Fig 2.5E).

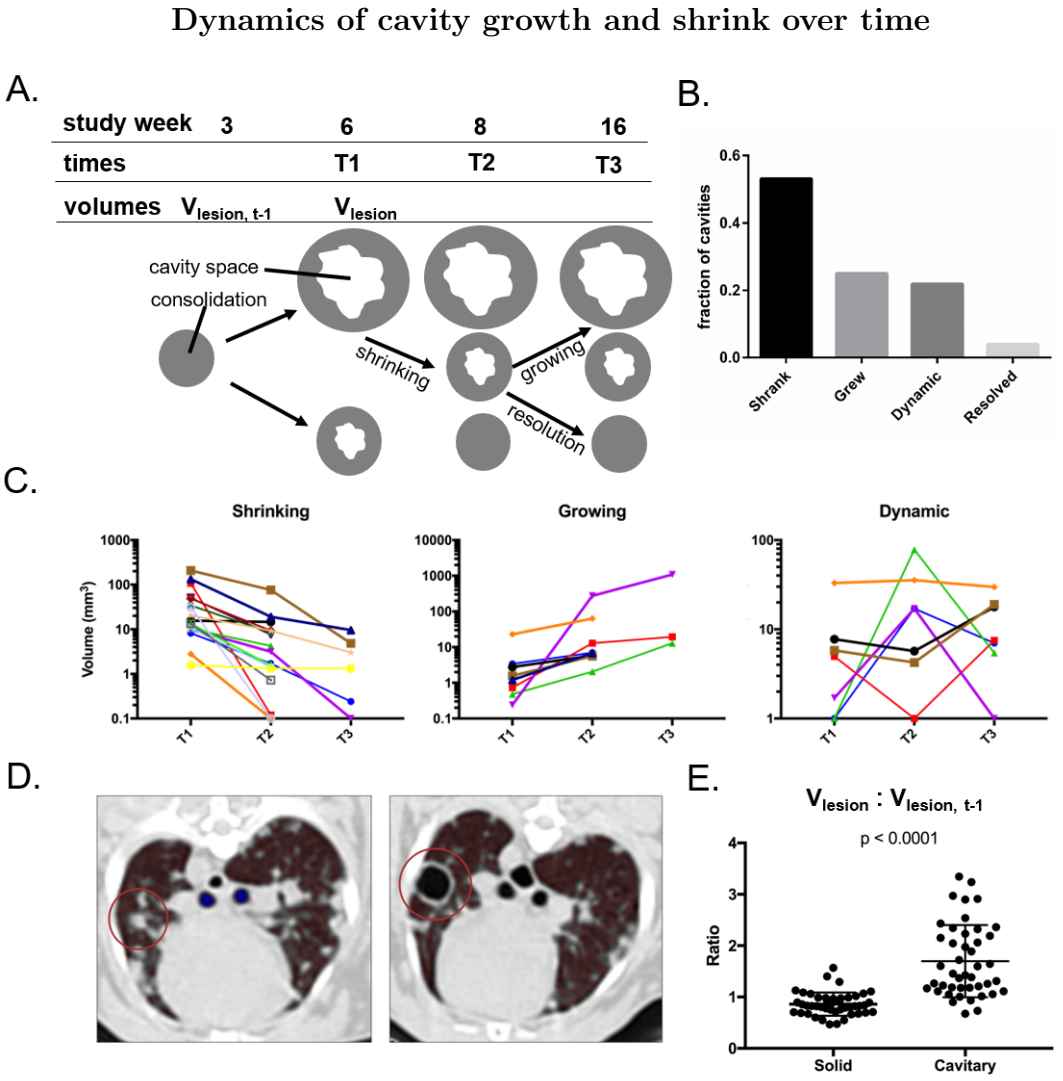

Figure 2.5: A study of the frequency of cavity growth and shrink over time in rabbits infected by repetitive aerosol exposure. (A) Study schematic showing the relationship between study week, CT-scan times T1, T2 and T3, and volumes V_{lesion} and $V_{lesion,\ t\text{-}1}$. The volume V_{lesion} is always the area of consolidation + the area of cavity-space if a cavity exists. (B) The fraction of all cavities identified that demonstrated each behavior. (C) Plots displaying V_{lesion} at each time-point. (D) An example transverse plane CT-scan reconstruction showing demonstrating cavitation from a consolidated focus. Scans were taken two-weeks apart. (E) The relative growth in lesion volume for consolidated foci that did not cavitate compared with those that did cavitate.

2.2.4 A bubble-like morphology occurs in more than 50% of cavities generated by repeated exposure

We spatially co-registered terminal CT-scans with high-resolution photographs of fixed lung-tissue. This technique allowed us to validate that cavities observed following histologic preparation were not artifacts of tissue sectioning, but rather cavities *in situ*. Dr. Elizabeth Ihms reviewed the histologic morphology of each lesion and inferred four distinct morphological sub-types (Fig 2.6). The category "smooth" or "bubble-like" accounted for 50% of all cavity-types (Fig 2.6A).

2.2.5 Histologic observations support the hypothesis that central necrosis and matrix depletion are prerequisites for cavitation

A large body of historic literature, in addition to our own observations, suggests that tuberculosis cavities arise from necrotic granulomas. Since we had not previously worked with a model that generates cavities by repetitive exposure to *M. tb*, we investigated whether the pathologic phenotype of lung destruction was similar to human disease. Histology samples collected from rabbits infected by repetitive exposure displayed many of the microscopic findings described in tuberculosis pathology reports (Fig 2.7)[4,14,132,135]. These hallmarks included granulomas, necrotic granulomas and cavities. Histologic observations from the repetitive exposure model show that the cytoarchitecture between necrotic granulomas and cavities was similar, further supporting a close relationship between the two lesions (Fig 2.7A and B, and Fig 2.8).

The cavities generated by repetitive exposure were marked by large proliferations of acid-fast bacteria along their inner surface and a wall enriched with fibrosis

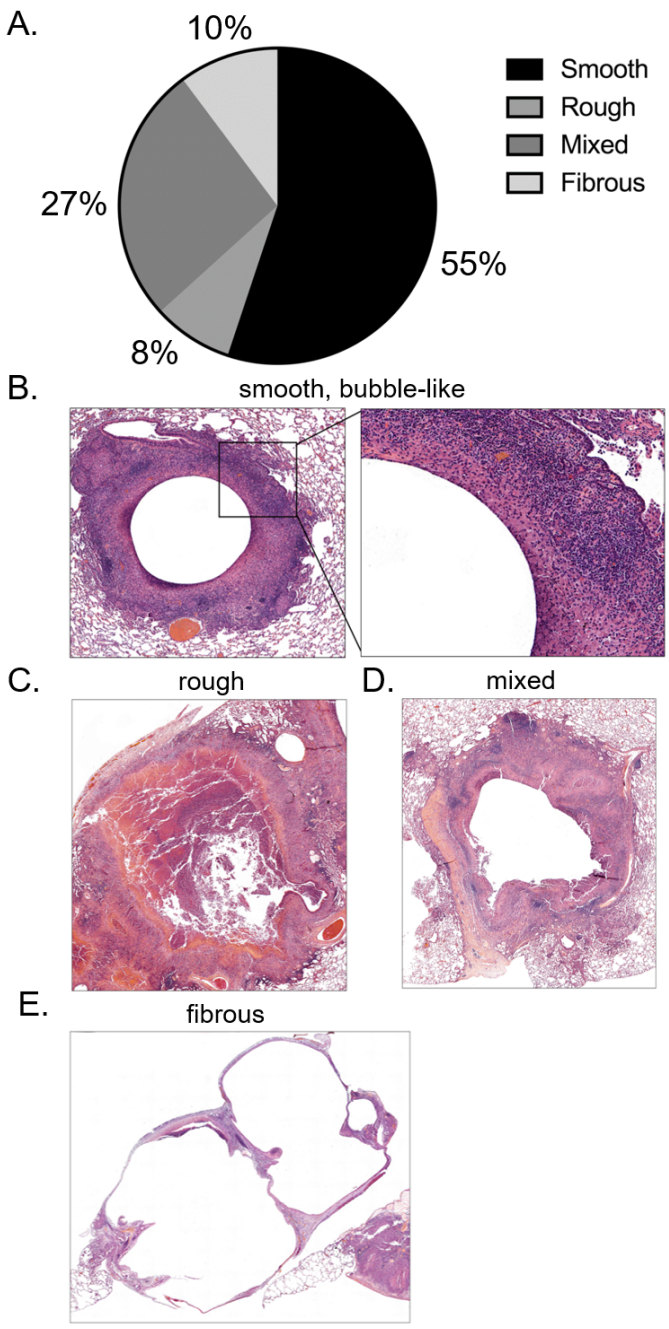

Figure 2.6: A study of the microscopic morphologies of rabbit cavities generated by repetitive aerosol exposure based on 49 cavities. (A) Frequency of each morphologic type. (B) Representative H&E section of a cavity showing "smooth" or "bubble-like" morphology. (C) Representative H&E section of a cavity showing "rough" morphology. (D) Representative H&E section of a cavity showing "mixed" morphology. (E) Representative H&E section of a cavity showing "fibrous" morphology.

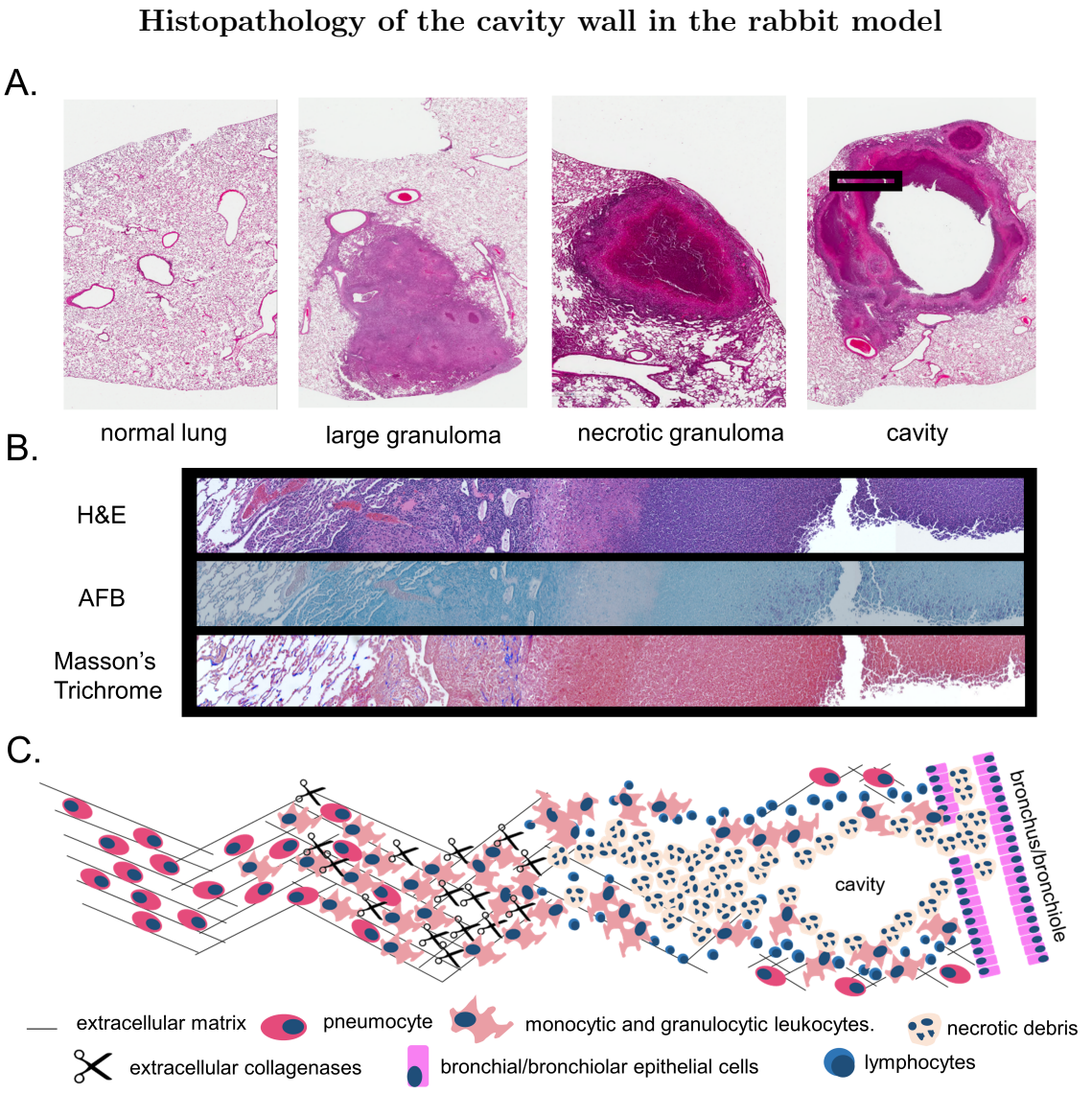

Figure 2.7: Histologic patterns of tuberculosis lesions in rabbits infected by repetitive aerosol exposure. (A) Representative H&E demonstrating lesions commonly observed in rabbits infected by repetitive aerosol exposure. (B) Serial sections from the boxed region demarcated in A stained with H&E, acid-fast bacilli, and Masson's trichrome stain. Masson's trichrome identifies collagen in blue hues. (C) Overview of the model for collagenase mediated destruction of extracellular matrix in proximity to a cavity.

(Fig 2.7B and Fig 2.8C). Since our investigations are predicated on the pathologic observation that matrix depletion predisposes to cavitation, we also confirmed that collagen matrix depletion was a hallmark of cavitary lesions from repetitive exposure (Fig 2.8). These observations show that repetitive aerosol exposure in rabbits generates a spectrum of histologic lesions commonly observed in tuberculosis pathology studies and validates the model for our studies by showing that pathologic matrix depletion is modeled by rabbits following repetitive aerosol infection.

2.3 Discussion

We have developed a novel model for cavitary tuberculosis based on repetitive aerosol exposure to virulent *M. tb.* Our data show that repetitive exposure over a two week period produced more advanced disease and more cavities than a single exposure, even when we carefully adjusted the concentrations bacteria in the aerosol inoculum to provide the same total exposure between groups. More generally, our findings provide experimental evidence that the pattern of exposure is a variable in determining the pattern of tuberculosis. Specifically, this finding suggests a link between repetitive exposure and tuberculosis exacerbation and is further supported by recent epidemiological evidence that multiple exposures to infected contacts increases the risk of tuberculosis progression[134,136]. An association between repetitive exposure and severe tuberculosis may have important implications for epidemiology and infection control in high-incidence regions of the world.

Our experiments did not evaluate the mechanism of repetitive-exposure related disease exacerbation; however, it is possible that the driver of more severe disease in repeatedly exposed animals is repeated priming of cell-mediated immunity. Although untested, repetitive exposure may cause a cascading set of T-cell priming and expan-

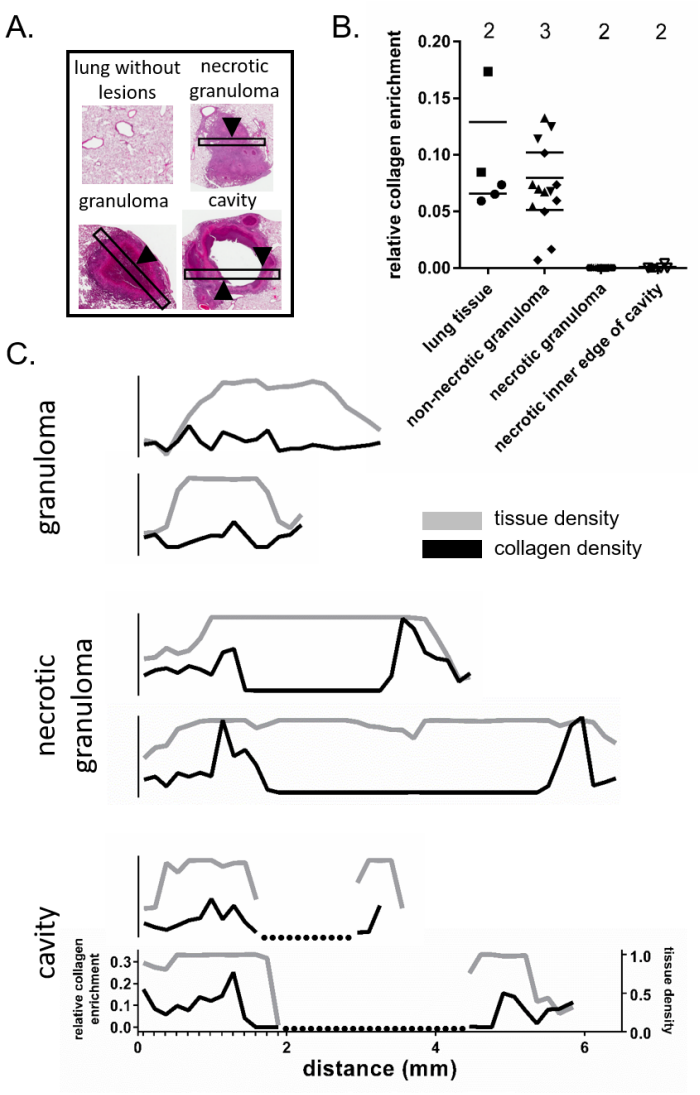

Figure 2.8: Collagen enrichment in lung lesions from rabbits infected with *M. tb.* (A) Examples of H&E stained tissue fields used for quantification of collagen enrichment analysis. Black rectangles represent example high-resolution fields used for quantification in B and traces in C. Arrow-heads indicate examples of the histologic regions surveyed during the relative collagen quantification reported in B. (B) Relative enrichment in collagen identified by blue hues in the Masson's trichrome stain. Surveys of collagen enrichment were random in normal appearing lung tissue and from regions 500 μm in length at the centers of lesion fields in granulomas and necrotic granulomas. Surveys of collagen enrichment from the cavity edge were defined as regions within 150 μm of the cavity edge. Multiple surveys were taken from non-overlapping areas within each region and the number above each category indicates the number of unique lesions surveyed. (C) Relative tissue density (grey line, right y-axis) and collagen density (black line, left y-axis) along linear traces crossing two granulomas, two necrotic granulomas, and two cavities. All traces are set to the same x and y scale and the minor hash marks in the lowest plot show the regular pattern of surveys continued along each lesion. Dotted lines indicate cavity space on histology.

sion events that disproportionately exacerbate the immune response against *M. tb* antigen in the lung[137].

Our data show that modeling cavitary tuberculosis by repetitive aerosol exposure also models a spectrum of human lesions and pathologic matrix depletion associated with caseous and cavitary pulmonary tuberculosis[138].

Our results demonstrate an entirely new system to study tuberculosis cavities. We show that repetitive exposure to aerosolized *M. tb* produces a pathologically relevant phenotype for screening pre-clinical agents toward the prevention and treatment of cavity formation.

2.3.1 Interpretations of dynamic cavity growth and shrink behavior

The dynamic growth and shrink behavior of cavities supports the conclusion that the size of the pre-cavitary consolidated focus is not a limit for the maximum size of the cavity derived from the pre-cavitary focus. Instead, cavities appear to have dynamic behavior over time and can grow, shrink, or resolve. One possible explanation for this dynamic behavior is the movement of caseum into and out of the cavity via the draining bronchus. However, this explanation only accounts for the dynamic size of the cavity-wall, but does not explain the ability of the entire cavitary focus (cavity-space and surrounding consolidation) to grow so that the new boundaries of the cavity-space exceed the original out-boundaries of consolidation. Therefore, it is likely that one or more physical or biochemical mechanisms drives large cavity expansion.

Our analysis of the ratio of cavity-lesion size (V_{lesion}) to the size of the pre-

cavitary focus compared to the same metric for lesions that did not cavitate provides another interesting insight into the cavitation event. In this comparison, cavitation was often accompanied by a sharp increase in overall lesion volume that was not observed in lesions that failed to cavitate. We argue that this is evidence for a stretching effect on the cavity wall. As central necrosis and matrix breakdown drive cavitation, the mechanical cross-sectional support within the lesion is reduced. As a result, the inspiration induced tension exhibited in all directions by alveoli stretches the cavity wall. The cavity wall is eventually balanced with the pull of alveoli by tangentially-vectored tension enforced by the fibrotic wall of the cavity. This explanation remains unsubstantiated, but the apices of the lungs are the sites of the greatest mechanical stress and we suggest that a tension-driven-expansion explanation may help explain why large cavities tend to occur in the apices of the lungs.

Another possible mechanism for cavity growth is continual necrosis and matrix-breakdown at the periphery of the cavity accompanied by further sloughing of new necrotic debris. This would have the effect of growing the overall size of the cavity-space beyond the boundaries of the pre-cavitary focus. Our studies provide insufficient evidence to rule out either tension-driven-expansion or peripheral remodeling as the major driver of large cavity expansion. Likewise, it is also possible that both mechanisms play a role in cavity expansion.

2.3.2 A positive-pressure model may explain the high-prevalence of cavities with a bubble-like morphology

Greater than 50% of the cavities observed following repeated aerosol exposure contained a "smooth" or "bubble-like" morphology. In her analysis, Dr. Elizabeth Ihms also noted that these cavities were, on average, younger than cavities show-

ing other morphologies. Corroborating our observations in the repetitive aerosol rabbit model, Ordonez *et al.*, also observed a similar "bubble-like" morphology in C3HeB/FeJ mice[139]. Several reports from tuberculosis pathology studies also noted the presence of a "bubble-like" cavity morphology. Therefore, we suggest a positive-pressure model best explains these observations. In this hypothesis, a necrotic granuloma connects to a bronchus and a small amount of necrotic debris occludes the draining bronchus. Respiratory inspiration pulls the walls of the cavity apart and creates a vacuum within the micro-cavity. The vacuum pulls small amounts of air into the cavity to create positive pressure when the respiratory muscles relax. This pattern of events may explain the earliest event in cavitation but this model requires further investigation. Finally, it is also possible that the bubble-like morphology is an artifact of both the rabbit and C3HeB/FeJ cavity models.

2.3.3 Limitations of the repetitive aerosol exposure model

There are several important limitations for the rabbit cavity model based on repetitive aerosol exposure. These limitations are important because they define the range of appropriate experimental applications for the repetitive aerosol exposure model.

First, the high rate of cavitation is artificial. Estimates for the frequency of cavitation among cases of active tuberculosis vary from 10 — 50%. In Chapter 1 we report a frequency of 15%. In contrast, the repetitive aerosol model develops cavities at a frequency between 60 — 80%. Therefore, the repetitive exposure model may not be appropriate for experiments where the frequency of cavitation is expected to be similar to the frequency observed in human tuberculosis.

Second, it is difficult to define the repetitive exposure model as a model of primary or post-primary tuberculosis. Post-primary tuberculosis is defined as tuber-

culosis in the context of a pre-existing adaptive-immune response. This distinction is not trivial since pathology studies demonstrate distinct patterns of disease for primary and post-primary tuberculosis. In the repetitive exposure model rabbits are naïve to tuberculosis antigen at the time of the first aerosol exposure. However, rabbits were shown to have acquired an adaptive-immune response to tuberculosis antigen by the end of the two-week exposure period (Fig 2.9A and B). Therefore, the first of five repetitive exposures may be considered a primary exposure event, but many of the disease foci probably develop in the context of an adaptive-immune response to *M. tb* antigen.

Finally, cavitation in the repetitive aerosol model occurs without polarized lung-lobe distribution (Fig 2.9C). Pathology studies describe post-primary disease foci predominately occurring in the apical lobes. Our studies show that the repetitive aerosol exposure model develops cavities distributed evenly through all lung lobes of the rabbit. The repetitive aerosol exposure model may not be appropriate for investigating hypotheses concerning the pathogenesis of apically-oriented post-primary disease.

These limitations aside, the high rate of cavitation seen in this model is advantageous for studies where cavities are analyzed as discrete biological occurrences. For our studies, the development of the repetitive exposure model enabled efficient screening for *in vivo* inhibitors of cavitation. These inhibition studies are the subjects of Chapters 3 and 4 of this manuscript.

Mantoux test results and the distribution of disease by lobe in rabbit lungs

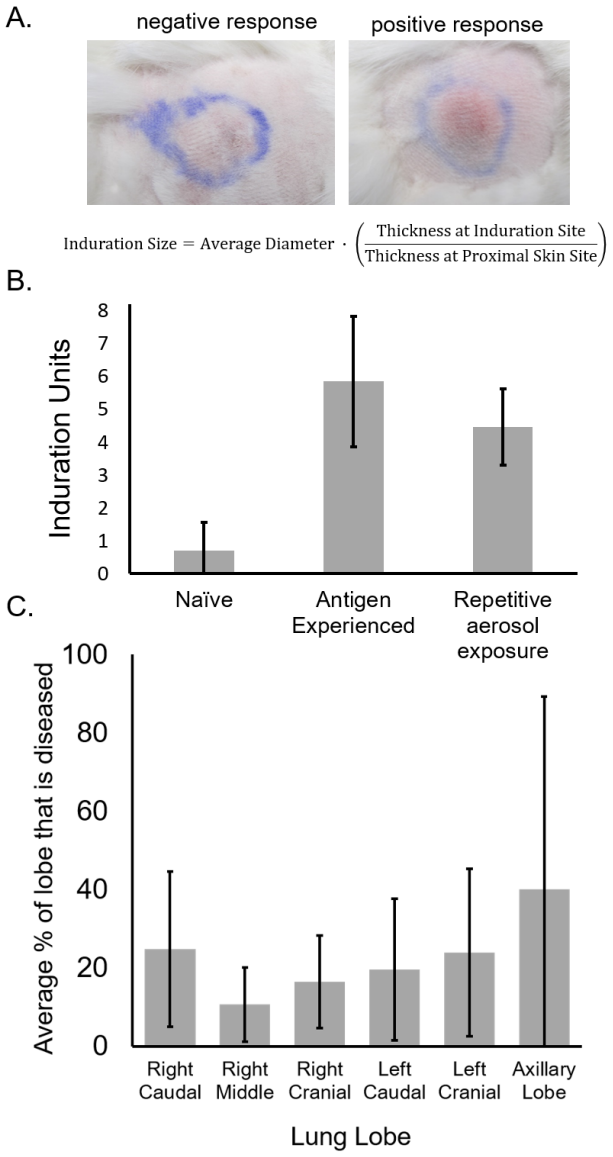

Figure 2.9: Mantoux test results and the distribution of disease by lobe in rabbit lungs. (A) An example of a negative PPD-reaction and a positive PPD-reaction in the rabbit model. The equation for calculating induration size is shown. The average diameter of the induration is measures as two perpendicular lengths taken across the injection site bounded by the start of the thickened region of skin. The thickness of the induration is calculated by caliper as the minimum thickenss of skin that can be pinched and held. (B) PPD-responses at the end of the two-week repetitive aerosol infection period compared with antigen-experienced controls and *M. tb*-antigen naïve rabbits. (C) The distribution of disease between lobes of rabbit lungs.

Chapter 3

Pharmacologic inhibition of the collagenase matrix metalloproteinases during cavity formation in the rabbit model

Michael E. Urbanowski · Elizabeth A. Ihms · Kristina Bigelow · André Kübler · Paul T. Elkington · William R. Bishai

"A cloud fell down from the heavens,
And broke on the mountains brow;
It scattered the dusky fragments
All over the vale below.

The moon and the stars were anxious
To know what its fate might be;
So they rushed to the azure op'ning,
And all peered down to see."

A Starry Night
by Paul Lawrence Dunbar.
Widely regarded as one of the greatest poets
and writers in 1900, died of tuberculosis in 1906
at the age of 33.

3.1 Introduction

In the previous chapter we describe a novel rabbit model for cavitary tuberculosis based on repetitive aerosol exposure. This model reliably generates multiple cavitary foci in 60 — 80% of study animals in a short period of time. Compared with single exposures of the same total bacterial burden, repetitive exposure generated more advanced disease and more cavitary foci, suggesting that repetitive exposure to aerosolized bacilli may be an important determinant for the severity of tuberculosis in high-incidence settings. We also confirmed that this model develops human-like tuberculosis cavities where matrix depletion was a pathologic feature of cavity development. Based on these observations, we endorse the repetitive aerosol exposure model as an advantageous tool for studying cavitation.

The collagenase MMPs and cathepsin K are the two lead candidates for molecular mediators of tissue matrix destruction in tuberculosis identified by Kübler *et al*[91,131]. In this chapter, we apply the repetitive aerosol exposure model to screen cipemastat, a potent inhibitor of the collagenase matrix metalloproteinases (MMPs), as a targeted inhibitor and therapeutic agent to limit tuberculosis cavitation[140,141].

3.1.1 The biology of matrix metalloproteinases

The MMPs are a group of 23 homologous metalloproteinases that are unified by the need for zinc binding within their active-sites and their ability to act as extracellular endopeptidases[142]. MMPs act as critical mediators over cell-cell interactions, over cell-extracellular matrix interactions, and over interactions between cells and soluble factors. The MMP family proteins were originally recognized for their proteolytic activity against collagenous substrates in tadpoles[143]. More formally, the MMPs are

defined as a subfamily of the zinc metalloprotease family M10 with distinct activities against extracellular and cell-surface associated targets[142]. A closely related group of proteins are the disintegrin and metalloprotease (ADAMs) which localize to the mammalian cell membrane and function both as sheddases that cleaving other membrane-targeted substrates and as mediators over cell-cell interactions[144].

Substrate specificities distinguish the 23 MMP isoforms. The original MMPs were noted for their collagenase activity. In humans, the canonical collagenases are MMP-1, 8 and 13, while the human MMP gelatinases are MMP-2 and MMP-9. Additional substrate groups include the stromelysins (MMP-3, MMP-10, MMP-11), the matrilysins (MMP-7 and MMP-26). Although these groups help distinguish the MMPs, there is often overlap in the substrate profile, even between group members[145]. Expression of functional MMPs is highly regulated based on tissue type and physiological context. Therefore, it is now recognized that the MMPs are part of a complex cellular toolbox of extracellular proteases with diverse, though specific, biological functions[142]. For instance, MMP-1 (a collagenase) is further characterized to cleave type I collagen and fibronectin (allowing cell migration), IGFBP-3 (to increase the bioavailability of IGF1), participate in the processing of IL-1 (to dampen inflammation), and PAR1 (activation of PAR1)[146,147]. Likewise, MMP-9 (a gelatinase) is further characterized to cleave plasminogen, IL-1 (similar to MMP-1, to dampen inflammation), IL-2R (to reduce inflammation), precursor TGF, and collagen IV (to induce thymic neovascularization)[148].

Super-cellular localization and domain composition are also used to group the MMPs[145,149]. All MMPs contain a conserved signal-peptide domain, propeptide domain, and zinc-coordinating catalytic domains responsible for endopeptidase activity. The MMPs 1, 3, 8, 10, 12, 13, 19, 20 and 27 contain an additional hemopexin domain that confers substrate specificity, mediates pro-peptide activation, and me-

diates TIMP-mediated inactivation. The specific functions and substrate specificity conferred by the hemopexin domain very among individual MMPs. The gelatinase MMPs 2 and 9 contain both a hemopexin domain and a set of three repeated type-II fibronectin domains located within the catalytic domain. The fibronectin domains mediate extracellular binding with gelatin, collagen, and laminins. The MMPs-14, 15, 16, 17 24, and 25 contain a transmembrane domain (MMP-14, 15, 16, 24) or a GPI anchor domain (MMP-17 and 25) and together are referred to as the membrane-type MMPs. Most membrane-type MMPs are capable of activating pro-MMP2 and degrading collagen.

The expression and activity of MMPs are highly regulated[150]. At a tissue-level, transcription factors, especially AP-1, NFAT, and NF-κB regulate the expression of MMPs[151]. A few studies also suggest that epigenetic modifications to DNA control the accessibility of MMP genes to transcriptional machinery, though most MMPs cluster together in a small region of chromosome 11 in the absence of CpG islands[152]. Furthermore, all MMPs are translated as propeptides with a propeptide domain at their N-terminal end which covers the catalytic site of the catalytic domain. Proteolytic cleavage of the N-terminal propeptide domain is required before MMPs can become active[153] and is mediated by the action of serine proteases such as plasmin[154]. A special, though important, case of propeptide cleavage and activation is the activation of MMP-9 by MMP-3[155]. Therefore, MMPs can also act as activators of other MMPs[156,157].

MMP activity is also regulated by proteins called tissue inhibitors of metalloproteinases (TIMPs)[96,158]. TIMPs are produced and released by mammalian cells and are highly conserved among mammalian lineages. There are four TIMP genes in humans. In general, TIMP-2 and TIMP-3 are capable of inhibiting all MMPs and many ADAMs while TIMP-1 and TIMP-4 are more specific for various members of

the MMP and ADAM families. The TIMPs provide an additional level of spatial regulation over the extracellular MMPs so the ratio of MMP to TIMP concentration is a determinant over MMP activity.

The MMPs also have diverse physiological roles and MMP biology is still a very active area of research. Here highlighted are three well-described physiological roles for MMPs.

1. **Embryogenesis:** MMPs were first described in the context of tadpole development[143] and subsequent studies showed that MMPs were dramatically up-regulated during embryogenesis in humans and mouse models[159,160] . Therefore, MMPs play a critical role in tissue pattern formation and morphogenesis and are primary agents in extracellular matrix remodeling.

2. **Cell migration:** MMPs are critical for the movement of cells through tissues of the body[161,162]. One example is the movement of immune cells through tissues to the site of an infection. These immune cells secrete soluble MMPs and transmembrane-domain containing MMPs at the leading edge of cell migration to facilitate matrix breakdown ahead of the migration path[163–166].

3. **Immune modulation:** A growing body of literature describes the immune-modulating effects of MMPs[167] . In these studies, immune modulation is achieved by a combination of substrate specificity and regulation over MMP activity. The best-describe example of MMP-immune modulation is the cleavage of members of the TNF superfamily by ADAM17 and MMP-8[168–170].

In additional to the physiological roles identified for MMPs, MMPs are also implicated in disease[171]. Again, here highlighted are three examples of the roles that MMPs play in the pathophysiology of disease.

1. **Cancer metastasis:** MMPs are implicated in cancer tissue invasion and metastasis[152,172]. Cancer cells express MMPs during primary tumor cell invasion, to move through the endothelial barrier of blood vessels and into tissues during metastasis, and to promote angiogenesis.

2. **Autoimmune arthritis:** The collagenase MMPs-1 and 13 may mediate autoimmune arthritis[173]. An imbalance of the MMP-TIMP ratio at joints is driven by increased TNFα signaling to cause joint damage.

3. **Multiple sclerosis:** MMP protein concentration is increased in the CSF of patients with multiple sclerosis and in the brains of animals modeling multiple sclerosis[174]. Furthermore, experimental treatment with MMP inhibitors in models of multiple sclerosis reduced the extent of brain damage. The mechanism of MMPs influence on multiple sclerosis pathology is less clear and may involve a combination of immune modulation and enhanced penetration of immune cells through the blood brain barrier.

3.1.2 A role for MMPs in tuberculosis

Several studies implicate MMPs as a biochemical drivers of cavitation. Transcription analysis of sputum and bronchoalveolar lavage samples from patients with active tuberculosis show the increased presence of MMP transcripts compared to samples from individuals without active tuberculosis[87–89]. These observations were further supported by experiments in model systems. Volkman *et al.* demonstrated that the zebrafish homologue of human gelatinase MMP-9 helped mediate granuloma formation[90] and Ordonez *et al.*, visualized MMP-9 using *ex vivo* optical imaging in mouse lungs[139]. Finally, Elkington and Friedland have extensively investigated and discussed the pathophysiological niche for MMPs in tuberculosis[78,86,89,103,175].

Kübler and colleagues worked in a rabbit model and confirmed that MMP-1 expression was spatially organized with regions of tuberculosis lung disease. Their work also establishes the validity of the rabbit model in studies to address the proteolytic basis of cavitation. Kübler *et al.* performed RNA-seq on tissue collected from rabbits modeling cavitary disease and showed that MMP-1 transcripts increased in diseased lungs[91]. Elegantly, Kübler *et al.* also took advantage of the spatial separation between lesions enabled by the size of the rabbit lungs[91]. The investigators collected tissue from regions with varying proximity to the cavity wall and showed that there was spatial specificity to MMP-1 expression. Regions closer to the cavity wall expressed more MMP-1. These results demonstrate that MMP-1 transcripts accumulate in the areas near *M. tb*-induced lung damage suggesting that MMP-1 activity might drive tissue destruction in tuberculosis[131]. We hypothesized that if MMP-1 was the major driver of tissue matrix destruction in tuberculosis patients, then inhibiting MMP-1 should prevent cavities (Fig 2.7C).

3.1.3 Cipemastat: a potent and selective inhibitor of the collagenase MMPs

We undertook a literature search for selective inhibitors of MMPs and obtained Cipemastat (Ro 32-3555, trade name Trocade), a potent inhibitor of MMP-1. The drug was originally developed by the Roche Corporation as an anti-arthritis agent but discontinued in the 2000s[140,141]. The use of cipemastat for our studies is advantageous several reasons. It was shown to inhibit MMP-mediated tissue destruction during *in vitro* assays, in mammalian model systems, and in humans. Cipemastat is also highly specific for the collagenase MMPs 1, 8 and 13 with IC_{50} values between 3 and 4 nanomolar. By comparison, the IC_{50} values for non-collagenase MMP-3 (a stromelysin) and MMP-2 (a gelatinase) are 527 nanomolar and 154 nanomolar re-

spectively. Finally, cipemastat also had good pharmacokinetic profile in mammalian models. The T_{max} in rats is reported as 0.05 hours, a half-life of 3.8 hours, and a C_{max} of 1,492 ng/mL following single oral dose of 25 mg/kg in rats[141].

3.2 Results

3.2.1 The collagenase MMP-inhibitor cipemastat is orally bioavailable in rabbits and reaches therapeutic concentrations in the peripheral blood

We first confirmed that cipemastat did not have intrinsic anti-mycobacterial properties but was able to inhibit MMP-1 *in vitro* (Table 3.1 and Fig 3.1). Next, we conducted a pharmacokinetic study to confirm that cipemastat was orally bioavailable in rabbits and had suitable kinetics for a daily dosing regimen (Table 3.2). During the PK study, 3 rabbits were given a single oral dose of cipemastat at a concentration of 100 mg/kg of body weight, a dose that was shown to be within the tolerability and efficacy range in humans and animal studies[176,177].

Table 3.1: Results of anti-mycobacterial activity testing for cipemastat

			1	2	3	4	5	6	7	8	9	10	11
	concentration		128	64	32	16	8	4	2	1	0.5	0.25	**Bacteria**
A	cipemastat-1	% inhibition	-5.6089	-6.0562	-2.3157	-1.6928	-4.295	-5.3816	1.34171	-5.8437	-1.3343	-8.564	57338
B	cipemastat-1	raw counts	57234	57491	55483	55099	56514	57133	53420	57374	54842	58848	53265
C	cipemastat-2	% inhibition	1.91277	-1.7797	3.10479	-0.1497	0.92959	3.19534	-0.9887	-3.6629	-0.037	-0.9351	51419
D	cipemastat-2	raw counts	53132	55071	52479	54228	53634	52415	54664	56123	54196	54733	49964
E	cipemastat-3	% inhibition	-3.8459	-1.7095	-1.3343	4.02144	2.77028	5.7531	9.50286	-0.6893	2.5097	6.83792	57488
F	cipemastat-3	raw counts	56208	55049	54836	52010	52623	51006	48971	54460	52777	50408	55186
	concentration		1.28	0.6	0.32	0.16	0.08	0.04	0.02	0.01	0.005	0	
G	isoniazid	% inhibition	96.6217	95.9582	91.9848	88.7914	86.9266	86.1375	83.7812	80.3197	74.1785	-3.0105	57567
		raw counts	8742	6734	6906	7048	7561	7703	8814	10668	13971	55736	

***In vitro* inhibition of MMP-1 by cipemastat**

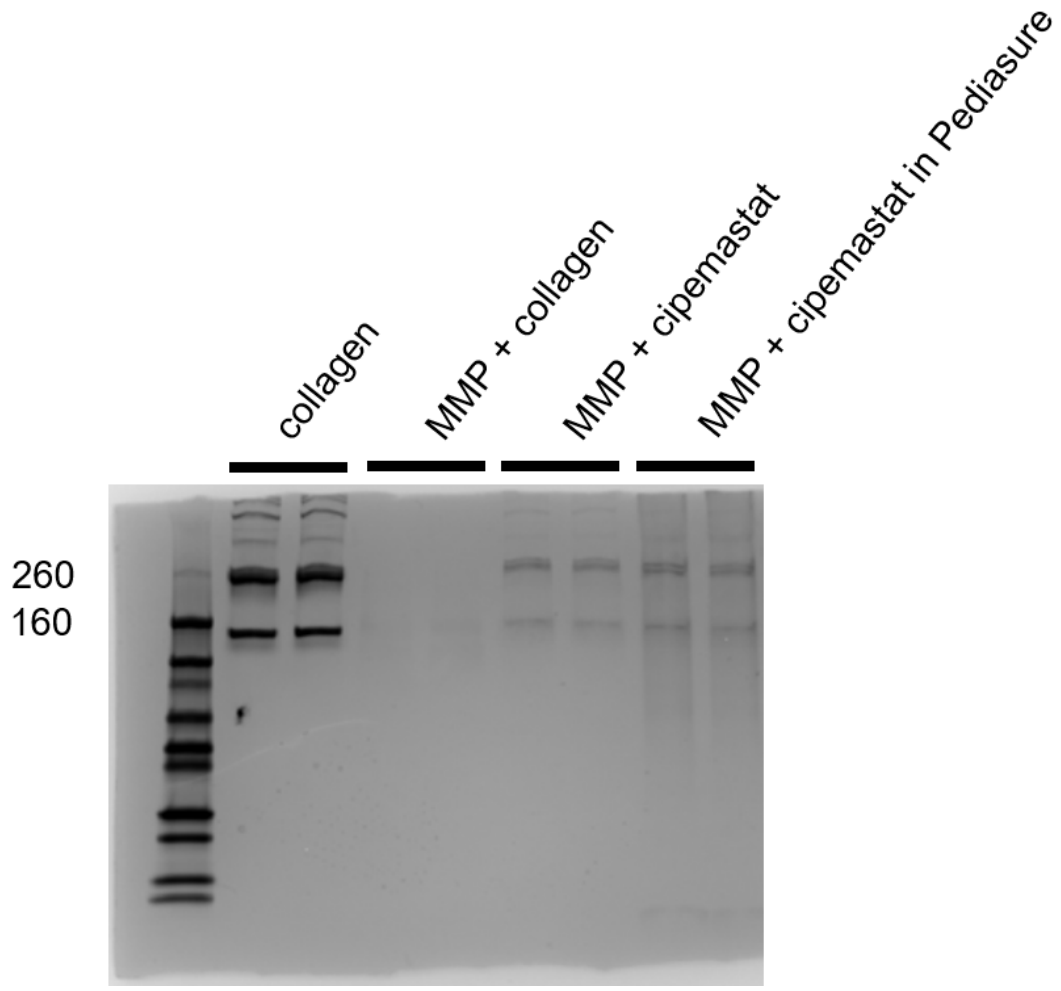

Figure 3.1: Coomassie blue stained gel electrophoresis of collagen incubated in the presence of human MMP-1, Trocade + MMP-1, and Troacade + MMP-1 in PediaSure vehicle.

The results of the PK study showed a 24-hour $AUC_{0\text{-}24\ hours}$ of 21.79 h·μg/mL (49.9 μM·h), consistent with previouly published oral dosing studies (Table 1)[176,177] (Table 3.2 and Fig 3.2). Importantly, we found that the plasma concentration remained above the published IC_{50} of cipemastat for MMP-1 at 26 ng/mL (60 nM) for 22 out of 24 hours following a single oral dose[141]. These results suggest that cipemastat shows good oral bioavaliability in rabbits and confirms that a daily dosing regimen is sufficient to maintain plasma concentration levels above the IC_{50} during most of a 24 hour period.

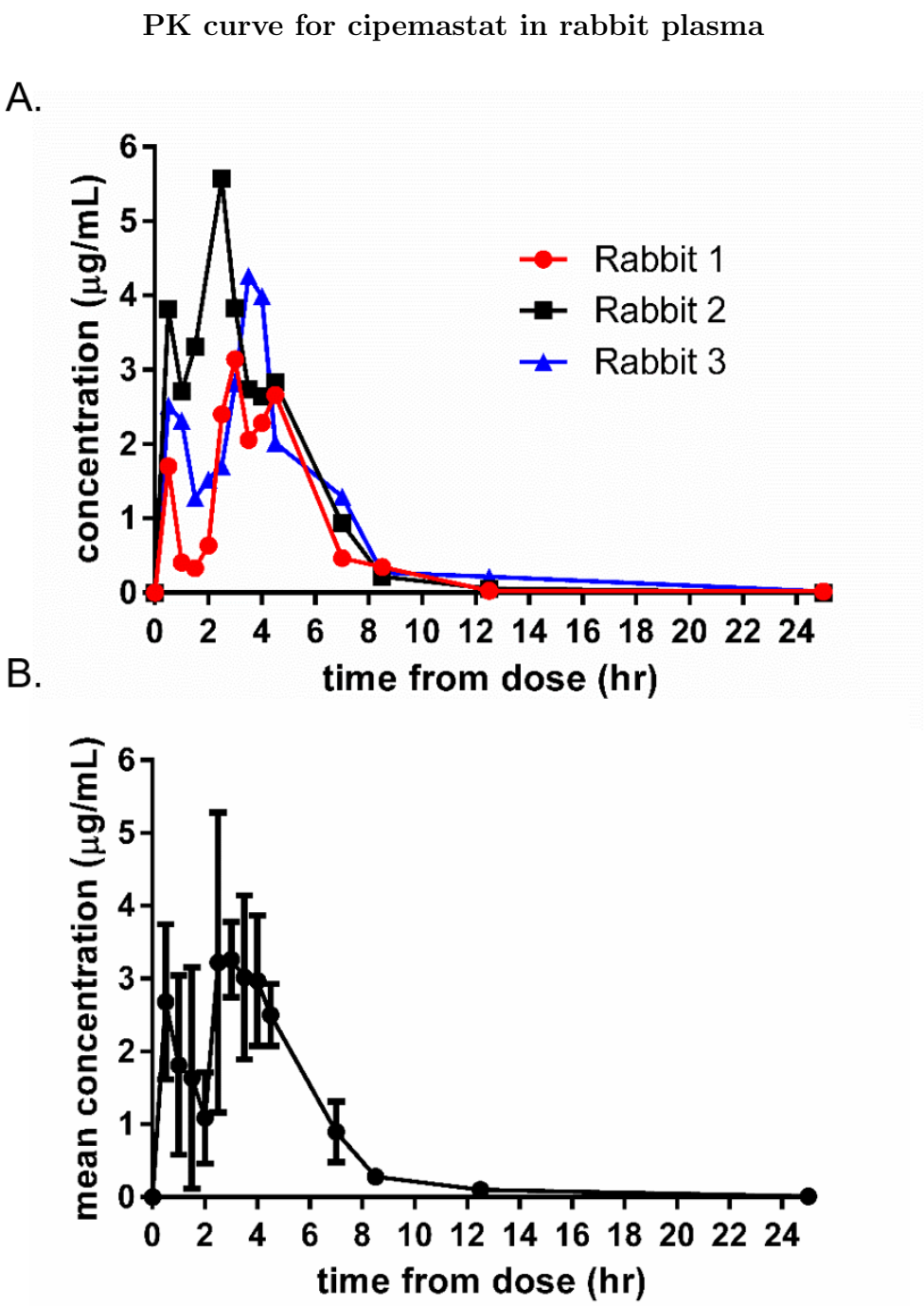

Figure 3.2: Plasma concentration curves of cipemastat in rabbit plasma following a single oral 100 mg/kg dose. (A) Graph showing traces for individual rabbits in the PK study. (B) Graph showing a curve representing the arithmetic means with standard-error bars of PK curves from the three rabbits shown in A.

Table 3.2: Pharmacokinetic data for cipemastat in rabbit plasma showing mean curve attributes following a single oral bolus dose of 100 mg/kg.

	parameter			
drug	**ACU$_{0\text{-}24}$ (hr·μg/mL)**	**C$_{max}$ (μg/mL)**	**T$_{max}$ (hr)**	**T$_{1/2}$ (hr)**
cipemastat	19.92 (16.42-23.44)	3.02 (1.99-4.44)	2.47 (1.98-3.07)	1.87 (1.22-2.23)

Note: Ranges in parentheses correspond to ± 1 standard error of the mean.

3.2.2 Cipemastat monotherapy did not protect against extensive lung destruction and cavitation

We randomized 18 rabbits into an vehicle group (n=8) and a cipemastat group (n=10). All rabbits received 1 mL of PediaSure per kilogram of body weight. Rabbits in the cipemastat group received 100 mg/kg of cipemastat in PediaSure, the same dosed that was validated during our PK study. Cipemastat was given orally from study weeks 5 through 10. This treatment window was consistent with the five weeks preceding the maximum frequency of cavitation and the time during which we predict that pathologic lesions will undergo matrix depletion (Fig 3.3). Two rabbits were excluded from our analysis due to poor adherence to oral dosing. One rabbit was excluded from the cipemastat group and one rabbit was excluded from the vehicle group. Our results are based on 7 control group rabbits and 9 cipemastat treated rabbits.

During weeks 7, 9, 12 and 14 we performed breath-hold computerized tomography (CT) scans on all study rabbits. These CT scans revealed no difference in the number of cavities or severity of cavitation between the control and treatment groups throughout the study (Fig 3.4 and Fig 3.5A, 6B). We did notice a repeated trend toward worse cavitary disease among rabbits in the cipemastat-treated group. The animals were sacrificed during week 14 and the lungs were fixed and scored for disease severity by two independent blinded observers (Fig 3.5C). We also quantified the extent of disease within the lungs by cutting the lungs in serial sections in the transverse plane and reporting the overall percentage of all lung slices with grossly visible disease (Fig 3.5C). Neither severity scoring nor disease quantification showed a difference between experimental groups.

3.2.3 Collagen content at cavity walls was not changed by cipemastat treatment

Tuberculosis lung lesions are often encircled by a fibrotic wall[132]. This pathologic matrix deposition is also a feature of rabbits modeling cavitary tuberculosis (Fig 2.7B and Fig 3.5D). Since cipemastat inhibits collagenase activity, we predicted that cipemastat administration should increase the collagen content around tuberculosis lesions. We used hue-thresholding to quantify the amount of collagen identified in blue by applying Masson's trichrome stain to formalin-fixed parafin-embedded lung sections of cavities (Fig 3.5D). Using this method we were unable to identify any difference in the collagenous content of cavity walls suggesting that cipemastat treatment did not change the phenotype of pathologic collagen accumulation around cavities in the rabbit model (Fig 3.5D).

3.3 Discussion

We took advantage of the repetitive aerosol exposure model to screen cipemistat, a potent and specific MMP-1 inhibitor, as an inhibitor of cavitation[141]. Our study was supported by a molecular phenotype in which MMP-1 expression increased around tuberculous lesions with central matrix destruction[131]. In these experiments, we administered cipemistat for four weeks preceding the development of caseous and cavitary lesions in the repetitive aerosol model. However, our results did not show a reduction in cavitation or disease severity.

As part of our investigations, we confirmed that the plasma concentrations of cipemistat were well above the IC_{50} during the 24 hour dosing cycle. We did not sample the concentration of cipemistat in tuberculosis lesions, therefore it is possible

that cipemistat did not reach inhibitory concentrations within granulomas undergoing matrix destruction. Furthermore, MMP activity may be highly localized in pericellular niches[178]. Alternatively, MMP-1 may act in conjunction with other extracellular collagenases to drive matrix depletion and that the inactivation of MMP-1 did not appreciably change the dynamics of cavity formation, reflecting redundancy in the proteolytic cascade. Finally, it is possible that MMP-1 is not a mediator of matrix depletion and cavitation. The increased expression of MMP-1 at tuberculosis lesions may be purely associative or indicate another role for MMP-1 in the pathobiology of tuberculosis.

3.3.1 Reconsidering the role of MMPs in tuberculosis lung pathology

The results presented in this chapter show that cipemastat monotherapy of 100 mg/kg by body-weight was unable to protect against cavitation in a rabbit model of cavitary tuberculosis. It is possible that MMPs are not the primary mediators of extracellular matrix destruction. Conversely, the introduction highlights a large body of literature supporting a role for MMPs in tuberculosis[89,90,103,131]. Recent investigations highlight MMPs as immune-modulators by acting as extracellular cytokine sheddases[167]. Therefore, it is possible that MMPs act as mediators over the immune response to tuberculosis rather than at the final step in matrix breakdown. One attractive hypothesis concerns the circular effects of MMP activation and TNFα production. MMP expression is driven by inflammatory cytokines including TNFα, but MMPs also show proteolytic specificity for pro-protein members of the TNFα family of inflammatory molecules. It is possible that MMP activity in tuberculous lesions is responsible for TNFα activation. A roll for MMPs as the primary mediators of TNFα activation may help explain our observation that cipemastat treatment was associated with a trend

toward worse disease and cavitation during our rabbit study. Further investigations are needed to clarify the contributions and redundancies of individual MMPs to lung inflammation in tuberculosis[179].

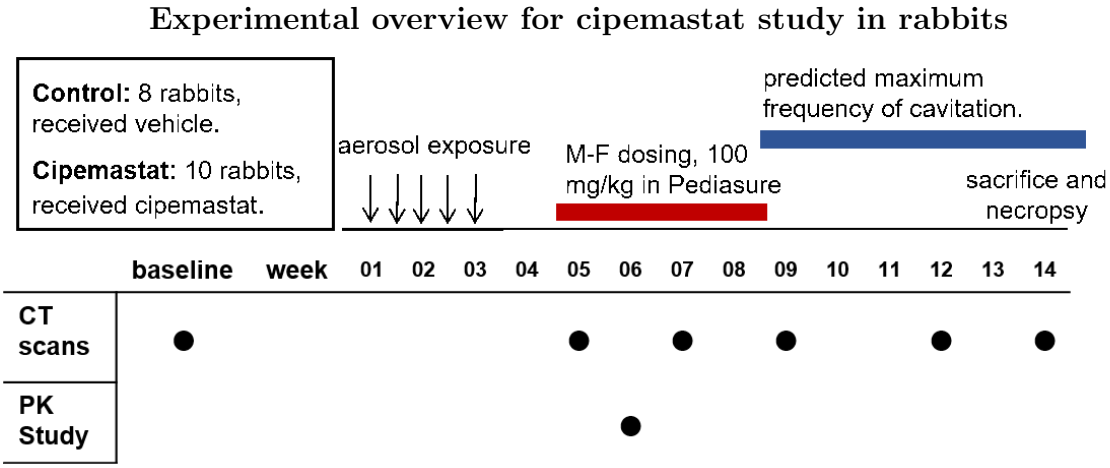

Figure 3.3: Experimental overview to investigate the pharmacologic inhibition of tissue destruction and cavitation using cipemastat in rabbits infected with *M. tb*.

Comparison of fixed lungs from control rabbits and rabbits treated with cipemastat

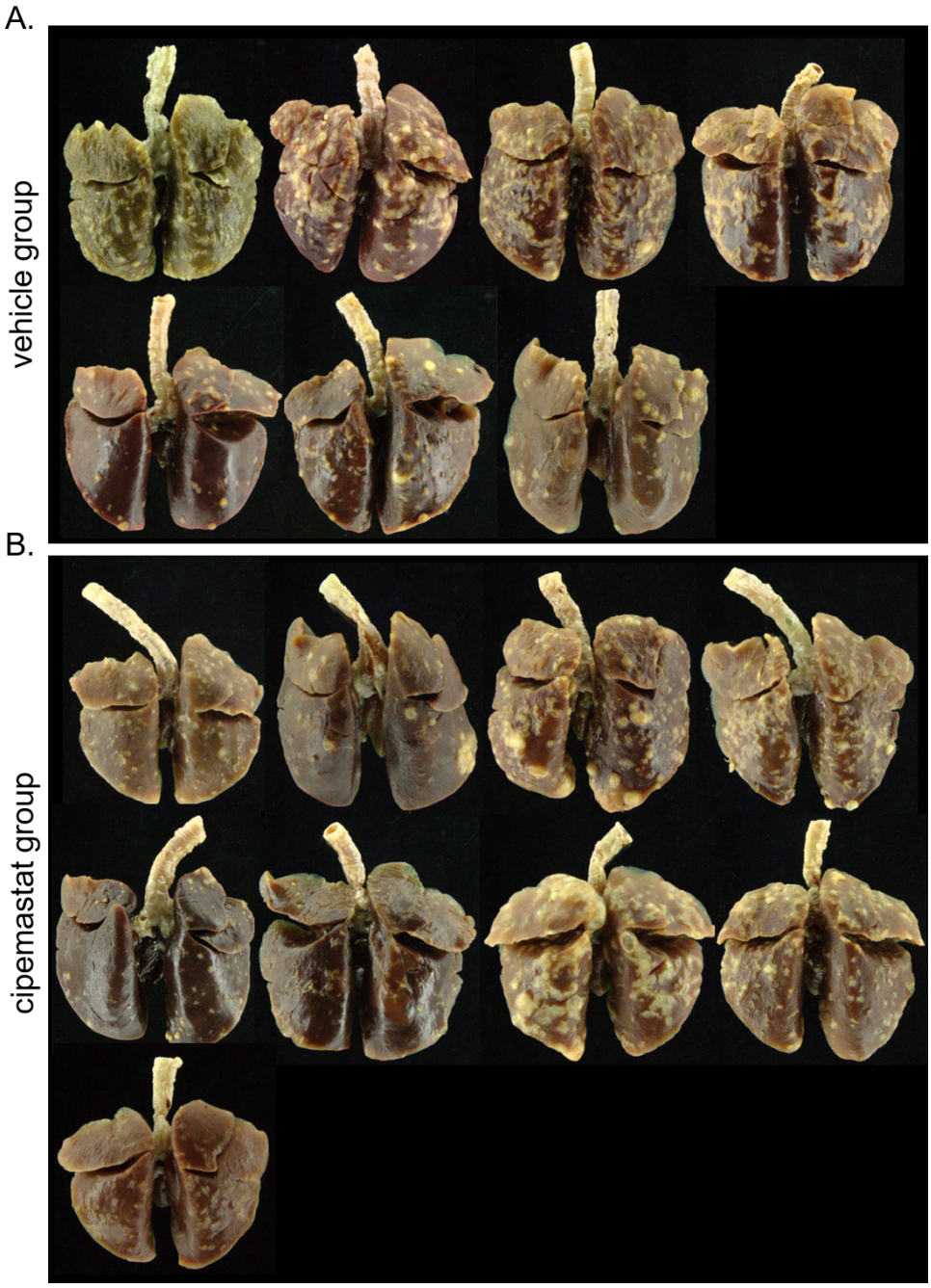

Figure 3.4: Comparison of fixed lungs from control rabbits and rabbits treated with cipemastat. Gross images of formalin fixed lungs showing the dorsal aspect of the lungs. (A) Lungs from rabbits in the vehicle treated group. (B) Lungs from rabbits in the cipemastat treated group.

Disease severity and cavitation in cipemastat treated rabbits compared with controls

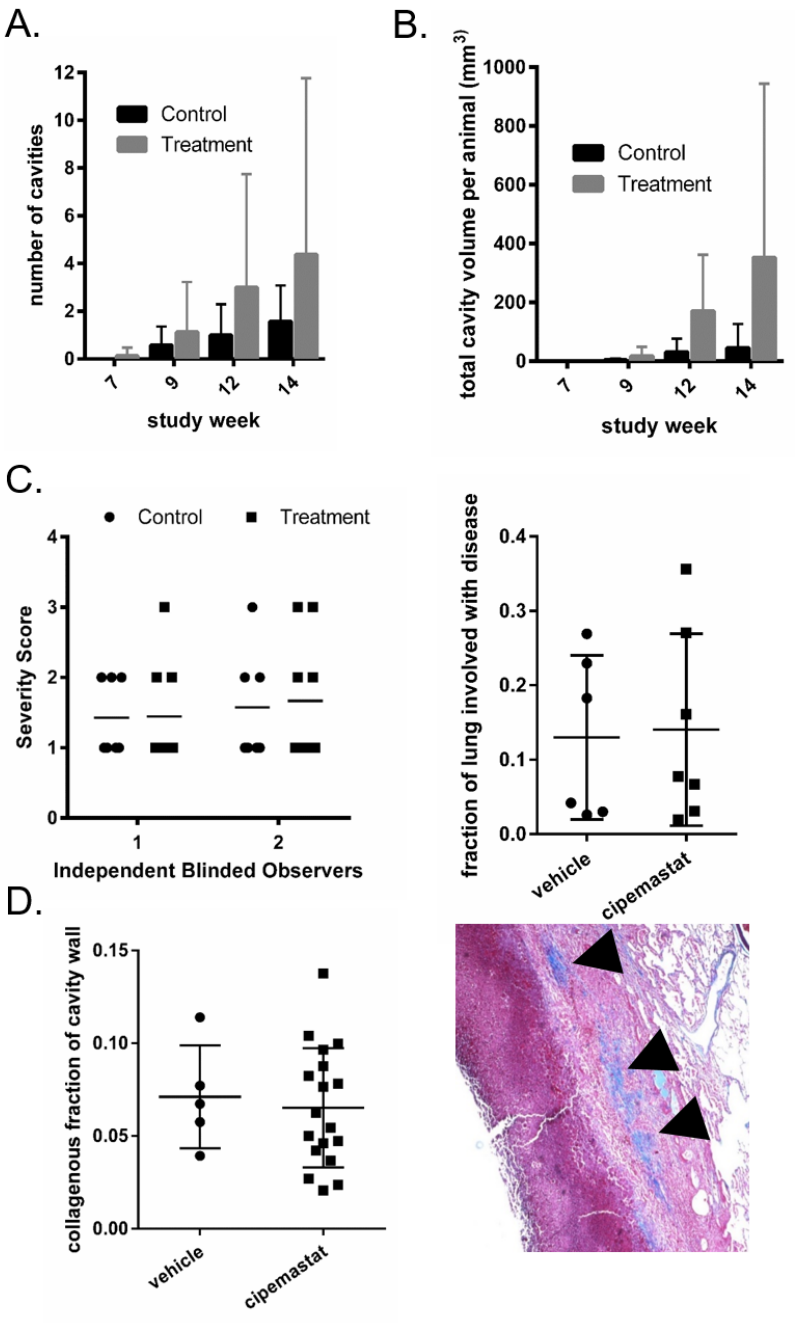

Figure 3.5: The extent of disease severity and cavitation in cipemastat treated rabbits compared with controls. (A) Average number of cavities per animal for weeks 7, 9, 12 and 14. (B) Average volume of the lung identified as cavity volume by CT-scan and segmentation analysis for weeks 7, 9, 12 and 14. (C) Disease severity scores of lungs assigned subjectively by two independent blinded observers and quantified as the fraction of lung identified as disease in transversely splayed lungs. (D) Quantification of collagen accumulation at the walls of cavities in *M. tb*-infected rabbits. The example of a cavity wall shows regions identified as collagen.

Chapter 4

Preliminary studies on the use of odanacatib to inhibit cathepsin K during cavity formation in the rabbit model

Michael E. Urbanowski · Kristina Bigelow · Kevin Bock · Marlene Orandle · André Kübler · William R. Bishai

"In my own studies on tuberculosis I began by using the known methods, without success. But several casual observations have induced me to forego these methods and to strike out in a new direction, which has finally led me to positive results"

by Robert Koch.
translated from German
Die Ätiologie der Tuberkulose (1882)

4.1 Introduction

The collagenase MMPs and cathepsin K are the two lead candidates for molecular mediators of tissue matrix destruction in tuberculosis identified by Kübler *et al*[91,131]. In the previous chapter we tested whether inhibition of the collagenase MMPs was able to reduce tissue destruction and prevent cavitation. Our findings showed that MMP inhibition did not reduce the occurrence or extent of cavitation in our model system and suggest that MMP may not be a key mediator in the tissue destruction phenotype that enables cavitation in tuberculosis. Therefore, in this chapter, we turn our attention to the second lead candidate mediator, cathepsin K.

Here we provide a series of preliminary experiments aimed to further understand the role of cathepsin K in tuberculosis lung destruction. During our investigations, we also obtained a small molecule inhibitor of cathepsin K, odanacatib, through a drug grant from Merck. We conducted a single oral bolus dosing study and show the pharmacokinetic profile of odanacatib in rabbit plasma. We next used these data to drive a repetitive dosing predictive model to identify steady-state plasma concentration. This model provides the basis for a proposed rabbit study using odanacatib to inhibit cathepsin K *in vivo*. In the final section of this chapter we propose a study designed to address whether cathepsin K is the critical mediator of lung matrix destruction in tuberculosis.

4.1.1 The biology of cathepsin K

Cathepsin K is a member of a group of human cathepsins[180]. The term "cathepsin" is derived from the greek word "kathepsein" meaning "to digest," but does not imply homology among the cathepsin proteases[181]. The term was derived from ini-

tial studies that identified the cathepsins as enzymatic mediators of protein digestion in lysosomes. Indeed, the cathepsin family is divided by differences in the cleaved residue on target proteins. Cathepsins B, C, F, H, K, L, O, S, V, W, and X are cysteine proteases. Cathepsins A and G are serine proteases. Finally, Cathepsins D and E are aspartic proteases. The cysteine cathepsin sub-group are a homologous group of proteins and are further divided as endopeptidases (cathepsins F, K, L, S and V), carboxypeptidases (cathepsin X)[180,182], dipeptidyle peptidase (cathepsin C), aminopeptidases (cathepsin H), or peptidyl dipeptidases (cathepsin X). Formally, the cysteine cathepsins are classified as the papain-like C1 family proteins of the CA superfamily of proteases[181].

Most of the cysteine cathepsins are expressed in all cells of the human body, but the expression of cysteine cathepsins K, S, V and W is restricted based on physiological context. Cathepsin K is predominately expressed by osteoclasts and synovial fibroblasts, but also to a lesser degree in hematopoietic epithelial and fibroblast cells[180,183–185]. The gene for cathepsin K is *CTSK* and is located on a central region of chromosome 1. At the cell level the cysteine cathepsins are found in both the lysosomes and in the extacellular compartment as secreted proteins. These localizations are consistent with two roles for the cysteine cathepsins. First, they act as digestive proteins in lysosomes. Second, they have physiological roles as extracellular proteases.

Cathepsin K was originally noticed for its robust ability to cleave bovine skin collagen during *in vitro* assays[98,186,187]. Compared with the other cysteine cathepsins, cathepsin K has the strongest proteolytic activity against collagen[94]. Congruent with these observations, cathepsin K is the only cysteine cathepsin able to cleave both non-helical and triple-helical collagen conformations under the physiological conditions of the extracellular environment[188–190]. Therefore, the contemporary perspective on cathepsin K is as the primary protein mediators of bone-matrix breakdown

by osteoclasts[191].

Although the physiological role of cathepsin K was established in the 1990s, a corresponding biochemical model was not formalized until the late 2000s. Part of the reason for the delay was a set of seemingly paradoxical biochemical observations. First, cathepsin K showed biochemical activity in the range pH 7.0 — pH 5.0[98,188,189,192] with optimal activity at lysosomal pH, but significantly lower activity closer to pH 7.0 at the pH of the extracellular environment[193]. This observation was consistent with the lysosomal role of cathepsin K but did not explain the strong collagenase activity observed outside the cell. The second observation was based on the amino acid sequence of cathepsin K. Investigators noticed that cathepsin K and closely related cathepsin L contained an allosteric globular region enriched with positively-charged amino-acids[192,194]. This spatially ordered positively-charged region was distinct from other cysteine cathepsins. Finally, studies on cathepsin L revealed that the allosteric positively-charged surface of cathepsin L-like proteins was optimal for binding to negatively-charged glycosaminoglycans (GAGs) and that the binding of GAGs to cathepsin L caused the optimal proteolytic activity to shift towards pH 7.0[94,195,196]. These findings were later confirmed for cathepsin K[192,194,197,198].

The current biochemical model for cathepsin K activity is based on compartment-specific control mediated by pH and GAG binding to cathepsin K. Cathepsin K is translated in the endoplasmic reticulum and trafficked through the Golgi apparatus as a proenzyme with a pro-peptide occluding the active site. This mechanism of pro-enzyme inhibition is conserved among the cysteine cathepsins[95,199]. The cysteine cathespins are then trafficked as proenzymes from the Golgi to the acidic lysosome. The acidic lysosome confers a higher degree of molecular movement on the cysteine cathespsins and this higher degree of molecular movement mediates activation. Among the milieu of cysteine cathepsins in the lysosome is cathepsin B.

Pro-cathepsin B in the acidic environment has enough molecular instability to switch between a closed (inactive) and an open (slightly active) protease form[200,201]. The slightly active protease form is enough to cleave the pro-peptide from of a nearby cysteine cathepsin, leading to chain-reaction auto-activation in the lysosome. For cathepsin K, the proenzyme form is a 37 kDa molecule that is cleaved to an active 27 kDa enzymatically active protein[191].

Following secretion and in the extracellular compartment, cathepsin K returns to a basal level of activity at pH 7.2. The binding of a negatively-charged collagen-matrix associated sulfated-GAGs chondroitin-4-sulfate, chondroitin-6-sulfate, dermatin sulfate, or hyaluronan at the allosteric positively-charged surface site increases the stability of the cathepsin K substrate interaction enough to promote optimal activity at neutral pH[198,202–204]. Therefore, environmental specificity is a major regulatory factor over cathepsin K activity. It is also likely that the GAG-cathepsin K complex is self-potentiating since the cleavage of collagen matrix releases more GAGs into the peri-cellular environment[205]. Additional specificity is conferred by cathepsin K specific active-site confirmation that enables binding to triple-helical collagen[190].

Cathepsin K is also susceptible to proteolytic inactivation. The major protein inhibitors of the cysteine cathepsins are the cystatins, thyropins and serpins[181], but the major mechanism of extracellular cathepsin K inhibition is auto-proteolytic degradation[192]. Therefore, cathepsin K activation is tightly regulated in the extracellular environment by substrate-specific factors while inactivation is controlled by self-limiting proteolytic degradation by cathepsin K and other endopeptidases in the extracellular environment.

Cathepsin K is the predominant protein mediator of bone absorption, but it is also implicated in several diseases. Inactivating or partially inactivating mutations in cathepsin K lead to pycnodysostosis, a congenital disorder characterized by atypically

dense and brittle bones[206]. Increased activity in adults is also thought to be a primary driver of osteoporosis[180].

4.1.2 A role for cathepsin K in tuberculosis.

As mentioned in the introduction, cathepsin K was identified as a candidate biochemical mediator of lung-matrix destruction by an RNA-seq study in rabbits modeling cavitary tuberculosis[91]. Several additional lines of evidence suggest a role for cathepsin K in lung matrix destruction during tuberculosis.

1. **Cathepsin K protects against pathologic pulmonary fibrosis.** Bhling *et al.* used mice deficient in cathepsin K production ($CTSK^{-/-}$ mice) in a drug-inducible model of pulmonary fibrosis[207]. Their investigations showed that the induced fibrosis in $CTSK^{-/-}$ mice was worse than in $CTSK^{+/+}$ mice. When cathepsin K overexpressing mice were used in similar experiments, cathepsin K overexpressing mice showed less pathologic fibrosis than wild-type mice[208]. The investigators concluded that cathepsin K was protective against pathologic fibrosis.

   Tuberculosis is a classic example of granulomatous pneumonia common to pathogenic pulmonary insults that cannot be readily cleared by the immune system. Granulomas may persist for months or years within the lungs of those with tuberculosis, and often the alveolar architecture within a granuloma is first degraded and then replaced with fibrotic collagen filaments. Therefore, cathepsin K may play a pivotal role in degrading the extracellular matrix of the lung during pathologic insult.

2. **Cathepsin K gene transcripts accumulate in the lungs of patients**

with necrotic tuberculosis granulomas. Kim *et al*, found that cathepsin K expression was increased in lungs of individuals with tuberculosis granulomas[88]. This study shows that cathepsin K is transcriptionally upregulated as part of the host response to *M. tb* infection and concentrates within granulomas.

3. **Multinucleated giant cells from tuberculosis lungs express cathepsin K.** Park *et al.*, stained granulomatous lesions from tuberculosis patients and showed that multinucleated giant cells within granulomas express cathepsin K[92]. Multinucleated giant cells are thought to occur by the fusion of macrophages and although they are not pathognomonic for tuberculosis, they are commonly observed in tuberculosis granulomas. The observation that multinucleated giant cells express cathepsin K is particularly interesting finding since osteoclasts and multinucleated giant cells share a common monocytic progenitor cell as part of their lineages of differentiation[209].

4. **Cathepsin K plasma protein levels are elevated in patients with tuberculosis.** Kübler *et al.*, performed ELISAs on sputum-culture confirmed patients with active tuberculosis and healthy blood-donor control patients and found that the plasma levels of cathepsin K were significantly higher in individuals with tuberculosis[91].

5. **Cathepsin K gene expression is regulated downstream of TNFα signaling and other common immunological pathways.** The control of cathepsin K gene expression was characterized in osteoclasts[101]. These studies show that cathepsin K is regulated along a RANKL/NFAT signaling axis. RANKL is part of the TNFα superfamily, and TNFα was also shown to influence osteoclast development and stimulate cathepsin K production.

   The members of the TNFα superfamily of signaling molecules are also common pro-inflammatory signaling molecules and have been shown to drive granuloma

development in tuberculosis[210].

6. **Dannenberg *et al.*, identified cathepsin proteases as likely mediators of tissue breakdown.** Work done by the laboratory of Arthur Dannenberg and collaborators in the 1970s independently identified lysosomal cathepsins as potential mediators of tissue destruction in tuberculosis[83,84,211].

7. **Mineralization and ossification of tuberculous lung lesions is a well-described outcome during chronic infection.** Finally, we highlight that calcification (sometimes termed ossification) is a well-described development in persistent tuberculous lung lesions. Although purely associative, it is interesting to consider that chronic insult and cytokine production may create a metaplastic osteogenic site in the lungs[14,27].

4.1.3 Odanacatib: a potent and selective inhibitor of rabbit and human cathepsin K

We are interested in cathepsin K with two objectives in mind. First, cathepsin K may be the critical mediator over lung matrix destruction in tuberculosis. This objective is part of our ongoing studies aimed at identifying the critical mediators of lung matrix destruction in tuberculosis. Second, cathepsin K may be a clinical target for host-directed therapy in tuberculosis. We hypothesize that the inhibition of cathepsin K will promote lung matrix stabilization during the inflammatory response in granulomas, thereby preventing cavitation and disease transmission.

To test our hypothesis, we looked for a potent, selective, and bioavailable inhibitor of cathepsin K. Many cathepsin K inhibitors have been synthesized during the past 20 years[212]. Considering that cathepsin K is the focus of our hypothesis, we are interested in several properties:

1. selectivity for cathepsin K over the other conserved cathepsins.

2. activity against rabbit cathepsin K.

3. activity again human cathepsin K.

Our literature review revealed odanacatib as a well tolerated, potent, and selective inhibitor of cathepsin K in human studies[213,214]. During our search we also considered several other related molecules including L-87372448[215] and its parent molecule, L-00623549[216] as a relatively selective cathepsin K inhibitor. These small molecules were advantageous because they were relatively selective against human and murine cathepsin K and had previously been tested as pre-clinical agents in mammalian models. Therefore, the use of these molecules meant that we could also employ mouse models as part of our experiments[217].

Odanacatib was selected as the highest-priority small-molecule inhibitor of cathepsin K for our investigations. This selection was based on several considerations. First, the IC_{50} of odanacatib against human cathepsin K is 0.2 nM. Strikingly, IC_{50} of odanacatib against rat and mouse cathepsin K is nearly 500 times higher[212]. Furthermore, the rabbit model is advantageous because rabbit cathepsin K shows high sequence homology with human cathepsin K (94% in rabbits versus 87% in mouse and 88% in rat)and because Gauthier *et al.* (2008) showed that the IC_{50} of odanacatib for rabbit cathepsin K was similar to that of human cathepsin K (1.0 nM for rabbit cathepsin K versus 0.2 nM for human cathepsin K)[213]. Finally, ovariectomized rabbits were recently used to model osteoporosis and treated with odanacatib to show biological effect[218,219]. Therefore, we reason that the use of odanacatib to inhibit cathepsin K in the rabbit model of cavitary tuberculosis is an appropriate system for this study from both a pathologic and biochemical perspective.

Odanacatib was also advantageous because it was shown to be well-tolerated

during dosing in both mammalian and human studies[214,218,220,221]. Odanacatib was developed by the Merck corporation as a treatment for osteoporosis. The drug was terminated during phase III clinical trials due to an unacceptable risk of stroke[222]. During all clinical trials, odanacatib continued to show clinical efficacy in reducing bone matrix depletion.

4.2 Results

4.2.1 Cathepsin K expression is increased following *in vitro* infection of macrophages with *M. tb*

We began our studies on cathepsin K in tuberculosis pathology by asking whether increased cathepsin K gene expression was a feature of a global transcriptional response to infection by *M. tb*. We used unstimulated murine J774 macrophages, a common laboratory macrophage line, for our *in vitro* studies. Macrophages were seeded onto 6-well plates at a concentration of 10^5 cells/mL and exposed to approximately 10^6 bacilli to cause a multiplicity of exposure of 1:10. The multiplicity of exposure was carefully chosen following a series of careful titration experiments to yield >90% macrophage viability after 24 hours. During our experiments, the supernatant was washed after a four-hour infection period and the infected macrophages were allowed to incubate for an additional 24 hours. RNA was extracted from all wells of the experiment and transcript levels were determined by Q-PCR (Fig 4.1).

The results of three biological replicates demonstrate that cathepsin K transcription was greater in macrophages infected with *M. tb* compared with media-wash controls (Fig 4.1B). In our panel, cathepsin B and cathepsin C transcription was

In vitro Cathepsin K gene transcription changes following macrophage infection by *M. tb*

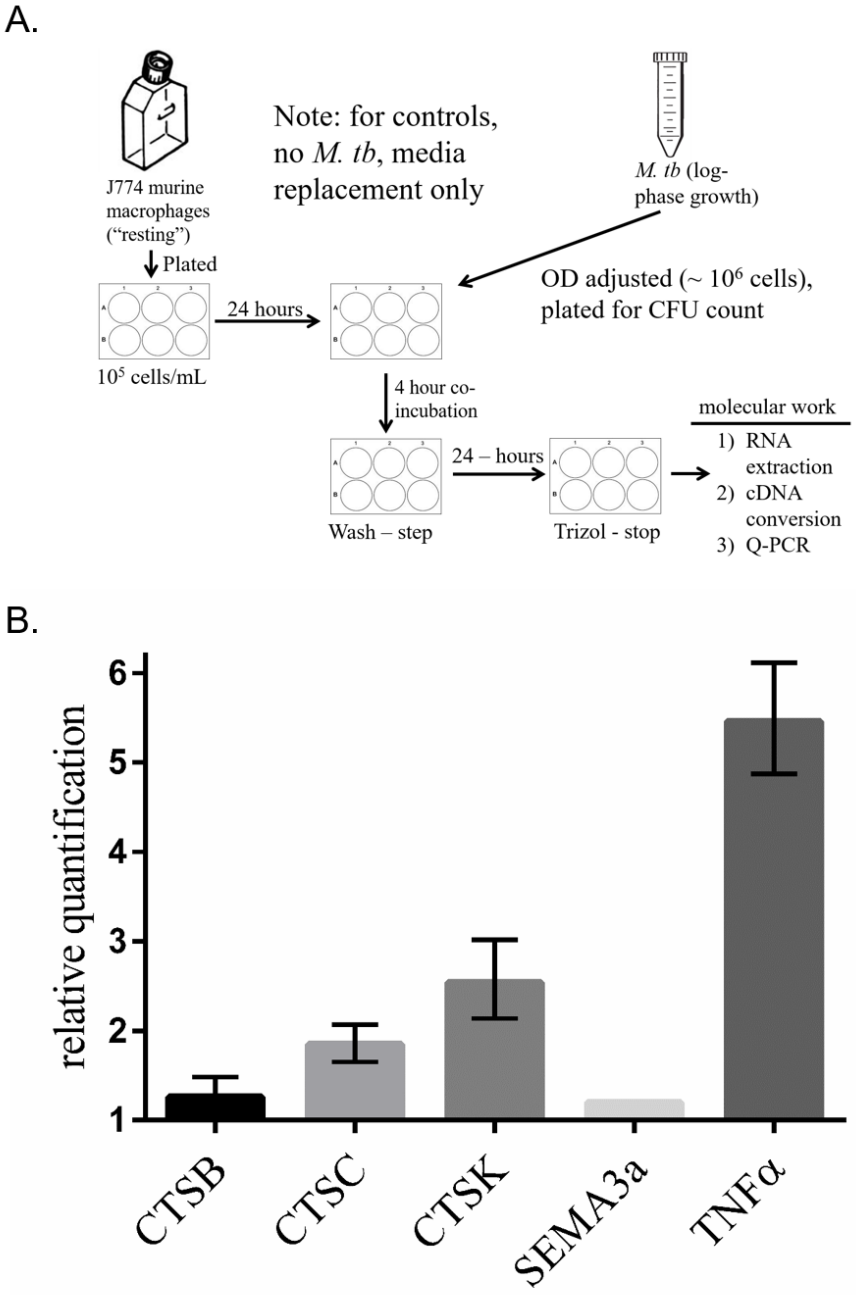

Figure 4.1: The influence of *in vitro M. tb* infection on cathepsin K transcription in macrophages. (A) Overview of *in vitro* macrophage infection study design. (B) Relative accumulation of selected gene transcripts assessed by Q-PCR in infected macrophages. All fold-changes are given relative to uninfected sham-treated (media exchange) controls.

also increased, but to a lesser extent than cathepsin K. As a negative control, we probed the transcriptional changes in SEMA3a, a protein implicated in control over neuronal growth. The levels of SEMA3a were not changed following *M. tb* infection. We used TNFα gene transcription as a positive control and noted that TNFα was highly upregulated following *M. tb* infection. Taken together, these results indicate that cathepsin K transcription is increased in macrophages following *in vitro* infection with *M. tb*.

4.2.2 Immunohistochemistry staining shows that cathepsin K is enriched in the walls of rabbit cavities.

We next asked whether cathepsin K could be detected in the lungs of rabbits infected with *M. tb* and whether the spatial distribution of cathepsin K was focused at the sites of granulomas and the walls of cavities. We obtained fixed tissue samples from rabbits modeling tuberculosis cavities and stained these tissue sections using an anti-human cathepsin K antibody (Fig 4.2).

The pattern of staining revealed that cathepsin K was enriched in the walls of cavities. Staining was not observed, as expected, in the necrotic zone of the cavity (Fig 4.2D). As a control, we also stained tissue sections without a primary anti-human cathepsin K antibody and confirmed that these slides showed no staining consistent with the signal from vulcan fast red chromogen used during these experiments (data not shown). These results demonstrate that cathepsin K protein is enriched in the walls of cavities and provides further evidence that cathepsin K expression is upregulated in the lungs during the granulomatous response to *M. tb* infection.

Anti-cathepsin K immunohistochemisty staining of rabbit cavity walls

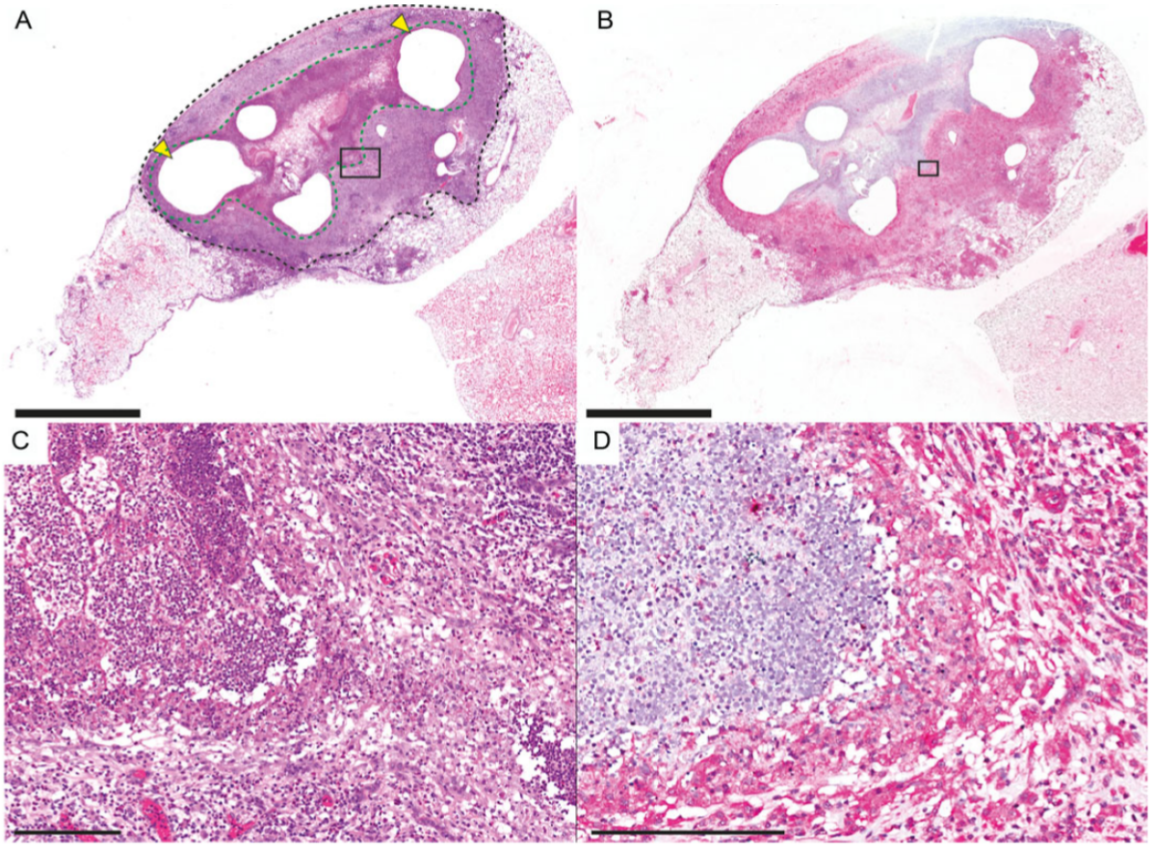

Figure 4.2: Anti-cathepsin K immunohistochemisty staining of rabbit cavity walls. (A) H&E staining of cavity from a rabbit infected with *M. tb*. Black dashed line indicates the boundary of granulomatous pneumonia. Green dashed line indicates the boundary of necrosis. Yellow arrows indicate cavity space. (B) A serial section with A, stained with anti-cathepsin K. The chromogen is vulcan-fast-red. Scale bars for A and B = 5 mm. (C) Enlarged area from the box drawn in A. (D) Enlarged area from the box drawn in B. Scale bars from C and D = 200 μm.

4.2.3 Cathepsin K transcripts accumulate in the cavity walls of rabbits modeling tuberculosis cavities.

Our previous results indicated that cathepsin K was expressed in the lungs of rabbits infected with *M. tb* and that the highest expression levels coincided with granulomatous inflammation and in the walls of cavities. Next, we performed a survey of cathespin K gene expression in a similar method to the survey performed by Kübler *et al*[91]. We modeled cavities using a bronchoscope to deliver a high concentration of *M. tb* bacilli directly into the lungs. Kübler previously characterized this model to show pathologic patterns consistent with tuberculosis cavitation[56]. Rabbits underwent cavitation one month following bronchoscopic inoculation and we extracted tissue from the rabbit lungs at varying distances from the walls of cavities. We then extracted RNA from these samples and performed Q-PCR analysis to assess the relative enrichment of cathespin K transcripts (Fig 4.3).

We compared tissue from normal-appearing lung regions to tissue close to cavity walls and tissue from the cavity walls and saw that tissue close to the cavity wall and from the cavity wall showed increased levels of cathepsin K gene expression. From these experiments, we concluded that the rabbit response to *M. tb* infection included a phenotype with increased cathepsin K expression, similar to the pattern observed in tuberculosis.

4.2.4 Plasma concentrations of odanacatib in rabbits following a single oral bolus dose confirms suitable pharmacokinetics for *in vivo* studies.

We wrote and received a drug grant from Merck to investigate the effects of odanacatib-mediated cathepsin K inhibition on tuberculosis cavitation. From this grant, we

Relative abundance of cathepsin K transcripts in the walls of rabbit cavities

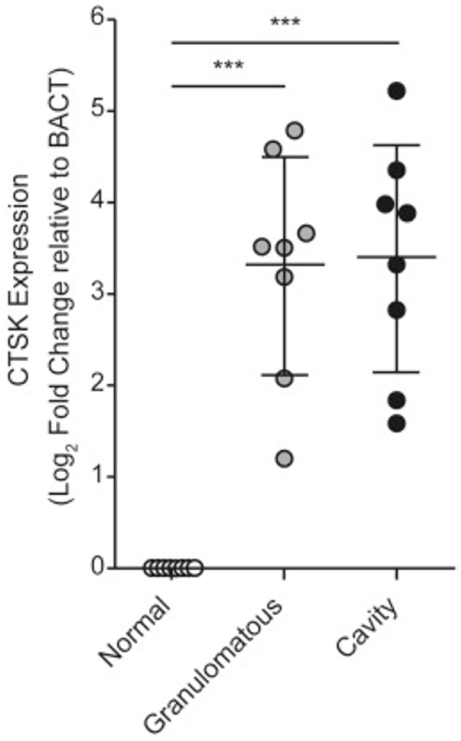

Figure 4.3: Relative abundance of cathepsin K transcripts in the walls of rabbit cavities compared to areas not involved with disease. Relative abundance of transcripts was assessed by Q-PCR.

received 150 grams of odanacatib for our study. We began our investigations by performing a single oral bolus dose pharmacokinetic study. During this study, we administered 5 mg/kg odanacatib *per os* in corn oil to three rabbits. This dose was similar to the dose of odanacatib used during human studies and was shown to be safe, tolerable, and efficacious[214]. We collected plasma from rabbits at various time-points following dosing according to our study plan. The plasma samples were analyzed using a liquid-chromatography mass-spectrometry protocol optimized for the detection of odanacatib (Fig 4.4).

The results of our initial PK study showed that 5 mg/kg oral dosing achieved a C_{max} of 284 nanomolar and this was consistent with previously published results following scaled dosing in humans[214] (Table 4.1). However, our study reported a significantly longer period between dosing and C_{max} with a T_{max} of 72 hours compared with 10 hours reported by Stoch *et al*[214]. We hypothesize that this difference may be due to the use of corn oil which is known to delay uptake of drugs in rabbits.

Concentrations of odanacatib in plasma following a single oral dose

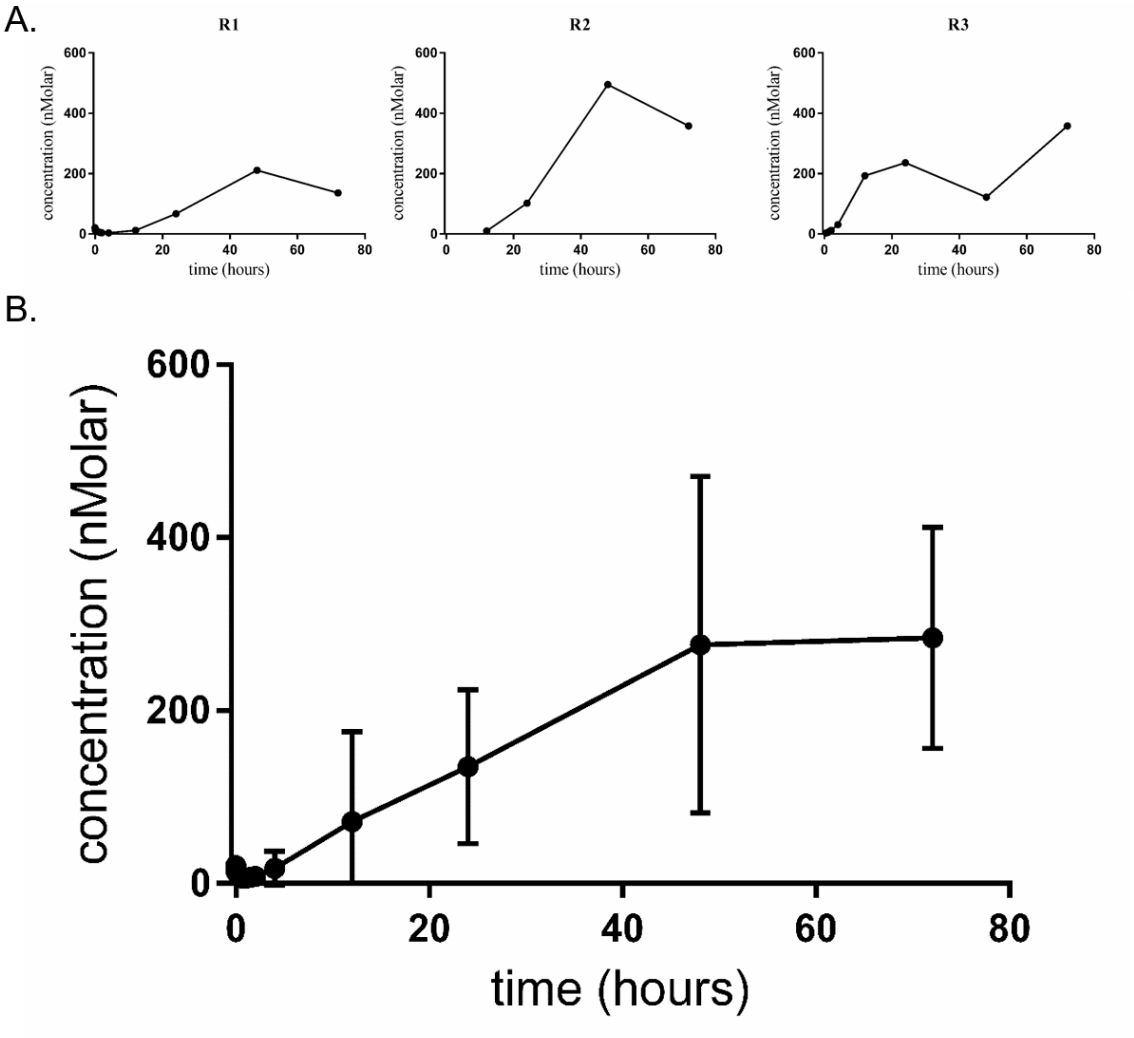

Figure 4.4: Concentrations of odanacatib over time in rabbit plasma following a single oral bolus dose of 5 mg/kg by body weight. Plasma concentrations of odanacatib were assessed by LC-MS. (A) Individual concentration curves for each of the three rabbits involved in the study. (B) Consensus curve generated from the three curves in A.

Table 4.1: Pharmacokinetic data for odanacatib in rabbit plasma showing mean curve attributes following a single oral bolus dose of 5 mg/kg.

	parameter			
drug	**$ACU_{0\text{-}24}$ (hr·nanomolar)**	**C_{max} (nanomolar)**	**T_{max} (hr)**	**$T_{1/2}$ (hr)**
odanacatib	13,394 (10,334-16,252)	284 (210-358)	72	37.9

Note: Ranges in parentheses correspond to ± 1 standard error of the mean.

4.2.5 A pharmacokinetic model for repetitive dosing predicts a dosing pattern of 10 mg/kg daily achieves steady-state concentrations between 300 and 600 nanomolar.

We next sought to design and implement a study where odanacatib was used to inhibit cathepsin K. One critical parameter for this study-design is the dosing strategy. From previous reports, we identified 300 — 600 nanomolar as a steady-state plasma concentration range that will achieve pharmacologic inhibition of cathepsin K.

We implemented our steady-state model using the parameters derived from our pharmacokinetic study (Fig 4.5). These parameters were:

1. $\mathbf{C_{max}}$**:** The maximum concentration achieved during single oral bolus dosing.
2. $\mathbf{T_{max}}$**:** The time until the maximum concentration.
3. $\mathbf{T_{1/2}}$**:** The half-life of the drug in the plasma.
4. $\mathbf{T_{lag}}$**:** The time between dosing and the initial increase in plasma concentration.

The simulation suggested that a dosing strategy of either 2 mg/kg every 24 hours or 4 mg/kg every 48 hours would achieve steady-state concentrations between 300 — 600 nanomolar (Fig 4.5A). However, we noticed that although most of the parameters used to drive our steady-state model agreed with previously published reports, our described T_{max} was considerably longer than the 10 hours reported previously[214]. Therefore, we implemented our steady-state model again, but this time substituting our estimate for T_{max} with the previously reported T_{max} of 10 hours (Fig 4.5B). The output from our revised simulation suggested that a dosing strategy of either 10 mg/kg every 24 hours or a dosing strategy of 20 mg/kg every 48 hours would maintain steady-state concentrations between 300 — 600 nanomolar. We selected 10

mg/kg every 24 hours as a conservative strategy to build a study-design for inhibition of cathepsin K during cavity formation in rabbits.

4.2.6 A proposed study-design to investigate the effects of cathepsin K inhibition during cavity formation in rabbits.

Study overview: Rabbits will be infected by five low-dose aerosol exposures to tuberculosis. From our previous work, we expect that cavitation will occur at a high frequency (60-80% of animals) between study weeks 8 – 10. We identified a treatment period beginning at study-week 2 and continuing through study-week 10. During this time we expect pre-cavity lesions to undergo a necrotic transition, the commitment step toward cavitation.

Fifteen rabbits will be randomized to a treatment group receiving odanacatib and 10 rabbits will be randomized to a control group to receive vehicle. Our previous work with this model suggests that these numbers will sufficiently power the study to discern a true change in the frequency of cavitation (see methods appendix A for details of power calculation). Rabbits in the treatment group will receive 40 mg/kg/day *per os* between weeks five and ten. The study will last a total of 14 weeks (Fig 4.6).

Study outcomes and evaluation: Data collected from this study will be in three different modalities: (1) computer tomography (CT) scans, (2) gross pathology quantification, and (3) histology and immunohistochemistry.

1. **CT scans:** Our biosafety-level 3 animal facility allows us to collected CT scans of infected rabbits. To monitor cavitation during the study we will collect

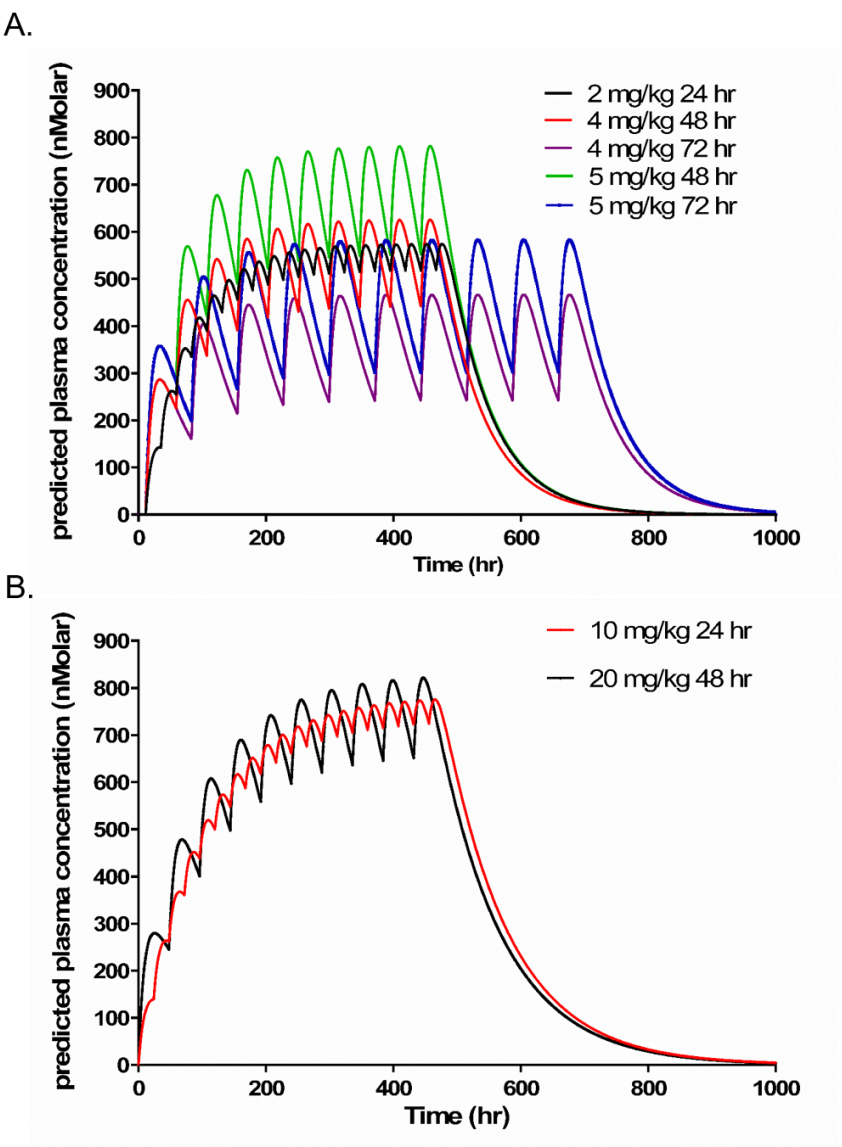

Figure 4.5: Predicted steady-state plasma concentrations of odanacatib during repetitive dosing. (A)Predicted plasma concentrations of odanacatib over time when all parameters for the steady-state predictive algorithm are based on the single oral bolus dosing study. (B) Predictive plasma concentrations of odanacatib over time when the T_{max} is set to 10 hours based on previous reports. All other parameters are the same as in A.

high-resolution CT scans of rabbits once every two weeks. These data will be quantified to give disease metrics at intermediate study time-points including number of cavities per animal and the average size of cavities between groups.

2. **Gross pathology quantification:** Following the study end-point the rabbits will be sacrificed. Lung, spleen, lymph nodes, liver, and bone-samples will be collected and fixed. Fixed lung will be dissected and photographed. These photographs will be used to quantify the extent of disease in lungs and validate radiological findings.

3. **Histology and immunohistochemistry:** Once the fixed organs are dissected and photographed, we will systematically collect histology samples. Samples will be paraffin embedded, section, and stained with H&E, Masson's trichrome stain and an anti-cathepsin K antibody that we previously optimized for rabbit samples. Using the Masson's trichrome stain, we expect to quantify the extent of collagen remaining in infected foci and the extent of collagen deposition around fibro-necrotic lesions.

Ethical considerations and safe animal practices: All animals will be housed in the Animal Biosafety-level 3 facility at the Johns Hopkins University School of Medicine. Researchers working with infected animals adhere to strict facility guidelines regarding appropriate personal protective equipment. All animals in the study will be monitored daily for fecal/urine output, appearance and weight. Animals that show signs of distress or disease will be evaluated by a member of the Johns Hopkins veterinary team. All procedures described in this proposed study are acceptable under an active IRB protocol in the Bishai Laboratory as approved by the Johns Hopkins University Animal Care and Use Committee.

4.3 Discussion

Our studies further support that cathepsin K expression is increased in the lungs of tuberculosis patients. These studies agree with past work by Kim *et al.* who showed that cathespin K transcription was increased in the caseous pneumonia of tuberculosis cavities and by Park *et al.*, who observed that multinucleated giant cells in tuberculosis lesions express cathepsin K by immunohistochemistry staining[88,92]. Our work is a continuation of Kübler *et al.*'s studies demonstrating that increased cathepsin K expression is also a feature of the host-response to *M. tb* infection in rabbits[91].

In the studies described above we demonstrate that macrophages infected by *M. tb* show increased transcription of cathepsin K by Q-PCR. This experiment shows that macrophages in mono-cell culture can express cathepsin K when infected by *M. tb*, thereby providing plausible *in vitro* evidence that macrophages and multinucleated giant cells can be the agents of cathepsin K expression in granulomatous pneumonia. Our *in vitro* experiments are not able to determine whether the observed increase in cathepsin K transcription is a biologically relevant process and so it is possible that cellular members of the granuloma (*ie.* fibroblasts, neutrophils, or lymphocytes) also participate in cathepsin K expression. It is also possible that a biologically relevant increase in cathepsin K expression within granulomas is driven by cytokine cross-talk between different cell-types.

We also show that the walls of rabbit cavities are enriched in cathepsin K by immunohistochemical staining. Again, this survey has several limitations. First, a review of the stained tissue section shows little variability in vulcan fast red chromogen hue between cell-types of the cavity wall. We propose two possibilities.

1. Many cells of the cavity wall are influenced by cytokines to increase cathespin K expression in granulocytic pneumonia.

2. Staining was not specific for cathespin K.

Two lines of evidence argue against non-specific staining.

1. We noticed that the necrotic debris at the interior edge of the cavity did not stain brightly for cathepsin K and this supports specificity for the primary antibody. We expect the necrotic debris of the cavity edge to be enriched in "protein-spill" from dying cells, and so would likely stain brightest if non-specific staining was a major contributor to the Vulcan-fast-red signal.

2. Our control slides, stained only with secondary-antibody, were devoid of vulcan-fast-red hue.

The second important limitation of our immunohistochemistry survey relates to the biology of Cathepsin K. Our primary anti-cathepsin K antibody is not specific for active cathepsin K and likely recognizes the 37 kDa inactive form with similar affinity to the 27 kDa active form. Therefore, the immunohistochemistry assay results presented above should not be interpreted as areas of increased cathepsin K activity.

We used Q-PCR to survey regions of rabbit lung of varying proximity to cavities induced by *M. tb* infection. Our results show a proximity-dependent increase in the transcription of cathepsin K. Tissue areas closer to the walls of cavities showed an increased concentration of cathepsin K transcripts. These studies further support granulomas and cavity-walls as the epicenters of cathespin K production. These results also validate the rabbit model as an appropriate system to further study the role of cathepsin K in the development of tuberculosis cavities.

In our final set of investigations, we obtained 150g of odanacatib and conducted a preliminary pharmacokinetic study in rabbits by measuring the plasma concentration of odanacatib following single oral bolus dosing. The results of our pharmacokinetic study show that odanacatib has good properties for an *in vivo* study to investigate the effects of cathespin K inhibition during cavity formation. Our proposed study design is also described.

We hypothesize that the inhibition of cathepsin K will stabilize the extracellular matrix of lung tissue, thereby preventing cavitation following repetitive aerosol challenge. In our study design we defined sensitive metrics for cavity formation and progression that will allow us to assess the effects of cathespin K inhibition. However, in careful consideration of our hypothesis, we also propose several potential pitfalls during our study.

1. **Inhibition of cathepsin K may damage the immune response.** If monocytes use cathepsin K as a way to move through lung tissue, the inhibition of cathepsin K may prevent monocyte migration to the foci of lung infection.

2. **The disruption of collagen breakdown may cause increased fibrosis.** Bhling *et al.* and Srivastava *et al.*, concluded that cathespin K was protective against pathologic lung fibrosis. It is possible that inhibition of cathepsin K in the context of *M. tb* infection will cause wide-spread pathologic fibrosis[207,208].

3. **It may be impossible to uncouple matrix breakdown from necrosis at the border between the cellular and necrotic regions of the cavity wall.** Finally, it is possible that matrix breakdown is an unavoidable consequence of widespread necrosis and that cell death releases a proteolytic cascade of lysosomal enzymes. If this is the case, then multiple proteolytic enzymes from many families might participate in matrix breakdown, therefore single-agent

small-molecule therapy is unlikely to change the rate of cavitation.

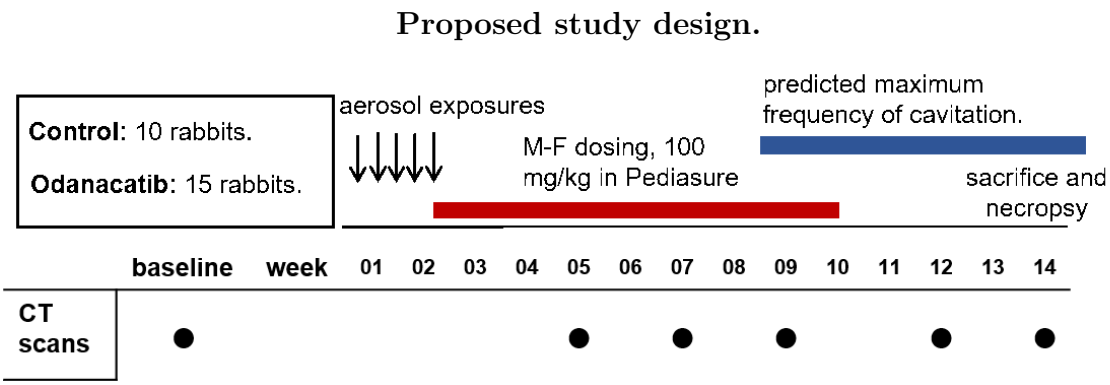

Figure 4.6: Proposed study design to investigate the effects of odanacatib-mediated inhibition of cathepsin K during cavity formation in rabbits.

References

1. Palaci, M. *et al.* Cavitary Disease and Quantitative Sputum Bacillary Load in Cases of Pulmonary Tuberculosis. *J Clin Microbiol* **45,** 4064–4066. ISSN: 0095-1137 (Dec. 2007).
2. Gadkowski, L. B. & Stout, J. E. Cavitary pulmonary disease. *Clin. Microbiol. Rev.* **21,** 305–333, table of contents. ISSN: 1098-6618 (Apr. 2008).
3. Ors, F. *et al.* High-resolution CT findings in patients with pulmonary tuberculosis: correlation with the degree of smear positivity. *J Thorac Imaging* **22,** 154–159. ISSN: 0883-5993 (May 2007).
4. Rom, W. N. & Garay, S. M. *Tuberculosis* 2nd ed. 944 pp. ISBN: 0-7817-3678-1 (Lippincott Williams & Wilkins, Philadelphia, 2004).
5. Leung, A. N. Pulmonary Tuberculosis: The Essentials. *Radiology* **210,** 307–322. ISSN: 0033-8419 (Feb. 1, 1999).
6. Li, B.-G. *et al.* The value of multislice spiral CT features of cavitary walls in differentiating between peripheral lung cancer cavities and single pulmonary tuberculous thick-walled cavities. *Br J Radiol* **85,** 147–152. ISSN: 1748-880X (Feb. 2012).
7. Zvetina, J. R. *et al.* Pulmonary cavitations in Mycobacterium kansasii: distinctions from M. tuberculosis. *AJR Am J Roentgenol* **143,** 127–130. ISSN: 0361-803X (July 1984).
8. Parkar, A. & Kandiah, P. Differential Diagnosis of Cavitary Lung Lesions. *Journal of the Belgian Society of Radiology* **100.** ISSN: 2514-8281. doi:10.5334/jbr-btr.1202. http://www.jbsr.be/articles/10.5334/jbr-btr.1202/ (2017) (Nov. 19, 2016).
9. Rozenshtein, A., Hao, F., Starc, M. T. & Pearson, G. D. N. Radiographic appearance of pulmonary tuberculosis: dogma disproved. *AJR Am J Roentgenol* **204,** 974–978. ISSN: 1546-3141 (May 2015).
10. *TB Central - About* https://tbportals.niaid.nih.gov/About (2018).

11. Gomes, M., Saad Jr., R. & Stirbulov, R. Pulmonary tuberculosis: relationship between sputum bacilloscopy and radiological lesions. *Revista do Instituto de Medicina Tropical de São Paulo* **45,** 275–281. ISSN: 0036-4665 (Oct. 2003).

12. Gallant, J. E. & Ko, A. H. Cavitary Pulmonary Lesions in Patients Infected with Human Immunodeficiency Virus. *Clinical Infectious Diseases* **22,** 671–682. ISSN: 1058-4838 (1996).

13. Riley, R. L. *et al.* AERIAL DISSEMINATION OF PULMONARY TUBERCULOSIS A TWO-YEAR STUDY OF CONTAGION IN A TUBERCULOSIS WARD. *Am J Epidemiol* **70,** 185–196. ISSN: 0002-9262 (Sept. 1, 1959).

14. Canetti, G. *The Tubercle Bacillus in the Pulmonary Lesion of Man* 1st ed. (Springer Publishing Co., 1955).

15. Lohmann, E. M. *et al.* Grading of a positive sputum smear and the risk of Mycobacterium tuberculosis transmission. *The International Journal of Tuberculosis and Lung Disease* **16,** 1477–1484 (Nov. 1, 2012).

16. Bailey, W. C. *et al.* Predictive Model to Identify Positive Tuberculosis Skin Test Results During Contact Investigations. *JAMA* **287,** 996–1002. ISSN: 0098-7484 (Feb. 27, 2002).

17. Grosset, J. Mycobacterium tuberculosis in the Extracellular Compartment: an Underestimated Adversary. *Antimicrob Agents Chemother* **47,** 833–836. ISSN: 0066-4804 (Mar. 2003).

18. Kaplan, G. *et al.* Mycobacterium tuberculosis growth at the cavity surface: a microenvironment with failed immunity. *Infect. Immun.* **71,** 7099–7108. ISSN: 0019-9567 (Dec. 2003).

19. Yoder, M. A., Lamichhane, G. & Bishai, W. R. Cavitary pulmonary tuberculosis: The Holy Grail of disease transmission. *CURR. SCI., Current science, Current Science (India), Current Science Bangalore, Current Science, India* **86,** 74–81. ISSN: 0011-3891 (Jan. 10, 2004).

20. Prideaux, B. *et al.* The association between sterilizing activity and drug distribution into tuberculosis lesions. *Nat. Med.* ISSN: 1546-170X. doi:10.1038/nm.3937 (Sept. 7, 2015).

21. Datta, M. *et al.* Anti-vascular endothelial growth factor treatment normalizes tuberculosis granuloma vasculature and improves small molecule delivery. *Proc Natl Acad Sci U S A* **112,** 1827–1832. ISSN: 0027-8424 (Feb. 10, 2015).

22. Dartois, V. The path of anti-tuberculosis drugs: from blood to lesions to mycobacterial cells. *Nat. Rev. Microbiol.* **12,** 159–167. ISSN: 1740-1534 (Mar. 2014).

23. Sarathy, J. P. *et al.* Prediction of Drug Penetration in Tuberculosis Lesions. *ACS Infect Dis* **2,** 552–563. ISSN: 2373-8227 (Aug. 12, 2016).

24. Chakaya, J., Kirenga, B. & Getahun, H. Long term complications after completion of pulmonary tuberculosis treatment: A quest for a public health approach. *Journal of Clinical Tuberculosis and Other Mycobacterial Diseases* **3,** 10–12. ISSN: 2405-5794 (May 1, 2016).

25. Davies. Aspergilloma and residual tuberculous cavities—the results of a resurvey. *Tubercle* **51,** 227–245. ISSN: 0041-3879 (Sept. 1, 1970).

26. Dannenberg, A. M. & Collins, F. M. Progressive pulmonary tuberculosis is not due to increasing numbers of viable bacilli in rabbits, mice and guinea pigs, but is due to a continuous host response to mycobacterial products. *Tuberculosis* **81,** 229–242. ISSN: 1472-9792 (June 1, 2001).

27. Dannenberg, A. M. *Pathogenesis of Human Pulmonary Tuberculosis* (ASM Press, 2006).

28. Helke, K. L., Mankowski, J. L. & Manabe, Y. C. Animal models of cavitation in pulmonary tuberculosis. *Tuberculosis (Edinb)* **86,** 337–348. ISSN: 1472-9792 (Sept. 2006).

29. Chaparas, S. D., Good, R. C. & Janicki, B. W. Tuberculin-induced lymphocyte transformation and skin reactivity in monkeys vaccinated or not vaccinated with Bacille Calmette-Guérin, then challenged with virulent Mycobacterium tuberculosis. *Am. Rev. Respir. Dis.* **112,** 43–47. ISSN: 0003-0805 (July 1975).

30. Kaushal, D., Mehra, S., Didier, P. & Lackner, A. The non-human primate model of tuberculosis. *J Med Primatol* **41,** 191–201. ISSN: 0047-2565 (June 2012).

31. McMurray, D. N. A Nonhuman Primate Model for Preclinical Testing of New Tuberculosis Vaccines. *Clin Infect Dis* **30,** S210–S212. ISSN: 1058-4838 (Supplement_3 June 1, 2000).

32. Scanga, C. A. & Flynn, J. L. Modeling tuberculosis in nonhuman primates. *Cold Spring Harb Perspect Med* **4,** a018564. ISSN: 2157-1422 (Dec. 2014).

33. Peña, J. C. & Ho, W.-Z. Monkey Models of Tuberculosis: Lessons Learned. *Infect. Immun.* **83,** 852–862. ISSN: 0019-9567, 1098-5522 (Mar. 1, 2015).

34. Schmidt, L. H. Some observations on the utility of simian pulmonary tuberculosis in defining the therapeutic potentialities of isoniazid. *Am Rev Tuberc* **74,** 138–153, discussion, 153–159. ISSN: 0096-0381 (Aug. 1956).

35. Good, R. C. Simian Tuberculosis: Immunologic Aspects*. *Annals of the New York Academy of Sciences* **154,** 200–213. ISSN: 1749-6632 (Sept. 1, 1968).

36. Barclay, W. R., Anacker, R. L., Brehmer, W., Leif, W. & Ribi, E. Aerosol-Induced Tuberculosis in Subhuman Primates and the Course of the Disease After Intravenous BCG Vaccination. *Infect Immun* **2,** 574–582. ISSN: 0019-9567 (Nov. 1970).

37. Schmidt, L. H. Studies on the Antituberculous Activity of Ethambutol in Monkeys*. *Annals of the New York Academy of Sciences* **135,** 747–758. ISSN: 1749-6632 (Apr. 1, 1966).

38. Maiello, P. *et al.* Rhesus Macaques Are More Susceptible to Progressive Tuberculosis than Cynomolgus Macaques: a Quantitative Comparison. *Infect. Immun.* **86,** e00505–17. ISSN: 0019-9567, 1098-5522 (Feb. 1, 2018).

39. Sharpe, S. A. *et al.* An aerosol challenge model of tuberculosis in Mauritian cynomolgus macaques. *PLOS ONE* **12,** e0171906. ISSN: 1932-6203 (Mar. 8, 2017).

40. Walsh, G. P. *et al.* The Philippine cynomolgus monkey (Macaca fasicularis) provides a new nonhuman primate model of tuberculosis that resembles human disease. *Nature Medicine* **2,** 430–436. ISSN: 1546-170X (Apr. 1996).

41. Capuano, S. V. *et al.* Experimental Mycobacterium tuberculosis Infection of Cynomolgus Macaques Closely Resembles the Various Manifestations of Human M. tuberculosis Infection. *Infect Immun* **71,** 5831–5844. ISSN: 0019-9567 (Oct. 2003).

42. Lin, P. L. *et al.* Quantitative Comparison of Active and Latent Tuberculosis in the Cynomolgus Macaque Model. *Infect Immun* **77,** 4631–4642. ISSN: 0019-9567 (Oct. 2009).

43. Lin, P. L. *et al.* Radiologic responses in cynomolgous macaques for assessing tuberculosis chemotherapy regimens. *Antimicrob. Agents Chemother.* ISSN: 1098-6596. doi:10.1128/AAC.00277-13 (June 24, 2013).

44. Curths, C., Knauf, S. & Kaup, F.-J. Respiratory Animal Models in the Common Marmoset (Callithrix jacchus). *Veterinary Sciences* **1,** 63–76 (June 20, 2014).

45. Brok, H. P., Hornby, R. J., Griffiths, G. D., Scott, L. A. & Hart, B. A. An extensive monoclonal antibody panel for the phenotyping of leukocyte subsets in the common marmoset and the cotton-top tamarin. *Cytometry* **45,** 294–303. ISSN: 0196-4763 (Dec. 1, 2001).

46. Via, L. E. *et al.* Differential virulence and disease progression following Mycobacterium tuberculosis complex infection of the common marmoset (Callithrix jacchus). *Infect. Immun.* **81,** 2909–2919. ISSN: 1098-5522 (Aug. 2013).

47. Via, L. E. *et al.* A sterilizing tuberculosis treatment regimen is associated with faster clearance of bacteria in cavitary lesions in marmosets. *Antimicrob. Agents Chemother.* **59,** 4181–4189. ISSN: 1098-6596 (July 2015).

48. Cadena, A. M. *et al.* Very Low Doses of Mycobacterium tuberculosis Yield Diverse Host Outcomes in Common Marmosets (Callithrix jacchus). *Comp Med* **66,** 412–419. ISSN: 1532-0820 (Oct. 2016).

49. Lurie, M. B. *Resistance to Tuberculosis: Experimental Studies in Native and Acquired Defensive Mechanisms* (Harvard University Press, Cambridge, MA, 1964).

50. Yamamura, Y., Maeda, H., Ogawa, Y. & Hashimoto, T. Experimental Pulmonary Cavity Formation by Mycobacterial Components and Synthetic Adjuvants. *Microbiology and Immunology* **30,** 1175–1187. ISSN: 1348-0421 (Nov. 1, 1986).

51. Maeda, H., Yamamura, Y., Ogawa, Y., Maeda, J. & Yamamura, Y. Mycobacterial Antigens Relating to Experimental Pulmonary Cavity Formation. *Am Rev Respir Dis* **115,** 617–623. ISSN: 0003-0805 (Apr. 1, 1977).

52. Azuma, I., Sugimura, K., Taniyama, T., Yamawaki, M. & Yamamura, Y. Adjuvant activity of mycobacterial fractions: adjuvant activity of synthetic N-acetylmuramyl-dipeptide and the related compounds. *Infect Immun* **14,** 18–27. ISSN: 0019-9567 (July 1976).

53. Yamamura, Y. *et al. Experimental formation of the tuberculous cavity in the rabbit's lung; experimental study on the tuberculous allergy.* 1954.

54. Converse, P. J. *et al.* Cavitary tuberculosis produced in rabbits by aerosolized virulent tubercle bacilli. *Infect. Immun.* **64,** 4776–4787. ISSN: 0019-9567, 1098-5522 (Nov. 1, 1996).

55. Nedeltchev, G. G. *et al.* Extrapulmonary dissemination of Mycobacterium bovis but not Mycobacterium tuberculosis in a bronchoscopic rabbit model of cavitary tuberculosis. *Infect. Immun.* **77,** 598–603. ISSN: 1098-5522 (Feb. 2009).

56. Kubler, A. *Development and Investigation of a Rabbit Model of Tuberculosis Tissue Destruction* PhD thesis (Imperial College London, London, United Kingdom, July 2013). 265 pp.

57. Wells, W. F. & Lurie, M. B. Experimental Air-borne Disease. Quantitative Natural Respiratory Contagion of Tuberculosis. *American Journal of Hygiene* **34.** ISSN: 0096-5294. `https://www.cabdirect.org/cabdirect/abstract/19422700054` (2018) (1941).

58. Nuermberger, E. Using Animal Models to Develop New Treatments for Tuberculosis. *Semin Respir Crit Care Med* **29,** 542–551. ISSN: 1069-3424, 1098-9048 (Oct. 2008).

59. Gumbo, T., Lenaerts, A. J., Hanna, D., Romero, K. & Nuermberger, E. Nonclinical Models for Antituberculosis Drug Development: A Landscape Analysis. *J Infect Dis* **211,** S83–S95. ISSN: 0022-1899 (suppl_3 June 15, 2015).

60. Dooley, K. E., Phillips, P. P., Nahid, P. & Hoelscher, M. Challenges in the clinical assessment of novel tuberculosis drugs. *Adv Drug Deliv Rev* **102,** 116–122. ISSN: 0169-409X (July 1, 2016).

61. Pan, H. *et al.* Ipr1 gene mediates innate immunity to tuberculosis. *Nature* **434,** 767–772. ISSN: 1476-4687 (Apr. 7, 2005).

62. Pichugin, A. V., Yan, B.-S., Sloutsky, A., Kobzik, L. & Kramnik, I. Dominant role of the sst1 locus in pathogenesis of necrotizing lung granulomas during chronic tuberculosis infection and reactivation in genetically resistant hosts. *Am. J. Pathol.* **174,** 2190–2201. ISSN: 1525-2191 (June 2009).

63. Yan, B.-S. *et al.* Progression of pulmonary tuberculosis and efficiency of bacillus Calmette-Guérin vaccination are genetically controlled via a common sst1-mediated mechanism of innate immunity. *J. Immunol.* **179,** 6919–6932. ISSN: 0022-1767 (Nov. 15, 2007).

64. He, X. *et al.* The sst1 resistance locus regulates evasion of type I interferon signaling by Chlamydia pneumoniae as a disease tolerance mechanism. *PLoS Pathog.* **9,** e1003569. ISSN: 1553-7374 (2013).

65. Harper, J. *et al.* Mouse model of necrotic tuberculosis granulomas develops hypoxic lesions. *J. Infect. Dis.* **205,** 595–602. ISSN: 1537-6613 (Feb. 15, 2012).

66. Driver, E. R. *et al.* Evaluation of a mouse model of necrotic granuloma formation using C3HeB/FeJ mice for testing of drugs against Mycobacterium tuberculosis. *Antimicrob. Agents Chemother.* **56,** 3181–3195. ISSN: 1098-6596 (June 2012).

67. Ordonez, A. A., DeMarco, V. P., Klunk, M. H., Pokkali, S. & Jain, S. K. Imaging Chronic Tuberculous Lesions Using Sodium [18F]Fluoride Positron Emission Tomography in Mice. *Mol Imaging Biol* **17,** 609–614. ISSN: 1536-1632 (Oct. 2015).

68. Lanoix, J.-P., Lenaerts, A. J. & Nuermberger, E. L. Heterogeneous disease progression and treatment response in a C3HeB/FeJ mouse model of tuberculosis. *Dis Model Mech* **8,** 603–610. ISSN: 1754-8403 (June 1, 2015).

69. Ordonez, A. A. *et al.* Radioiodinated DPA-713 Imaging Correlates with Bactericidal Activity of Tuberculosis Treatments in Mice. *Antimicrob Agents Chemother* **59,** 642–649. ISSN: 0066-4804 (Jan. 2015).

70. Lenaerts, A., Barry, C. E. & Dartois, V. Heterogeneity in tuberculosis pathology, microenvironments and therapeutic responses. *Immunol Rev* **264,** 288–307. ISSN: 0105-2896 (Mar. 2015).

71. Hunter, R. L. Pathology of post primary tuberculosis of the lung: an illustrated critical review. *Tuberculosis (Edinb)* **91,** 497–509. ISSN: 1873-281X (Nov. 2011).

72. Irwin, S. M. *et al.* Presence of multiple lesion types with vastly different microenvironments in C3HeB/FeJ mice following aerosol infection with Mycobacterium tuberculosis. *Disease Models & Mechanisms* **8,** 591–602. ISSN: 1754-8403, 1754-8411 (June 1, 2015).

73. DeMarco, V. P. *et al.* Determination of [11C]Rifampin Pharmacokinetics within Mycobacterium tuberculosis-Infected Mice by Using Dynamic Positron Emission Tomography Bioimaging. *Antimicrob. Agents Chemother.* **59,** 5768–5774. ISSN: 0066-4804, 1098-6596 (Sept. 1, 2015).

74. Kjellsson, M. C. *et al.* Pharmacokinetic evaluation of the penetration of antituberculosis agents in rabbit pulmonary lesions. *Antimicrob. Agents Chemother.* **56,** 446–457. ISSN: 1098-6596 (Jan. 2012).

75. Lanoix, J.-P. *et al.* Selective Inactivity of Pyrazinamide against Tuberculosis in C3HeB/FeJ Mice Is Best Explained by Neutral pH of Caseum. *Antimicrob. Agents Chemother.* **60,** 735–743. ISSN: 0066-4804, 1098-6596 (Feb. 1, 2016).

76. Weinstein, E. A. *et al.* Noninvasive determination of 2-[18F]-fluoroisonicotinic acid hydrazide pharmacokinetics by positron emission tomography in Mycobacterium tuberculosis-infected mice. *Antimicrob. Agents Chemother.* **56,** 6284–6290. ISSN: 1098-6596 (Dec. 2012).

77. Luna, B. *et al.* In vivo prediction of tuberculosis-associated cavity formation in rabbits. *J. Infect. Dis.* **211,** 481–485. ISSN: 1537-6613 (Feb. 1, 2015).

78. Elkington, P. T., Ugarte-Gil, C. A. & Friedland, J. S. Matrix metalloproteinases in tuberculosis. *European Respiratory Journal* **38,** 456–464. ISSN: 0903-1936, 1399-3003 (Aug. 1, 2011).

79. Dannenberg, A. M. & Bennett, W. E. HYDROLYTIC ENZYMES OF RABBIT MONONUCLEAR EXUDATE CELLS. I. QUANTITATIVE ASSAY AND PROPERTIES OF CERTAIN PROTEASES, NON-SPECIFIC ESTERASES, AND LIPASES OF MONONUCLEAR AND POLYMORPHONUCLEAR CELLS AND ERYTHROCYTES. *J. Cell Biol.* **21,** 1–13. ISSN: 0021-9525 (Apr. 1964).

80. Carson, M. E. & Dannenberg, A. M. Hydrolytic Enzymes of Rabbit Mononuclear Exudate Cells: II. Lysozyme: Properties and Quantitative Assay in Tuberculous and Control Inbred Rabbits. *The Journal of Immunology* **94,** 99–104. ISSN: 0022-1767, 1550-6606 (Jan. 1, 1965).

81. Mizunoe, K. & Dannenberg, A. M. Hydrolases of rabbit macrophages. 3. Effect of BCG vaccination, tissue culture, and ingested tubercle bacilli. *Proc. Soc. Exp. Biol. Med.* **120,** 284–290. ISSN: 0037-9727 (Nov. 1965).

82. Meyers, O. T., Dannenberg, A. M. & Mizunoe, K. Polymorphonuclear exudate cells and pulmonary alveolar macrophages. 3. Deoxyribonuclease and ribonuclease: properties and quantitative assay in macrophages from tuberculous and control inbred rabbits. *J Reticuloendothel Soc* **7,** 15–31. ISSN: 0033-6890 (Jan. 1970).

83. McAdoo, M. H., Dannenberg, A. M., Hayes, C. J., James, S. P. & Sanner, J. H. Inhibition of cathepsin D-type proteinase of macrophages by pepstatin, a specific pepsin inhibitor, and other substances. *Infect. Immun.* **7,** 655–665. ISSN: 0019-9567 (Apr. 1973).

84. Rojas-Espinosa, O., Dannenberg, A. M., Sternberger, L. A. & Tsuda, T. The Role of Cathepsin D in the Pathogenesis of Tuberculosis. *Am J Pathol* **74,** 1–17. ISSN: 0002-9440 (Jan. 1974).

85. Elkington, P. T. G. & Friedland, J. S. Matrix metalloproteinases in destructive pulmonary pathology. *Thorax* **61,** 259–266. ISSN: 0040-6376 (Mar. 2006).

86. Elkington, P. T., D'Armiento, J. M. & Friedland, J. S. Tuberculosis Immunopathology: The Neglected Role of Extracellular Matrix Destruction. *Sci Transl Med* **3,** 71ps6. ISSN: 1946-6234 (Feb. 23, 2011).

87. Elkington, P. *et al.* MMP-1 drives immunopathology in human tuberculosis and transgenic mice. *J Clin Invest* **121,** 1827–1833. ISSN: 0021-9738 (May 2, 2011).

88. Kim, M.-J. *et al.* Caseation of human tuberculosis granulomas correlates with elevated host lipid metabolism. *EMBO Mol Med* **2,** 258–274. ISSN: 1757-4684 (July 2010).

89. Elkington, P. T., Green, J. A. & Friedland, J. S. in *Macrophages and Dendritic Cells* DOI: 10.1007/978-1-59745-396-7_16, 253–265 (Humana Press, 2009). ISBN: 978-1-58829-972-7. `https://link.springer.com/protocol/10.1007/978-1-59745-396-7_16` (2018).

90. Volkman, H. E. *et al.* Tuberculous granuloma induction via interaction of a bacterial secreted protein with host epithelium. *Science* **327,** 466–469. ISSN: 1095-9203 (Jan. 22, 2010).

91. Kubler, A. *et al.* Cathepsin K Contributes to Cavitation and Collagen Turnover in Pulmonary Tuberculosis. *J. Infect. Dis.* **213,** 618–627. ISSN: 1537-6613 (Feb. 15, 2016).

92. Park, J. K. *et al.* Expression of cathepsin K and tartrate-resistant acid phosphatase is not confined to osteoclasts but is a general feature of multinucleated giant cells: systematic analysis. *Rheumatology (Oxford)* **52,** 1529–1533. ISSN: 1462-0332 (Aug. 2013).

93. Nagase, H., Enghild, J. J., Suzuki, K. & Salvesen, G. Stepwise activation mechanisms of the precursor of matrix metalloproteinase 3 (stromelysin) by proteinases and (4-aminophenyl)mercuric acetate. *Biochemistry* **29,** 5783–5789. ISSN: 0006-2960 (June 19, 1990).

94. Turk, B. *et al.* Regulation of the Activity of Lysosomal Cysteine Proteinases by pH-Induced Inactivation and/or Endogenous Protein Inhibitors, Cystatins. *Biological Chemistry Hoppe-Seyler* **376,** 225–230. ISSN: 0177-3593 (1995).

95. Cygler, M. *et al.* Structure of rat procathepsin B: model for inhibition of cysteine protease activity by the proregion. *Structure* **4,** 405–416. ISSN: 0969-2126 (Apr. 1, 1996).

96. Brew, K., Dinakarpandian, D. & Nagase, H. Tissue inhibitors of metalloproteinases: evolution, structure and function. *Biochim. Biophys. Acta* **1477,** 267–283. ISSN: 0006-3002 (Mar. 7, 2000).

97. Buck, M. R., Karustis, D. G., Day, N. A., Honn, K. V. & Sloane, B. F. Degradation of extracellular-matrix proteins by human cathepsin B from normal and tumour tissues. *Biochem J* **282,** 273–278. ISSN: 0264-6021 (Pt 1 Feb. 15, 1992).

98. Brömme, D., Okamoto, K., Wang, B. B. & Biroc, S. Human cathepsin O2, a matrix protein-degrading cysteine protease expressed in osteoclasts. Functional expression of human cathepsin O2 in Spodoptera frugiperda and characterization of the enzyme. *J. Biol. Chem.* **271,** 2126–2132. ISSN: 0021-9258 (Jan. 26, 1996).

99. Chung, L. *et al.* Collagenase unwinds triple-helical collagen prior to peptide bond hydrolysis. *EMBO J* **23,** 3020–3030. ISSN: 0261-4189 (Aug. 4, 2004).

100. Shipley, J. M. *et al.* The Structural Basis for the Elastolytic Activity of the 92-kDa and 72-kDa Gelatinases ROLE OF THE FIBRONECTIN TYPE II-LIKE REPEATS. *J. Biol. Chem.* **271,** 4335–4341. ISSN: 0021-9258, 1083-351X (Feb. 23, 1996).

101. Troen, B. R. The Regulation of Cathepsin K Gene Expression. *Annals of the New York Academy of Sciences* **1068,** 165–172. ISSN: 1749-6632 (Apr. 1, 2006).

102. O'Kane, C. M. *et al.* STAT3, p38 MAPK, and NF-/*kappa*B Drive Unopposed Monocyte-Dependent Fibroblast MMP-1 Secretion in Tuberculosis. *Am J Respir Cell Mol Biol* **43,** 465–474. ISSN: 1044-1549 (Oct. 2010).

103. Rand, L., Green, J. A., Saraiva, L., Friedland, J. S. & Elkington, P. T. G. Matrix Metalloproteinase-1 Is Regulated in Tuberculosis by a p38 MAPK-Dependent, p-Aminosalicylic Acid-Sensitive Signaling Cascade. *The Journal of Immunology* **182,** 5865–5872. ISSN: 0022-1767, 1550-6606 (May 1, 2009).

104. Harris, J. E., Green, J. A., Elkington, P. T. & Friedland, J. S. Monocytes infected with Mycobacterium tuberculosis regulate MAP kinase-dependent astrocyte MMP-9 secretion. *Journal of Leukocyte Biology* **81,** 548–556. ISSN: 1938-3673 (Feb. 1, 2007).

105. Nagasawa, N., Yamashita, M. & Okamoto, H. Studies on the relationship between pulmonary tuberculous cavities and draining bronchi, by injecting acrylic resin. *Acta Tuberc Jpn* **3,** 35–47. ISSN: 0567-8161 (Dec. 1953).

106. Hermel, M. B. & Gershon-Cohen, J. Healing Mechanisms of Tuberculous Cavities. *Radiology* **63,** 544–549. ISSN: 0033-8419 (Oct. 1, 1954).

107. Hsu, T. *et al.* The primary mechanism of attenuation of bacillus Calmette–Guérin is a loss of secreted lytic function required for invasion of lung interstitial tissue. *Proc Natl Acad Sci U S A* **100,** 12420–12425. ISSN: 0027-8424 (Oct. 14, 2003).

108. Hunter, R. L., Olsen, M. R., Jagannath, C. & Actor, J. K. Multiple Roles of Cord Factor in the Pathogenesis of Primary, Secondary, and Cavitary Tuberculosis, Including a Revised Description of the Pathology of Secondary Disease. *Ann Clin Lab Sci* **36,** 371–386. ISSN: 0091-7370, 1550-8080 (Sept. 21, 2006).

109. Sakamoto, K. *et al.* Mycobacterial trehalose dimycolate reprograms macrophage global gene expression and activates matrix metalloproteinases. *Infect. Immun.* **81,** 764–776. ISSN: 1098-5522 (Mar. 2013).

110. Busi Rizzi, E., Schininà, V., Palmieri, F., Girardi, E. & Bibbolino, C. Cavitary pulmonary tuberculosis HIV-related. *Eur J Radiol* **52,** 170–174. ISSN: 0720-048X (Nov. 2004).

111. Comas, I. *et al.* Human T cell epitopes of Mycobacterium tuberculosis are evolutionarily hyperconserved. *Nat Genet* **42,** 498–503. ISSN: 1061-4036 (June 2010).

112. Canetti, G. Present aspects of bacterial resistance in tuberculosis. *Am. Rev. Respir. Dis.* **92,** 687–703. ISSN: 0003-0805 (Nov. 1965).

113. Belton, M. *et al.* Hypoxia and tissue destruction in pulmonary TB. *Thorax* **71,** 1145–1153. ISSN: 0040-6376 (Dec. 2016).

114. Corbetta, L. *et al.* Improvement in tubercular cavities following adjuvant treatment with endobronchial valves: a case report [Correspondence]. *The International Journal of Tuberculosis and Lung Disease* **17,** 850–851 (June 1, 2013).

115. Vadwai, V. *et al.* Clonal Population of Mycobacterium tuberculosis Strains Reside within Multiple Lung Cavities. *PLoS One* **6.** ISSN: 1932-6203. doi:10.1371/journal.pone.0024770. https://www.ncbi.nlm.nih.gov/pmc/articles/PMC3173478/ (2018) (Sept. 14, 2011).

116. Amberson, J. B. Clinical Studies of Healing of Pulmonary Tuberculosis. *Trans Am Climatol Clin Assoc* **43,** 144 (1927).

117. Ross, J. D. & Kay, D. T. A Review of 138 Cases of Closure of Tuberculous Lung Cavities Under Chemotherapy. *Thorax* **11,** 1–9. ISSN: 0040-6376, 1468-3296 (Mar. 1, 1956).

118. Fraser, R. S. Pulmonary aspergillosis: pathologic and pathogenetic features. *Pathol Annu* **28 Pt 1,** 231–277. ISSN: 0079-0184 (1993).

119. Beers, M. F. & Morrisey, E. E. The three R's of lung health and disease: repair, remodeling, and regeneration. *J Clin Invest* **121,** 2065–2073. ISSN: 0021-9738 (June 1, 2011).

120. Yang, C. *et al.* Mycobacterium tuberculosis Beijing Strains Favor Transmission but Not Drug Resistance in China. *Clin Infect Dis* **55,** 1179–1187. ISSN: 1058-4838 (Nov. 1, 2012).

121. Dowdy, D. W., Azman, A. S., Kendall, E. A. & Mathema, B. Transforming the Fight Against Tuberculosis: Targeting Catalysts of Transmission. *Clin Infect Dis* **59,** 1123–1129. ISSN: 1058-4838 (Oct. 15, 2014).

122. Ypma, R. J. F., Altes, H. K., Soolingen, D. v., Wallinga, J. & Ballegooijen, W. M. v. A Sign of Superspreading in Tuberculosis: Highly Skewed Distribution of Genotypic Cluster Sizes. *Epidemiology* **24,** 395–400. ISSN: 1044-3983 (May 1, 2013).

123. Stein, R. A. Super-spreaders in infectious diseases. *International Journal of Infectious Diseases* **15,** e510–e513. ISSN: 1201-9712 (Aug. 1, 2011).

124. Gardy, J. L. *et al.* Whole-Genome Sequencing and Social-Network Analysis of a Tuberculosis Outbreak. *New England Journal of Medicine* **364,** 730–739. ISSN: 0028-4793 (Feb. 24, 2011).

125. Curtis, A. B. *et al.* Extensive Transmission of Mycobacterium tuberculosis from a Child. *New England Journal of Medicine* **341,** 1491–1495. ISSN: 0028-4793 (Nov. 11, 1999).

126. Kline, S. E., Hedemark, L. L. & Davies, S. F. Outbreak of Tuberculosis among Regular Patrons of a Neighborhood Bar. *New England Journal of Medicine* **333,** 222–227. ISSN: 0028-4793 (July 27, 1995).

127. *WHO — Global tuberculosis report 2016* WHO. http://www.who.int/tb/publications/global_report/en/ (2017).

128. Singla, N., Singla, R., Fernandes, S. & Behera, D. *Post treatment sequelae of multi-drug resistant tuberculosis patients (PDF Download Available)* ResearchGate. https://www.researchgate.net/publication/44599152_Post_treatment_sequelae_of_multi-drug_resistant_tuberculosis_patients (2017).

129. Minchinton, A. I. & Tannock, I. F. Drug penetration in solid tumours. *Nature Reviews Cancer* **6,** 583–592. ISSN: 1474-1768 (Aug. 2006).

130. Al Shammari, B. *et al.* The Extracellular Matrix Regulates Granuloma Necrosis in Tuberculosis. *J Infect Dis* **212,** 463–473. ISSN: 0022-1899 (Aug. 1, 2015).

131. Kübler, A. *et al.* Mycobacterium tuberculosis dysregulates MMP/TIMP balance to drive rapid cavitation and unrestrained bacterial proliferation. *J. Pathol.* **235,** 431–444. ISSN: 1096-9896 (Feb. 2015).

132. *A Color Atlas of Comparative Pathology of Pulmonary Tuberculosis* (eds Leong, F. J., Dartois, V. & Dick, T.) 1st (CRC Press, Taylor & Francis Group, New York, 2011). 216 pp. ISBN: 978-1-4398-3527-2.

133. Gupta, U. D. & Katoch, V. M. Animal models of tuberculosis. *Tuberculosis (Edinb)* **85,** 277–293. ISSN: 1472-9792 (Nov. 2005).

134. Lee, R. S., Proulx, J.-F., Menzies, D. & Behr, M. A. Progression to tuberculosis disease increases with multiple exposures. *European Respiratory Journal* **48,** 1682–1689. ISSN: 0903-1936, 1399-3003 (Dec. 1, 2016).

135. Rich, A. *The Pathogenesis of Tuberculosis* 1st. 1008 pp. (Charles C Thomas, Baltimore, Maryland, 1944).

136. Nardell, E. & Churchyard, G. What is thwarting tuberculosis prevention in high-burden settings? *N. Engl. J. Med.* **365,** 79–81. ISSN: 1533-4406 (July 7, 2011).

137. Behar, S. M., Carpenter, S. M., Booty, M. G., Barber, D. L. & Jayaraman, P. Orchestration of pulmonary T cell immunity during Mycobacterium tuberculosis infection: immunity interruptus. *Semin. Immunol.* **26,** 559–577. ISSN: 1096-3618 (Dec. 2014).

138. *Dail and Hammar's Pulmonary Pathology* (ed Tomashefski, J. F.) 3rd ed. 2 vols. (Springer Publishing Co., 2008).

139. Ordonez, A. A. *et al.* Mouse model of pulmonary cavitary tuberculosis and expression of matrix metalloproteinase-9. *Dis Model Mech* **9,** 779–788. ISSN: 1754-8411 (2016).

140. Brewster, M., Lewis, J. E., Wilson, K. L., Greenham, A. K. & Bottomley, K. M. K. Ro 32-3555, an orally active collagenase selective inhibitor, prevents structural damage in the STR/ORT mouse model of osteoarthritis. *Arthritis & Rheumatism* **41,** 1639–1644. ISSN: 1529-0131 (Sept. 1, 1998).

141. Lewis, E. J. *et al.* Ro 32-3555, an orally active collagenase inhibitor, prevents cartilage breakdown in vitro and in vivo. *Br. J. Pharmacol.* **121,** 540–546. ISSN: 0007-1188 (June 1997).

142. Nagase, H., Visse, R. & Murphy, G. Structure and function of matrix metalloproteinases and TIMPs. *Cardiovasc Res* **69,** 562–573. ISSN: 0008-6363 (Feb. 15, 2006).

143. Gross, J. & Lapiere, C. M. COLLAGENOLYTIC ACTIVITY IN AMPHIBIAN TISSUES: A TISSUE CULTURE ASSAY*. *Proc Natl Acad Sci U S A* **48,** 1014–1022. ISSN: 0027-8424 (June 1962).

144. Giebeler, N. & Zigrino, P. A Disintegrin and Metalloprotease (ADAM): Historical Overview of Their Functions. *Toxins (Basel)* **8.** ISSN: 2072-6651. doi:10.3390/toxins8040122. https://www.ncbi.nlm.nih.gov/pmc/articles/PMC4848645/ (2018) (Apr. 23, 2016).

145. Visse, R. & Nagase, H. Matrix Metalloproteinases and Tissue Inhibitors of Metalloproteinases: Structure, Function, and Biochemistry. *Circulation Research* **92,** 827–839. ISSN: 0009-7330, 1524-4571 (May 2, 2003).

146. Boire, A. *et al.* PAR1 Is a Matrix Metalloprotease-1 Receptor that Promotes Invasion and Tumorigenesis of Breast Cancer Cells. *Cell* **120,** 303–313. ISSN: 0092-8674, 1097-4172 (Feb. 11, 2005).

147. Fowlkes, J. L., Enghild, J. J., Suzuki, K. & Nagase, H. Matrix metalloproteinases degrade insulin-like growth factor-binding protein-3 in dermal fibroblast cultures. *J. Biol. Chem.* **269,** 25742–25746. ISSN: 0021-9258, 1083-351X (Oct. 14, 1994).

148. Odaka, C., Tanioka, M. & Itoh, T. Matrix Metalloproteinase-9 in Macrophages Induces Thymic Neovascularization following Thymocyte Apoptosis. *The Journal of Immunology* **174,** 846–853. ISSN: 0022-1767, 1550-6606 (Jan. 15, 2005).

149. Maskos, K. & Bode, W. Structural basis of matrix metalloproteinases and tissue inhibitors of metalloproteinases. *Mol Biotechnol* **25,** 241–266. ISSN: 1073-6085, 1559-0305 (Nov. 1, 2003).

150. Hadler-Olsen, E. *et al.* Gelatin in situ zymography on fixed, paraffin-embedded tissue: zinc and ethanol fixation preserve enzyme activity. *J. Histochem. Cytochem.* **58,** 29–39. ISSN: 1551-5044 (Jan. 2010).

151. Fanjul-Fernández, M., Folgueras, A. R., Cabrera, S. & López-Otín, C. Matrix metalloproteinases: Evolution, gene regulation and functional analysis in mouse models. *Biochimica et Biophysica Acta (BBA) - Molecular Cell Research. Matrix Metalloproteinases* **1803,** 3–19. ISSN: 0167-4889 (Jan. 1, 2010).

152. Chernov, A. V. & Strongin, A. Y. Epigenetic regulation of matrix metalloproteinases and their collagen substrates in cancer. *Biomol Concepts* **2,** 135–147. ISSN: 1868-5021 (June 2011).

153. Van Wart, H. E. & Birkedal-Hansen, H. The cysteine switch: a principle of regulation of metalloproteinase activity with potential applicability to the entire matrix metalloproteinase gene family. *Proc Natl Acad Sci U S A* **87,** 5578–5582. ISSN: 0027-8424 (July 1990).

154. Monea, S., Lehti, K., Keski-Oja, J. & Mignatti, P. Plasmin activates pro-matrix metalloproteinase-2 with a membrane-type 1 matrix metalloproteinase-dependent mechanism. *J. Cell. Physiol.* **192,** 160–170. ISSN: 1097-4652 (Aug. 1, 2002).

155. Flores-Pliego, A. *et al.* Matrix Metalloproteinase-3 (MMP-3) Is an Endogenous Activator of the MMP-9 Secreted by Placental Leukocytes: Implication in Human Labor. *PLOS ONE* **10,** e0145366. ISSN: 1932-6203 (Dec. 29, 2015).

156. Murphy, G. *et al.* Mechanisms for pro matrix metalloproteinase activation. *APMIS* **107,** 38–44. ISSN: 1600-0463 (Mar. 1, 1999).

157. Saunders, W. B., Bayless, K. J. & Davis, G. E. MMP-1 activation by serine proteases and MMP-10 induces human capillary tubular network collapse and regression in 3D collagen matrices. *Journal of Cell Science* **118,** 2325–2340. ISSN: 0021-9533, 1477-9137 (May 15, 2005).

158. Woolley, D. E., Roberts, D. R. & Evanson, J. M. Inhibition of human collagenase activity by a small molecular weight serum protein. *Biochemical and Biophysical Research Communications* **66,** 747–754. ISSN: 0006-291X (Sept. 16, 1975).

159. Fata, J. E., Ho, A. T.-V., Leco, K. J., Moorehead, R. A. & Khokha*, R. Cellular turnover and extracellular matrix remodeling in female reproductive tissues: functions of metalloproteinases and their inhibitors. *CMLS, Cell. Mol. Life Sci.* **57,** 77–95. ISSN: 1420-682X, 1420-9071 (Jan. 1, 2000).

160. Nuttall, R. K. *et al.* Expression analysis of the entire MMP and TIMP gene families during mouse tissue development. *FEBS Letters* **563,** 129–134. ISSN: 1873-3468 (Apr. 9, 2004).

161. Newby, A. C. Matrix metalloproteinases regulate migration, proliferation, and death of vascular smooth muscle cells by degrading matrix and non-matrix substrates. *Cardiovasc Res* **69,** 614–624. ISSN: 0008-6363 (Feb. 15, 2006).

162. Madri, J. A. & Graesser, D. Cell migration in the immune system: the evolving inter-related roles of adhesion molecules and proteinases. *Dev. Immunol.* **7,** 103–116. ISSN: 1044-6672 (2000).

163. Larochelle, C., Alvarez, J. I. & Prat, A. How do immune cells overcome the blood–brain barrier in multiple sclerosis? *FEBS Letters. Autoimmunity: Rheumatoid Arthritis & Multiple Sclerosis* **585,** 3770–3780. ISSN: 0014-5793 (Dec. 1, 2011).

164. Agrawal, S. *et al.* Dystroglycan is selectively cleaved at the parenchymal basement membrane at sites of leukocyte extravasation in experimental autoimmune encephalomyelitis. *J Exp Med* **203,** 1007–1019. ISSN: 0022-1007 (Apr. 17, 2006).

165. Kim, Y. H., Kwon, H.-J. & Kim, D.-S. Matrix Metalloproteinase 9 (MMP-9)-dependent Processing of βig-h3 Protein Regulates Cell Migration, Invasion, and Adhesion. *J Biol Chem* **287,** 38957–38969. ISSN: 0021-9258 (Nov. 9, 2012).

166. Song, J., Wu, C., Zhang, X. & Sorokin, L. M. In Vivo Processing of CXCL5 (LIX) by Matrix Metalloproteinase (MMP)-2 and MMP-9 Promotes Early Neutrophil Recruitment in IL-1β–Induced Peritonitis. *The Journal of Immunology* **190,** 401–410. ISSN: 0022-1767, 1550-6606 (Jan. 1, 2013).

167. Khokha, R., Murthy, A. & Weiss, A. Metalloproteinases and their natural inhibitors in inflammation and immunity. *Nat. Rev. Immunol.* **13,** 649–665. ISSN: 1474-1741 (Sept. 2013).

168. Black, R. A. *et al.* A metalloproteinase disintegrin that releases tumour-necrosis factor-α from cells. *Nature* **385,** 729–733. ISSN: 1476-4687 (Feb. 1997).

169. Moss, M. L. *et al.* Cloning of a disintegrin metalloproteinase that processes precursor tumour-necrosis factor-α. *Nature* **385,** 733–736. ISSN: 1476-4687 (Feb. 1997).

170. Young, J. *et al.* Lymphotoxin-$\alpha\beta$ heterotrimers are cleaved by metalloproteinases and contribute to synovitis in rheumatoid arthritis. *Cytokine* **51,** 78–86. ISSN: 1043-4666 (July 1, 2010).

171. Malemud, C. J. Matrix metalloproteinases (MMPs) in health and disease: an overview. *Front. Biosci.* **11,** 1696–1701. ISSN: 1093-9946 (May 1, 2006).

172. Nabeshima, K., Inoue, T., Shimao, Y. & Sameshima, T. Matrix metalloproteinases in tumor invasion: Role for cell migration. *Pathology International* **52,** 255–264. ISSN: 1440-1827 (Apr. 1, 2002).

173. Burrage, P. S., Mix, K. S. & Brinckerhoff, C. E. Matrix metalloproteinases: role in arthritis. *Front. Biosci.* **11,** 529–543. ISSN: 1093-9946 (Jan. 1, 2006).

174. Yong, V. W., Power, C., Forsyth, P. & Edwards, D. R. Metalloproteinases in biology and pathology of the nervous system. *Nature Reviews Neuroscience* **2,** 502–511. ISSN: 1471-0048 (July 2001).

175. Elkington, P. T. & Friedland, J. S. Permutations of time and place in tuberculosis. *Lancet Infect Dis* **15,** 1357–1360. ISSN: 1474-4457 (Nov. 2015).

176. Hemmings, F. J., Farhan, M., Rowland, J., Banken, L. & Jain, R. Tolerability and pharmacokinetics of the collagenase-selective inhibitor Trocade in patients with rheumatoid arthritis. *Rheumatology (Oxford)* **40,** 537–543. ISSN: 1462-0324 (May 2001).

177. Ishikawa, T. *et al.* Prevention of progressive joint destruction in collagen-induced arthritis in rats by a novel matrix metalloproteinase inhibitor, FR255031. *Br. J. Pharmacol.* **144,** 133–143. ISSN: 0007-1188 (Jan. 2005).

178. Murphy, G. & Nagase, H. Localizing matrix metalloproteinase activities in the pericellular environment. *FEBS Journal* **278,** 2–15. ISSN: 1742-4658 (Jan. 1, 2011).

179. GREENLEE, K. J., WERB, Z. & KHERADMAND, F. Matrix Metalloproteinases in Lung: Multiple, Multifarious, and Multifaceted. *Physiol Rev* **87,** 69–98. ISSN: 0031-9333 (Jan. 2007).

180. Novinec, M. & Lenarčič, B. Cathepsin K: a unique collagenolytic cysteine peptidase. *Biological Chemistry* **394,** 1163–1179. ISSN: 1437-4315 (2013).

181. Turk, V. *et al.* Cysteine cathepsins: From structure, function and regulation to new frontiers. *Biochimica et Biophysica Acta (BBA) - Proteins and Proteomics. Proteolysis 50 years after the discovery of lysosome* **1824,** 68–88. ISSN: 1570-9639 (Jan. 2012).

182. Rossi, A., Deveraux, Q., Turk, B. & Sali, A. Comprehensive search for cysteine cathepsins in the human genome. *Biological Chemistry* **385,** 363–372 (2005).

183. Hou, W.-S. *et al.* Cathepsin K Is a Critical Protease in Synovial Fibroblast-Mediated Collagen Degradation. *Am J Pathol* **159,** 2167–2177. ISSN: 0002-9440 (Dec. 2001).

184. Inaoka, T. *et al.* Molecular Cloning of Human cDNA for Cathepsin K: Novel Cysteine Proteinase Predominantly Expressed in Bone. *Biochemical and Biophysical Research Communications* **206,** 89–96. ISSN: 0006-291X (Jan. 5, 1995).

185. Tezuka, K. *et al.* Molecular cloning of a possible cysteine proteinase predominantly expressed in osteoclasts. *J. Biol. Chem.* **269,** 1106–1109. ISSN: 0021-9258, 1083-351X (Jan. 14, 1994).

186. Inui, T. *et al.* Cathepsin K Antisense Oligodeoxynucleotide Inhibits Osteoclastic Bone Resorption. *J. Biol. Chem.* **272,** 8109–8112. ISSN: 0021-9258, 1083-351X (Mar. 28, 1997).

187. Votta, B. J. *et al.* Peptide Aldehyde Inhibitors of Cathepsin K Inhibit Bone Resorption Both In Vitro and In Vivo. *J Bone Miner Res* **12,** 1396–1406. ISSN: 1523-4681 (Sept. 1, 1997).

188. Garnero, P. *et al.* The Collagenolytic Activity of Cathepsin K Is Unique among Mammalian Proteinases. *J. Biol. Chem.* **273,** 32347–32352. ISSN: 0021-9258, 1083-351X (Nov. 27, 1998).

189. Kafienah, W., Brömme, D., Buttle, D. J., Croucher, L. J. & Hollander, A. P. Human cathepsin K cleaves native type I and II collagens at the N-terminal end of the triple helix. *Biochem J* **331,** 727–732. ISSN: 0264-6021 (Pt 3 May 1, 1998).

190. Bossard, M. J. *et al.* Proteolytic Activity of Human Osteoclast Cathepsin K EXPRESSION, PURIFICATION, ACTIVATION, AND SUBSTRATE IDENTIFICATION. *J. Biol. Chem.* **271,** 12517–12524. ISSN: 0021-9258, 1083-351X (May 24, 1996).

191. Costa, A. G., Cusano, N. E., Silva, B. C., Cremers, S. & Bilezikian, J. P. Cathepsin K: its skeletal actions and role as a therapeutic target in osteoporosis. *Nature Reviews Rheumatology* **7,** 447–456. ISSN: 1759-4804 (Aug. 2011).

192. Novinec, M., Kovačič, L., Lenarčič, B. & Baici, A. Conformational flexibility and allosteric regulation of cathepsin K. *Biochemical Journal* **429,** 379–389. ISSN: 0264-6021, 1470-8728 (July 15, 2010).

193. Jordans, S. *et al.* Monitoring compartment-specific substrate cleavage by cathepsins B, K, L, and S at physiological pH and redox conditions. *BMC Biochemistry* **10,** 23. ISSN: 1471-2091 (Sept. 22, 2009).

194. Li, Z., Kienetz, M., Cherney, M. M., James, M. N. G. & Brömme, D. The crystal and molecular structures of a cathepsin K:chondroitin sulfate complex. *J. Mol. Biol.* **383,** 78–91. ISSN: 1089-8638 (Oct. 31, 2008).

195. Dubin, G. Proteinaceous cysteine protease inhibitors. *CMLS, Cell. Mol. Life Sci.* **62,** 653. ISSN: 1420-682X, 1420-9071 (Mar. 1, 2005).

196. Mason, R. W. & Massey, S. D. Surface activation of pro-cathepsin L. *Biochemical and Biophysical Research Communications* **189,** 1659–1666. ISSN: 0006-291X (Dec. 30, 1992).

197. Almeida, P. C. *et al.* Cysteine Proteinase Activity Regulation A POSSIBLE ROLE OF HEPARIN AND HEPARIN-LIKE GLYCOSAMINOGLYCANS. *J. Biol. Chem.* **274,** 30433–30438. ISSN: 0021-9258, 1083-351X (Oct. 22, 1999).

198. Li, Z., Hou, W.-S. & Brömme, D. Collagenolytic Activity of Cathepsin K Is Specifically Modulated by Cartilage-Resident Chondroitin Sulfates. *Biochemistry* **39,** 529–536. ISSN: 0006-2960 (Jan. 1, 2000).

199. Sivaraman, J., Lalumière, M., Ménard, R. & Cygler, M. Crystal structure of wild-type human procathepsin K. *Protein Sci* **8,** 283–290. ISSN: 0961-8368 (Feb. 1999).

200. Rozman, J., Stojan, J., Kuhelj, R., Turk, V. & Turk, B. Autocatalytic processing of recombinant human procathepsin B is a bimolecular process11Dedicated to Prof. Pavao Mildner on the occasion of his 80th birthday. *FEBS Letters* **459,** 358–362. ISSN: 0014-5793 (Oct. 15, 1999).

201. Pungerčar, J. R. *et al.* Autocatalytic processing of procathepsin B is triggered by proenzyme activity. *FEBS J* **276,** 660–668. ISSN: 1742-464X (Feb. 2009).

202. Li, Z., Hou, W.-S., Escalante-Torres, C. R., Gelb, B. D. & Brömme, D. Collagenase Activity of Cathepsin K Depends on Complex Formation with Chondroitin Sulfate. *J. Biol. Chem.* **277,** 28669–28676. ISSN: 0021-9258, 1083-351X (Aug. 9, 2002).

203. Costa, M. G. *et al.* How does heparin prevent the pH inactivation of cathepsin B? Allosteric mechanism elucidated by docking and molecular dynamics. *BMC Genomics* **11,** S5. ISSN: 1471-2164 (Suppl 5 Dec. 22, 2010).

204. Almeida, P. C. *et al.* Cathepsin B Activity Regulation HEPARIN-LIKE GLYCOSAMINOGLYCANS PROTECT HUMAN CATHEPSIN B FROM ALKALINE pH-INDUCED INACTIVATION. *J. Biol. Chem.* **276,** 944–951. ISSN: 0021-9258, 1083-351X (Jan. 12, 2001).

205. Hou, W.-S., Li, Z., Büttner, F. H., Bartnik, E. & Brömme, D. Cleavage Site Specificity of Cathepsin K toward Cartilage Proteoglycans and Protease Complex Formation. *Biological Chemistry* **384,** 891–897 (2005).

206. Gelb, B. D., Shi, G.-P., Chapman, H. A. & Desnick, R. J. Pycnodysostosis, a Lysosomal Disease Caused by Cathepsin K Deficiency. *Science* **273,** 1236–1238. ISSN: 0036-8075, 1095-9203 (Aug. 30, 1996).

207. Bühling, F. *et al.* Pivotal Role of Cathepsin K in Lung Fibrosis. *Am J Pathol* **164,** 2203–2216. ISSN: 0002-9440 (June 2004).

208. Srivastava, M. *et al.* Overexpression of cathepsin K in mice decreases collagen deposition and lung resistance in response to bleomycin-induced pulmonary fibrosis. *Respir. Res.* **9,** 54. ISSN: 1465-993X (2008).

209. Udagawa, N. *et al.* Origin of osteoclasts: mature monocytes and macrophages are capable of differentiating into osteoclasts under a suitable microenvironment prepared by bone marrow-derived stromal cells. *Proc Natl Acad Sci U S A* **87,** 7260–7264. ISSN: 0027-8424 (Sept. 1990).

210. Ernst, J. D. The immunological life cycle of tuberculosis. *Nat. Rev. Immunol.* **12,** 581–591. ISSN: 1474-1741 (Aug. 2012).

211. Dannenberg, A. M. Liquefaction and cavity formation in pulmonary TB: a simple method in rabbit skin to test inhibitors. *Tuberculosis (Edinb)* **89,** 243–247. ISSN: 1873-281X (July 2009).

212. Desmarais, S., Massé, F. & Percival, M. D. Pharmacological inhibitors to identify roles of cathepsin K in cell-based studies: a comparison of available tools. *Biol. Chem.* **390,** 941–948. ISSN: 1437-4315 (Sept. 2009).

213. Gauthier, J. Y. *et al.* The discovery of odanacatib (MK-0822), a selective inhibitor of cathepsin K. *Bioorg. Med. Chem. Lett.* **18,** 923–928. ISSN: 1464-3405 (Feb. 1, 2008).

214. Stoch, S. A. *et al.* Odanacatib, a selective cathepsin K inhibitor to treat osteoporosis: safety, tolerability, pharmacokinetics and pharmacodynamics – results from single oral dose studies in healthy volunteers. *Br J Clin Pharmacol* **75,** 1240–1254. ISSN: 1365-2125 (May 1, 2013).

215. Li, C. S. *et al.* Identification of a potent and selective non-basic cathepsin K inhibitor. *Bioorganic & Medicinal Chemistry Letters* **16,** 1985–1989. ISSN: 0960-894X (Apr. 1, 2006).

216. Palmer, J. T. *et al.* Design and Synthesis of Tri-Ring P3 Benzamide-Containing Aminonitriles as Potent, Selective, Orally Effective Inhibitors of Cathepsin K. *J. Med. Chem.* **48,** 7520–7534. ISSN: 0022-2623 (Dec. 1, 2005).

217. Soung, D. Y., Gentile, M. A., Duong, L. T. & Drissi, H. Effects of pharmacological inhibition of cathepsin K on fracture repair in mice. *Bone* **55,** 248–255. ISSN: 8756-3282 (July 1, 2013).

218. Duong, L. T. *et al.* Odanacatib, effects of 16-month treatment and discontinuation of therapy on bone mass, turnover and strength in the ovariectomized rabbit model of osteopenia. *Bone* **93,** 86–96. ISSN: 1873-2763 (Dec. 2016).

219. Pennypacker, B. L. *et al.* Cathepsin K inhibitors prevent bone loss in estrogen-deficient rabbits. *J. Bone Miner. Res.* **26,** 252–262. ISSN: 1523-4681 (Feb. 2011).

220. Eisman, J. A. *et al.* Odanacatib in the treatment of postmenopausal women with low bone mineral density: three-year continued therapy and resolution of effect. *J. Bone Miner. Res.* **26,** 242–251. ISSN: 1523-4681 (Feb. 2011).

221. Kassahun, K. *et al.* Pharmacokinetics and metabolism in rats, dogs, and monkeys of the cathepsin k inhibitor odanacatib: demethylation of a methylsulfonyl moiety as a major metabolic pathway. *Drug Metab. Dispos.* **39,** 1079–1087. ISSN: 1521-009X (June 2011).

222. Mullard, A. *Merck & Co. drops osteoporosis drug odanacatib* Nature Reviews Drug Discovery. DOI: 10.1038/nrd.2016.207. `https://www.nature.com/articles/nrd.2016.207` (2018).

223. Hopfgartner, G., Husser, C. & Zell, M. Rapid screening and characterization of drug metabolites using a new quadrupole-linear ion trap mass spectrometer. *J Mass Spectrom* **38,** 138–150. ISSN: 1076-5174 (Feb. 2003).

224. J Schindelin, Arganda-Carreras & Frise. *Fiji: an open-source platform for biological-image analysis*

Appendices

Appendix A

Methods

A.1 Commitment to animal welfare and ethics statement

All animals will be housed in the Animal Biosafety-level 3 facility at the Johns Hopkins University School of Medicine. Researchers working with infected animals adhere to strict facility guidelines regarding appropriate personal protective equipment. All animals in the study will be monitored daily for fecal/urine output, appearance and weight. Animals that show signs of distress or disease will be evaluated by a member of the Johns Hopkins veterinary team.

All procedures described in this document are acceptable under an active IRB protocol in the Bishai Laboratory as approved by the Johns Hopkins University Animal Care and Use Committee: Protocol Number: RB14M418. Oversight and accreditation of the Johns Hopkins Animal Care and Use Committee and facilities is provided by the Association for the Assessment and Accreditation of Laboratory Animal Use (AAALAC) International.

A.2 Repetitive aerosol infection of rabbits

Female New Zealand White rabbits (2.5 — 3.5 kg) were purchased from Robinson Services (Mocksville, NC) and housed individually in a BSL-3 facility without cross-ventilation. Rabbits were infected in a Madison aerosol droplet generation chamber (College of Engineering Shops, University of Wisconsin, Madison, WI). The aerosol inoculum for the chamber was prepared by dilution of log-phase bacterial culture of *M. tb* H_{37}Rv to the appropriate OD_{600} for each experimental group.

A.3 Clinical care plan for study rabbits

A.3.1 Criteria for euthanasia

Weight Loss: Progressive 5-8% per week sustained over 3 weeks despite fluid administration and dietary supplementation.

Respiratory distress or dyspnea: (1) any indication of hunched posture and/or nostril flaring. (2) bluish visible mucosa, (2) loss of appetite, (3) CNS depression, (4) lack of grooming, (5) soiled fur are criteria for immediate euthanasia.

Low fecal/urine output: Sustained low fecal/urine output over 3 weeks despite fluid administration and dietary supplementation.

Poor appetite: Sustained poor appetite over 3 weeks despite fluid administration and dietary supplementation.

A.3.2 Intervention plan in cases of weight loss and/or low fecal/urine output

Fluid administration: Rabbits will receive 100-150 mL of lacate ringers per day. Urine output will be monitored.

Dietary supplementation: Rabbits will receive dietary supplements such as fresh/dried fruits and vegetables, additional alfalfa hay, enrichment treats and/or critical care recovery food.

Veterinary Consultation: An animal-resources veterinarian will be consulted.

Increased and progressive monitoring: Animals covered under the intervention plan will receive increased monitoring and their status will be recorded daily

Unchanged or progressive worsening: Animals that continue to decline in fecal/urine/appetite and/or dehydration metrics will trigger criteria for euthanasia (above).

A.3.3 Protocol for procedure-level rabbit anesthesia

Animals are weighed and clinical observations are recorded. Injectible anesthetics are dosed by body weight.

1. **Ketamine:** 17-35 mg/kg IM
2. **Acepromazine:** 0.1-0.25 mg/kg IM
3. **Xylazine:** 5-10 mg/kg IM

Maintenance of anesthesia was mediated by 1-2% isofluorane in an air/oxygen mixture.

A.3.4 Protocol for rabbit euthanasia

Rabbits undergo anesthesia under the standard protocol (above). The rabbit is injected with pentobarbital solution (Euthasol) administered IV at 100 mg/kg body weight. Pupil reactivity and absence of heart-beat by palpation will be used to confirm death.

A.4 Rabbit intubation and breath-holding for CT scans

Intubation is used to achieve a lung-field immobilizing breath-hold conditions during CT imaging. Rabbits undergo standard anesthesia (above) and are maintained on 1-2% isofluorane in an oxygen/air mixture. A cuffed pediatric endotracheal (ET) tube is placed under endoscopic guidance. Rabbits are placed into the CT scanner and the ET tube is connected to a pressure-regulator. Rabbits undergo breath-holding for a period of 12-seconds. This protocol is shown to be safe for rabbits and is approved as part of the Bishai Lab standard Animal Care and Use Committee protocol.

Intubation was also used for bronchoscopic instillation of *M. tb* suspension inoculation into the lungs. In this case, a non-cuffed pediatric ET tube was used to guide the bronchoscope probe to the site of infection. The non-cuffed pediatric ET tube is necessary to allow movement of air around the ET tube while the bronchoscope probe is in the lungs.

A.5 Cipemastat dosing

Cipemastat was obtained from the Roche Corporation (Basel, Switzerland) and the identity of the compound was confirmed by LC/MS.

Rabbits in the treatment group were given 100 mg/kg cipemastat orally by body weight adjusted weekly using PediaSure as a vehicle. The concentration of cipemastat in the vehicle was 100 mg/mL. Cipemastat treatment and vehicle shams were administered daily between study weeks 5 and 10.

A.6 Pharmacokinetic analysis of cipemastat in plasma

Three rabbits were given a single 100 mg/kg oral dose of cipemastat. Peripheral blood samples were collected every 30 minutes, then at 4, 6, 8, 12, and 24 hours.

Experimental samples were analyzed in tandem with a standard curve prepared in untreated rabbit plasma. Plasma concentrations of cipemastat were detected and quantified by liquid chromatography- tandem mass spectrometry (LC-MS/MS; AB SCIEX QTRAP 5500). Liquid chromatography was carried out by reverse phase

gradient elution between 90% mobile phase A (0.1% formic acid in water) to 95% mobile phase B (100% acetonitrile) over 2 minutes on a ZORBAX Eclipse Plus C18 column (2.1 x 50 mm, 3.5 μm, Agilent Technologies, Part No. 9597432-902). Selected ion monitoring of the cipemastat parent ion at m/z 437.2 identified daughter ions at m/z 262.2 and 404.3. These transitions were supported by predicted masses in a cipemastat fragmentation map and agree with transitions identified by Hopfgartner *et al.* (2003)[223].

Cipemastat concentration in eluate was measured as area under the curve for mass transition peaks. Analysis was conducted using Analyst (SCIEX) and companion software MultiQuant (SCIEX). Pharmacokinetics analysis (PK) of total drug exposure over time (AUC0-24), half-life ($T_{1/2}$), concentration maximum (C_{max}) and time of concentration maximum (T_{max}) were calculated using 2 compartment 1st order pharmacokinetics analysis with WinNonlin software (version 7.0, Pharsight Corp).

A.7 Computerized tomography scans

Rabbits were imaged using a CereTom 8-slice clinical computerized tomography (CT) scanner with a 32.5 cm bore diameter (NeuroLogica, Boston, MA). To achieve reconstructions in the absence of motion artifact, rabbits underwent breath-holding during CT scans as described by Kübler[56].

A.8 Identification of cavities from CT reconstructions

CT reconstructions were viewed using VivoQuant software (Invicro). Lung cavities were radiologically identified from CT scan reconstructions as a contiguous set of volume elements (voxels) whose size is defined by the limit-of-resolution of the CT scanner, within the lungs, with densities close to air (-1000 – 910 Hounsfield unit [HU]) and encapsulated by consolidation defined as a continuous region of voxels with densities similar to water (-725 – 1000 HU). This radiological definition was consistent with the consensus definition for cavities advanced by Gadkowski and Stout (2008)[2]. Contiguous airspace and consolidation regions were selected by connected thresholding in the density range for each landmark. Continuity of consolidation around the airspace was confirmed by eye.

A.9 Lung extraction and fixation

After 14 weeks, rabbits were sedated and euthanized. Lungs were removed and photographed and then gently infused with intratracheal 10% neutral buffered formalin and fixed for 48 hours.

A.10 Quantification of the extent of lung disease

Gross images were obtained using a Nikon D3200 digital camera and a Nikon NIKKOR lens and analyzed with ImageJ to identify the areas of visually diseased lung as a fraction of the total area of splayed lung[224]. This fraction was used as an estimate of the percentage of diseased lung.

A.11 Histology and trichrome quantification

Transverse lung slices were collected for paraffin embedding and histologic sectioning. Serial 5 μm sections were stained using hematoxylin and eosin (H&E), Masson's trichrome stain, or the acid-fast stain. Image capture for semi-quantitative trichrome quantification was performed on a Nikon Eclipse 90i microscope with attached Nikon DS-Ri1 color camera, and analyzed using NIS Elements Advanced Research software (Nikon Instruments, Melville, NY). Regions of interest (ROIs) included the full thickenss of the cavity wall while excluding necrotic debris and air space at the cavity interior. Positive staining was calculated as a percentage of the total ROI.

A.12 Collagen cleavage assay by MMP-1

Recombinant human MMP-1 (BioVision, Milpitas CA) was added to a solution of type I collagen (Thermo Fisher Scientific, Waltham MA) in PBS at a molar ratio of 1:5. 100 μL Novex Zymogram 1X Developing Buffer (Thermo Fisher Scientific, Waltham MA) with or without 1μg cipemestat was added to this solution prior to incubation at 37° C for 24 hours. At 24 hours, an equal volume of EDTA was added

to stop the cleavage reaction, and the products were briefly boiled and subjected to SDS-PAGE on a Mini-Protean TGX precast gel (Bio-Rad, Hercules CA).

A.13 Rabbit infection by bronchoscope guided instillation

Rabbits were anesthetized by the standard protocol (described above. A 2.0-mm flexible Pentax FB-8V pediatric broncoscope (Pentax, Montvale, New Jersey) was guided into 1 lower lobe. A length of 90 cm long TE-40 plastic tubing was advanced down the bronchoscope probe and into the distal branches of the bronchial tree until slight mechanical resistance was felt by the operator. 400 μL of $1.0 \cdot 10^4$ CFU/mL bacilli in PBS was instilled through the flexible tubing and into the lung. The deadspace of the 90cm of flexible tubing is 200 μL.

A.14 Histologic and immunohistochemical staining of rabbit samples

Tissue was resected, formalin fixed in 10% NBF and paraffin embedded. Tissue sections were cut into 4 μm sections. Serial sections were stained for both hematoxylin and eosine or remained unstained for immunohistochemistry.

For CTSK immunohistochemical analysis, sections were washed in xylene, rehydrated and heated by microwave for 20 minutes in unmaking solution (Vector Laboratories, Burlingame, California; reference H-3300). Tissues were incubated for 30 minutes in serum-free protein blocking agent (Dako, Carpinteria, California; reference X0909) and incubated with monoclonal mouse anti-human CTSK primary antibody (AbD Serotec, Oxford, United Kingdom; reference MCA5232Z; 60 minutes) and then with biotinylated goat anti-mouse F_c secondary antibody (30 minutes). The complex was coupled to alkaline phosphatase by biotin and avidin (Vector Laboratories, Burlingame, California; reference AK-5000). The development step used the Vulcan Fast Red chromagen (Biocare, Concord, California; reference FR805) and hematoxylin counterstain. To control for nonspecific signal from secondary antibody binding or chromogen development, we stained serial tissue sections in the absence of primary antibody.

A.15 Repetitive dose modeling for steady-state plasma concentration in rabbits

Pheonix modeling software was used to model various doses of odanacatib as steady-state concentration between 300 nM and 600 nM. Pharmacokinetic data was used to fit slopes for absorption and elimination kinetics.

A.16 Power calculations for rabbit studies

Power calculations for our rabbit studies are based on previous work in the rabbit model. A group of 12 rabbits was exposed to mycobacterial antigen before experimental infection and was compared with a group of rabbits that was not exposed to mycobacterial antigen before infection. The pre-infection antigenic challenge provides an experimental intervention known to produce a significant reduction in disease at 12-weeks in both guinea-pigs and rabbits.

Parameters for Power Calculations:

- **Mean Fraction of Lung as Disease in Antigen-experience group:** 0.05
- **Mean Fraction of Lung as Disease in Antigen-naïve group:** 0.15
- **Standard Deviation (Average for both groups):** 0.10
- **Sampling Ratio (antigen experience/antigen-nave):** Varies by experimental plan. For example, for the proposed odanacatib rabbit experiment this parameter is 1.33 (20/15, from experimental plan).
- **Power (1-β):** 0.90
- **Type I error rate, α:** 5%
- **Sample Size of the Antigen-nave group:** Varies by experimental plan. For example, for the proposed odanacatib rabbit experiment, this parameter is 15 rabbits.
- **Decide between one or two-sided sample test comparing the means of two groups for a difference:** Varies by hypothesis and experimental plan.

Appendix B

Innovations to reduce the pain and/or distress consistent with the 3Rs of animal welfare

B.1 Refinement: ET-tube placement by endoscopic guidance

The standard method of ET tube placement in rabbits is challenging because of the elongated oropharynx which precludes visual confirmation of the ET tube in the trachea and not the esophagus. The current standard of practice is blind placement of the ET tube. To refine this technique, we innovated the use of a bronchoscope running along the ET tube to visually confirm placement of the ET tube in the trachea. Using this new technique, we have shown a significant decrease in the time needed to place the ET tube and incidental jostling and trauma to the laryngeal anatomy during placement.

B.2 Reduction: Multi-parametric disease outcomes reduce number of study rabbits

Pathology data in rabbits is collected using three different modalities: (1) Progressive CT scans, (2) Gross Pathology, (3) Histology and immunohistochemistry. The use of these three sensitive metrics of disease severity and healing allows us to reduce the number of animals needed to test our hypothesis. CT scanning in-particular allows temporal following of disease and allows the research team to resolve trends in disease that might otherwise require intermediate animal-sacrifice time-points, greatly increasing the number of animals in these studies.

Appendix C

Typesetting of this manuscript

This manuscript was created using the LaTeX document preparation system. The type face is the serif font *Computer Modern* created by Donald Knuth. Figure elements are typeset in *Arial*. The type page is 8½ *x* 11 inches. A copy of the source code is available on request from Michael Urbanowski.

Michael E. Urbanowski

Curriculum vitae

Cancer Research
Building II, Room 176.
1550 Orleans Street,
Baltimore MD, 21231

michael.urbanowski@jhmi.edu

(508) 981 – 5176

EDUCATION

Undergraduate

B.S.	2011	Microbiology, The University of Massachusetts – Amherst, Amherst MA. Graduate with Departmental Honors
B.S.	2011	Public Health, The University of Massachusetts – Amherst, Amherst MA
Summa Cum Laude Honors	2011	The Commonwealth Honors College, The University of Massachusetts – Amherst, Amherst MA. Cumulative GPA: 3.842

Graduate

M.S.	2012	Graduate Program in Plant Biology, The University of Massachusetts – Amherst, Amherst, MA - Advisor: Dr. Tobias I. Baskin - Thesis: "Development of a Cytosolic pH - - Reporter for Tobacco BY-2 Plants"
Ph.D.	2018	Graduate Program in Pathobiology, The Johns Hopkins University School of Medicine. - Advisor: Dr. William R. Bishai - Thesis: "Studies on the Mechanism and Inhibition of Tuberculosis Cavitation"

PROFESSIONAL EXPERIENCE

Research and Laboratory Experience

2007 – 2012	Research Student, Laboratory of Dr. Tobias I. Baskin. Department of Biology, University of Massachusetts – Amherst. - Research in plant physiology - Fluorescent light microscopy - Polarized light microscopy. - Cell microinjection
2010 – 2012	Research Assistant in Pediatric Oncology, research group of Dr. Naheed Usmani, University of Massachusetts School of Medicine, Worcester, MA - Clinical data management.

- Patient consent, study enrollment and follow-up.
- Training: Ethical research for studies with human subjects.

2012 – 2018 Graduate Student, Laboratory of Dr. William R. Bishai. Department of Internal Medicine, Johns Hopkins University School of Medicine, Baltimore MD.

- Training: Laboratory radiation use training.
- Training: Animal biological safety level-3 training.
- Handling of small mammals as disease models
- LC/MS for small-molecule detection
- Disease histology and immunohistochemistry
- Clinical sample IRB application and sample protocol author.

Administration and Leadership

2009 - 2011 Residential Assistant at the University of Massachusetts Amherst, Amherst MA.

- In residence leadership
- Office administration
- Crisis management

2010 – 2011 President of the Undergraduate Biological Science Group at the University of Massachusetts – Amherst, Amherst MA.

- Curriculum design
- Representation of students

2014 – 2015 Chief Graduate Student for the Pathobiology Graduate Program at the Johns Hopkins University School of Medicine, Baltimore MD.

- Peer guidance and counseling
- Project management
- Meeting organization

Teaching Experience

2011 – 2012 Graduate Teaching Assistant, The University of Massachusetts – Amherst, Amherst MA

- Academic laboratory coordination and administration
- Lecturing

2013 – 2016 Graduate Teaching Assistant, Basic Mechanisms of Disease Course Graduate Course, The Johns Hopkins University School of Medicine, Baltimore MD

- Lecture topic: “A&P of the Circulatory System”
- Lecture topic: “A&P of the Respiratory System”

2015 – 2017 Graduate Teaching Assistant, Infectious Disease and Immunology Graduate Course, The Johns Hopkins University School of Medicine, Baltimore MD

PUBLICATIONS

Peer Reviewed Articles

Kubler A, Larsson C, Luna B, Andrade BB, Amaral EP, **Urbanowski M**, Orandle M, Bock K, Ammerman NC, Cheung LS, Winglee K, Halushka M, Park JK, Sher A, Friedland JS, Elkington PT, Bishai WR. "Cathepsin K Contributes to Cavitation and Collagen Turnover in Pulmonary Tuberculosis." *Journal of Infectious Disease*. September 27, 2015.

Pan SJ, Tapley A, Adamson J, Little T, **Urbanowski M**, Cohen K, Pym A, Almeida D, Dorasamy A, Layre E, Young DC, Singh R, Patel VB, Wallengren K, Ndung'u T, Wilson D, Moody DB, Bishai WR. Biomarkers for Tuberculosis Based on Secreted, Species-Specific, Bacterial Small Molecules. Journal of Infectious Disease. May 26, 2015.

Ordonez AA, Weinstein EA, Bambarger LE, Saini V, Chang YS, DeMarco VP, Klunk MH, **Urbanowski ME**, Moulton KL, Murawski AM, Pokkali S, Kalinda AS, Jain SK. A Systematic Approach to Developing Bacteria-Specific Imaging Tracers. *Journal of Nuclear Medicine*. September 15, 2016.

Urbanowski ME, Ihms EA, Bigelow K, Kubler A, Elkington PT, Bishai WR. Repetitive aerosol exposure promotes cavitary tuberculosis and enables screening for targeted inhibitors of extensive lung destruction. *Journal of Infectious Disease*. (Published Online March 15 2018).

Rifat D, Prideaux B, Radojka SM, **Urbanowski ME**, Parsons TL, Luna B, Marzinke MA, Ordonez AA, Demarco VP, Jain SK, Dartois V, Bishai WR, Dooley KE. Pharmacokinetics of rifapentine and rifampin in a rabbit model of tuberculosis and correlation with clinical trial data. *Science Translational Medicine*. April 4, 2018.

Review Articles

Abel L, Fellay J, Haas DW, Schurr E, Srikrishna G, **Urbanowski M**, Chaturvedi N, Srinivasan S, Johnson DH, Bishai WR. Genetics of human susceptibility to active and latent tuberculosis: present knowledge and future perspectives. *Lancet Infect Dis.* March 18th, 2018

Hunter RL, Actor JK, Hwang SA, Khan A, **Urbanowski ME**, Kaushal D, Jagannath C. Pathogenesis and Animal Models of Post-Primary (Bronchogenic) Tuberculosis, A Review. *Pathogens*. February 6th, 2018.

Opinion Pieces

Urbanowski M. "Argue and *Be* Wrong!" The Restriction Digest, a Publication of the Graduate Student Association at the Johns Hopkins

University School of Medicine. Retrieved from: http://restrictiondigest.weebly.com/blog/argue-and-be-wrong

AWARDS AND INTERNSHIPS

2009 – 2010	Howard Hughes Medical Institute Undergraduate Internist, Department of Biology, University of Massachusetts – Amherst, Amherst, MA
2010	Howard Hughes Medical Institute Undergraduate Summer Internist, Department of Biology, University of Massachusetts – Amherst, Amherst, MA
2010 – 2011	Junior Fellow in the Life Sciences at the University of Massachusetts – Amherst, Amherst MA
2017	Arthur M. Dannenberg Award – Research in Tuberculosis.

INVITED TALKS

June, 2017	Tuberculosis Research Day Symposium: "Modeling tuberculosis cavities using repetitive aerosol exposure to Mycobacterium tuberculosis"
October 2017	Johns Hopkins School of Public Health Tropical Medicine Dinner Club Short-Talk: "Modeling tuberculosis cavities using repetitive aerosol exposure to *Mycobacterium tuberculosis*"
March 2018	NIH RISE invited seminar speaker at Morgan State University: "The Hole Issue in Tuberculosis"

POSTER PRESENTATIONS

April 2015	Johns Hopkins Pathology Department Young Investigators Day: "Persistent Cavitary Disease in a Rabbit Model of Tuberculosis"
January 2017	Keystone Conference on Tuberculosis: "Cipemastat, a potent MMP-1 inhibitor, does not reduce cavity formation in the rabbit TB model."
April 2018	Keystone Conference on Tuberculosis: "Repetitive aerosol exposure exacerbates tuberculosis cavitation in a rabbit model.

MENTORSHIP

2015	Chase Weinberg, Undergraduate Summer Internist, Bishai Laboratory, The Johns Hopkins University School of Medicine, Baltimore MD
2015	Benjamin Merenbloom, Undergraduate Summer Internist, Bishai Laboratory, The Johns Hopkins University School of Medicine, Baltimore MD

2016	Maryalanna Williams, Merit Health Leadership Academy, High-School Participant, Bishai Laboratory, The Johns Hopkins University School of Medicine, Baltimore, MD

VOLUNTEER EXPERIENCE

2005 – 2008	Counselor – Camp Sunshine, Acadia ME: A residential camp for children with life-threatening illnesses and their families.
2007 – 2009, 2017	Counselor – The Hole In The Wall Gang Camp, Ashford CT: A residential camp for children with life-threatening hematologic diseases.
2007 – 2011	Volunteer – Habitat for Humanity, Pioneer Valley, MA
2009 – 2012	Study Assistant – Pediatric Oncology Survivorship Study and Pediatric Oncology Audit Project Assistant. University of Massachusetts School of Medicine, Worcester MA.
2014	Counselor – Heroes Journey, The Hole in the Wall Gang Camp, Ashford CT: A residential program for teenagers off-treatment for serious hematological disorders.